

Polyoxazoline-Silica Hybrid Nanoparticles

Thesis submitted to the
Faculty of Chemistry and Chemical Biology
in partial fulfillment of the requirements
for the Doctorate in Philosophy degree in Chemistry
(Dr. rer. nat.)

by

Golnaz Bissadi

Department of Chemistry and Chemical Biology
Technical University of Dortmund

Statement of Contributions and Collaborators

I hereby declare that I am the sole author of this thesis. I independently designed all the experimental studies, performed analytical studies and wrote all the chapters in this work.

My supervisor, Prof. Dr. Ralf Weberskirch, provided me with an excellent collaboration throughout this work with supervision, discussions, support, and editorial comments for all of my written work. The quality of this thesis has been tremendously improved through his guidance.

Golnaz Bissadi

Faculty of Chemistry and Chemical Biology
Technical University of Dortmund
Germany

The present work was carried out during the period from August 2014 to November 2016 under the direct supervision of Prof. Dr. Ralf Weberskirch at the Faculty of Chemistry and Chemical Biology at the Technical University of Dortmund.

Contributions:

G. Bissadi, R. Weberskirch, Efficient synthesis of polyoxazoline-silica hybrid nanoparticles by using the “grafting-onto” approach, *Polymer Chemistry*, 7 (2016) 1271-1280

G. Bissadi, R. Weberskirch, Formation of polyoxazoline-silica nanoparticles via the surface-initiated cationic polymerization of 2-methyl-2-oxazoline, *Polymer Chemistry*, 7 (2016) 5157-5168

Assessors:

1. Prof. Dr. Ralf Weberskirch
2. Prof. Dr. Jörg C. Tiller

Acknowledgement

First and foremost, I would like to acknowledge my supervisor, Prof. Dr. Ralf Weberskirch, for giving me the opportunity to work on this interesting research project. His dedicated supervision, continued support, mentorship, and guidance have provided me with the inspiration needed to complete my doctoral studies.

In addition to my supervisor, I would like to thank Prof. Dr. Jörg C. Tiller for kindly agreeing to be the second evaluator of my Ph.D. defense.

It is with great appreciation that I thank Prof. Dr. Jörg C. Tiller and Prof. Dr. Heinz Rehage for giving me the opportunity to use their analytical equipment.

I gratefully acknowledge a number of people who have provided help throughout this research. My sincere thanks also goes to Mrs. Monika Meuris from the group of Prof. Dr. Jörg C. Tiller for taking TEM images and all others who were involved with materials characterizations; the group of Prof. Dr. Heinz Rehage for providing the DLS device; the group of Prof. Dr. Michael Spitteller for providing the TGA and BET devices; and the entire NMR department, Dr. Wolf Hiller, Dr. Mathias Hehn, and Benjamin Kissel for the rapid measurement of my NMR samples.

I would like to thank Katja Weber for all of her support in the laboratory and for maintaining the lab equipment, as well as Andrea Bokelmann for her support in analytical questions. Furthermore, I would like to thank Silvia Lessing, Andreas Hammer, and Heidi Auer for all their assistance with any organizational issues.

I would also like thank to my colleagues past and present: Sotoodeh Mohammadi, Patrick Bolduan, Hanne Petersen, Omar Sallouh, Anne-Larissa Kampmann, Irene Pretzer, Dr. Andrea Ernst, David Pelzer, and Henning Sand for all of their helps.

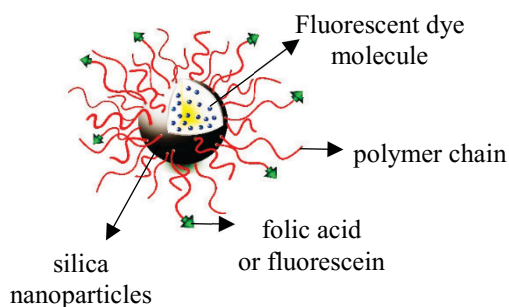
Further, I would like to acknowledge the work of undergraduate and graduate students who participated in this project: Tristan Jolmes, Paola Andrea Benitez Rengifo, Fabian Roesler, Christoph Drechsler, and Marco Schnurbus.

Finally, I would like to thank my wonderful family for their support, patience, encouragement, and understanding throughout this work. In addition, I would like to thank my husband, Amir, without whom none of this would have been possible.

Abstract

Core-shell nanoparticles have found increased attention in the past years due to their many potential applications in material science, i.e. catalysis, optics and biomedicine. In this thesis, well-defined silica nanoparticles (SNPs) coated with poly(2-methyl-2-oxazoline) (PMeOx) have been prepared and characterized for biomedical applications. SNPs were synthesized through the reverse microemulsion method followed by the chemical binding of PMeOx chains to the surface of the silica core via various approaches including “grafting to”, “grafting from”, and in-situ immobilization and polymerization of 2-methyl-2-oxazoline (MeOx).

For the synthesis of PMeOx-coated SNPs via the “grafting to” approach, two different methods were employed involving click chemistry and the silane coupling reaction; however, only the latter method resulted in a relatively higher grafting density. The hybrid nanoparticle synthesis was further improved by fabricating the polymer shell via the “grafting from” approach and immobilization of an initiator on the particle surface before polymerization. Grafting density and thickness of the polymeric shell was controlled by varying the polymerization time and monomer/initiator ratio concentration. These hybrid nanoparticles were further functionalized with fluorescein isothiocyanate and folic acid as a fluorescence imaging molecule and cancer-targeting ligand, respectively. Moreover, hybrid nanoparticles with tris(bipyridine)ruthenium(II) chloride as a fluorophore encapsulated in the silica core were prepared before the PMeOx shell was formed by the “grafting-from” method. Finally, a novel one-pot method was designed and optimized entitled “in situ immobilization and polymerization of monomer” for the synthesis of PMeOx-coated SNPs. This led to a grafting density similar to the “grafting to” approach with the advantage of a simplified the reaction procedure.



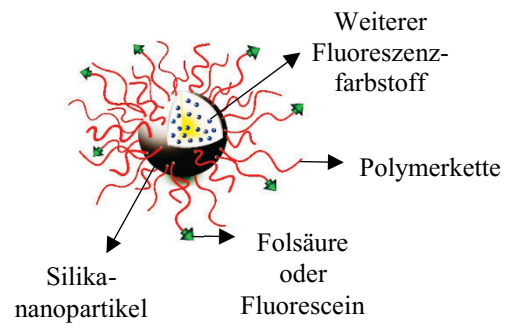
Scheme 1. Schematic picture of a silica polymer hybrid nanoparticle with surface functional groups (folic acid or fluorescein) and/or encapsulated dye molecules

Kurzfassung

Kern-Schale basierte Nanopartikel sind Materialien, die eine zunehmende Aufmerksamkeit erfahren aufgrund ihrer zahlreichen möglichen Anwendungen in den Materialwissenschaften, z. Bsp. der Katalyse, der Optik oder der Biomedizin. Im Rahmen dieser Arbeit wurden Silika-Nanopartikel (SNPs) hergestellt und charakterisiert für Biomedizinanwendungen, die mit einer Poly(2-methyl-2-oxazolin) (PMeOx) Hülle umgeben sind. SNPs wurden mithilfe der reversen Mikroemulsion hergestellt gefolgt von der kovalenten Kopplung der PMeOx-Ketten auf der Silikaoberfläche mithilfe verschiedener Techniken, wie die “grafting-to”, “grafting-from” und der in-situ Immobilisation und Polymerisation von 2-Methyl-2-oxazolin (MeOx).

Für die Herstellung der PMeOx-beschichteten SNPs nach der “grafting-to” Methode, wurden zwei unterschiedliche Ansätze untersucht, dazu gehören die Click-Chemie und die Silan-Kupplungsreaktion; wobei nur die letztere zu relativ hohen Pfropfdichten führte. Die Synthese der Silikahybridpartikel wurde weiter verbessert durch Bildung der Polymerhülle mithilfe des “grafting-from” Verfahrens und Immobilisierung eines Initiators auf der Partikeloberfläche vor der Polymerisation. Die Pfropfdichte und die Dicke der Polymerhülle wurden kontrolliert durch Variation der Polymerisationszeit und der Monomer / Initiatorverhältnisse. Die so erhaltenen Hybridnanopartikel wurden weiter funktionalisiert mit Fluoresceinisothiocyanat für die bildgebende Diagnostik und Folsäure für das Tumor-spezifische aktive Targeting. Darüber hinaus konnte gezeigt werden, daß Fluorophore, wie Tris(bipyridine)ruthenium(II) chlorid in den Silikakern verkapselt werden können bevor die Oberflächen-initiierte Polymerisation von 2-Methyl-2-oxazolin durchgeführt wurde.

Schließlich wurde eine Eintopfvariante entwickelt und optimiert, bei der in-situ der Initiator immobilisiert wird und die Polymerisation von 2-Methyl-2-oxazolin für die Bildung der PMeOx beschichteten SNPs abläuft. Dies führte zu einer Pfropfdichte ähnlich der, die bei der “grafting-to” Methode gefunden wurde, jedoch mit dem Vorteil der vereinfachten Reaktionsführung.



Schema 1. Schematische Darstellung eines Silikahybrid Polymernanopartikels mit Oberflächen-funktionalisierten Gruppen (Folsäure oder Fluorescein) und/oder eingekapselten Farbstoffen.

Table of Contents

Chapter 1. Introduction.....	1
Chapter 2. Literature Review.....	3
2.1 General description of core-shell nanoparticles.....	3
2.2 Nanoparticles in bioimaging.....	5
2.2.1 Properties of silica nanoparticles.....	6
2.2.2 Synthesis of silica nanoparticles.....	8
2.2.2.1 Size.....	10
2.2.2.2 Shape.....	11
2.2.2.3 Surface property.....	12
2.2.3 Synthesis of fluorescent dye-doped silica nanoparticles.....	13
2.3 Polymers in biomedical applications.....	15
2.3.1 Poly(2-oxazolines).....	16
2.3.2 Functionalization of Poly(2-oxazolines).....	19
2.4 Polymer chemistry for surface modification.....	23
2.4.1 “Grafting to” approach.....	24
2.4.2 “Grafting from” approach.....	26
2.4.3 “Grafting through” approach.....	28
2.4.4 Other approaches.....	29
Chapter 3. Overview of Project Objectives.....	31
Chapter 4. Synthesis of Polyoxazoline-Silica Hybrid Nanoparticles via “Grafting to” Approach.....	33
4.1 Introduction.....	33
4.2 Results and Discussion.....	37
4.2.1 Synthesis of the PMeOx-coated SNP through the “grafting to” approach.....	37
4.2.1.1 Click coupling between alkyne-functionalized PMeOx and azide-modified SNPs.....	37
4.2.1.2 Silane coupling reaction between silane agent-functionalized PMeOx and hydroxyl groups on the surface of SNPs.....	42
4.2.2 Synthesis of fluorescent-dye doped SNP-coated with PMeOx.....	47
4.2.3 Study the effect of different synthesis parameters on grafting density.....	51
4.2.3.1 The effect of synthetic parameters on grafting density of the PSNP-B.....	52
4.2.3.2 The effect of synthetic parameters on grafting density of the PSNP-D.....	55

4.3 Conclusion.....	57
4.4 Experimental	58
4.4.1 Synthesis of silica nanoparticles (SNPs)	58
4.4.2 Synthesis of azide-modified silica nanoparticles (SNP-N ₃).....	59
4.4.3 Synthesis of alkyne-functionalized PMeOx (P1)	60
4.4.4 Synthesis of trimethoxysilane-functionalized PMeOx (P2)	61
4.4.5 Click coupling between alkyne-functionalized PMeOx and azide-modified SNPs (PSNP-A).....	61
4.4.6 Coupling reaction between silane agent PMeOx and SNPs (PSNP-B, PSNP-C, and PSNP-D).....	62
4.4.7 Synthesis of Ru(bpy)-doped silica nanoparticles (SNP-Ru(bpy)).....	63
4.4.8 Synthesis of PMeOx coated SNP-Ru(bpy) via reverse microemulsion (PSNP-E)	64
4.4.9 Synthesis of FITC-doped silica nanoparticles (SNP-FITC).....	64
4.4.10 Synthesis of PMeOx coated SNP-FITC via reverse microemulsion (PSNP-F)	64
Chapter 5. Synthesis of Polyoxazoline-Silica Hybrid Nanoparticles via “Grafting from” Approach.....	65
5.1 Introduction	65
5.2 Results and discussion.....	68
5.2.1 Synthesis of the PMeOx-coated SNP via “grafting from” approach using 4-(bromomethyl)benzoic acid as an initiator	68
5.2.2 Synthesis of the PMeOx-coated SNP via “grafting from” approach using ((chloromethyl)phenylethyl)trimethoxysilane as an initiator	70
5.2.2.1 Immobilization of CTM on the surface of SNPs	71
5.2.2.2 Reaction time effect	73
5.2.2.3 Monomer concentration effect.....	77
5.2.2.4 Conjugation of folate and/or FITC to polymer-grafted-Silica nanoparticles.....	78
5.2.2.5 Synthesis of dye-encapsulated silica nanoparticle coated with a PMeOx shell.....	82
5.3 Conclusion.....	84
5.4 Experimental	85
5.4.1 Synthesis of silica nanoparticles (SNPs)	85
5.4.2 Synthesis of amino-modified SNP (SNP-NH ₂).....	85
5.4.3 Synthesis of bromide-modified SNP (SNP-BMBA)	86
5.4.4 Preparation of PSNP-G via “grafting from” approach	86
5.4.5 Synthesis of chloride-modified SNP (SNP-CTMS).....	87

5.4.6 Preparation of PSNP-H via “grafting from” approach	87
5.4.7 Synthesis of amine-functionalized hybrid nanoparticles (PSNP-I).....	88
5.4.8 Conjugation of FITC on PSNP-I (PSNP-I-FITC)	89
5.4.9 Conjugation of folic acid on PSNP-I (PSNP-I-FA).....	90
5.4.10 Synthesis of Ru(bpy)-doped SNP coated with PMeOx (PSNP-J).....	90
5.4.11 Etching silica nanoparticles	91
Chapter 6. Synthesis of Polyoxazoline-Silica Hybrid Nanoparticles via <i>In situ</i> Immobilization and Polymerization of 2-Methyl-2-oxazoline.....	93
Introduction	93
Results and discussion.....	95
Conclusion.....	102
Experimental	103
6.4.1 Synthesis of silica nanoparticles (SNPs)	103
6.4.2 Synthesis of PMeOx-coated SNPs	103
6.4.2.1 Synthesis of PSNP-K	103
6.4.2.2 Synthesis of PSNP-L.....	104
6.4.2.3 Synthesis of PSNP-M	104
6.4.3 Etching silica nanoparticles	105
Chapter 7. Characterization Techniques.....	107
7.1 Thermogravimetric analysis	107
7.2 Transmission electron microscopy.....	107
7.3 Fourier transform infrared spectroscopy	107
7.4 Nuclear magnetic resonance spectroscopy.....	108
7.5 Dynamic light scattering	108
7.6 Nitrogen adsorption.....	108
7.7 Elemental analysis.....	109
7.8 Size exclusion chromatography	109
7.9 Ultraviolet-visible spectroscopy.....	109
Chapter 8. Conclusions and Recommendations	111
Chapter 9. References.....	115
Chapter 10. Appendix.....	133
10.1 Nomenclature	133
10.1.1 Abbreviations.....	133

10.1.2 Symbols	135
10.2 List of Figures	136
10.3 List of Tables.....	140
10.4 ¹ H NMR spectra of P1 and P2	141
10.5 UV-Vis Calibration	142

Chapter 1. Introduction

Nanoparticles (NPs) have mainly been investigated in recent years as a prospective biomedical tool, which can contribute immensely to various fields such as drug delivery, gene delivery, and imaging [1,2]. The key feature that makes NPs interesting in life sciences is their high surface-to-volume ratio. This allows them to be modified adequately and consequently improves their pharmacokinetic properties, increases their vascular circulation lifetime, and enhances their bioavailability [1]. Moreover, these nano-sized particles allow large numbers of drug molecules, imaging, and therapeutic agents to be encapsulated inside or to be attached on their surface [3]. The surface modification of NPs with polymers has recently gained much attention since the polymer coating alters the interfacial properties of the NPs as it increases their dispersibility, enhances the thermal and chemical stability of their core, decreases their toxicity, improves their biocompatibility, and facilitates their conjugation with other bioactive molecules [1]. These novel core-shell nanoparticles (CSNPs) have therefore performed better than simple NPs in biomedical applications, when core and shell have a suitable composition. A schematic illustration of cancer diagnosis and therapy with NPs is shown in Figure 1.1.

Various types of inorganic NPs can be used in biomedical applications, such as silica, gold, silver, and iron oxide nanoparticles [4]. Silica nanoparticles (SNPs) are among the most interesting and well-known NPs. They have received increasing attention as drug delivery vehicles or bioimaging agents [5] owing to their ease of synthesis [6], particle size uniformity [7], relatively low cost [8], excellent biocompatibility [6,9], hydrophilicity [6], and versatility of the possible surface modifications [9]. In bioimaging applications, SNPs have the potential to encapsulate the imaging molecules and therefore overcome some limitations of conventional fluorescent dyes such as poor hydrophilicity, low photostability, and insufficient stability in biological system [10]. However, the major challenge is related to the surface properties of SNPs since many studies reported the adsorption of proteins on the surface of these nanoparticles, possibly affecting their colloidal stability and toxicity [11,12]. To address this problem, the surface of SNPs can be modified with hydrophilic polymers that can prevent non-specific protein adsorption [11].

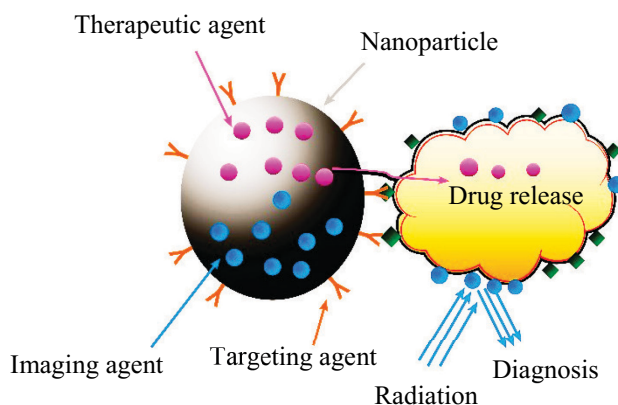


Figure 1.1 Schematic illustration of cancer diagnosis and therapy with nanoparticles, based on Ahmed et al. [2].

Generally, the surface of inorganic NPs can be modified with polymer chains by either physical interaction or covalent attachment. Covalent grafting techniques are preferable due to the enhanced stability of the tethered polymer layer [13,14]. These approaches have been mainly used to attach polymer layers to the NP surface: “grafting to” involves a coupling technique, “grafting from” uses surface-initiated polymerization, and “grafting through” involves a macromonomer that can be copolymerized with the other monomers in the surrounding medium [15–19]. More specifically, the surface modification of SNPs with hydrophilic polymers is essential for *in vivo* applications owing to the improved circulation time of the particles. Among the polymers that can be used as a shell, polyethylene glycol (PEG) is one of the most interesting polymers in biomedical applications [20–22]; however, it has some limitations owing to its possible interaction with the immune system and possible degradation under stress [21,23–25]. To circumvent these problems, poly(2-methyl-2-oxazoline) (PMeOx) and poly(2-ethyl-2-oxazoline) (PEtOx) have been proposed as a promising alternatives for this challenge in biomedical applications, because they combine essential properties such as hydrophilicity, biocompatibility, versatile end group chemistry [21], chemical stability [26], and stealth behavior similar to PEG [27]. Mansfield et al. recently reported similar abilities of poly(2-ethyl-2-oxazoline) (PEtOx) and PEG-coated SNPs to improve the diffusivity of SNPs in mucin dispersions and through the gastric mucosa [27]. It should be noted that the ease of synthesis also plays an undeniable role in attracting the attention of researchers to this novel class of materials [1]. This current study aims at modifying the surface of SNPs with poly(2-methyl-2-oxazoline), PMeOx, for bioimaging applications, by using several chemical strategies.

Chapter 2. Literature Review

2.1 General description of core-shell nanoparticles

Core-shell nanoparticles are defined as nano-sized particles that contain an inner material (core) that is surrounded by an outer layer material (shell) [28]. These novel materials are well-known for their improved stability, physical, and chemical properties, as the shell is able to protect the core from the surrounding environment [29]. In addition, CSNPs may have properties that arise from the synergy between cores and shells [30].

Core-shell nanoparticles can be composed of various combinations of materials, including inorganic/inorganic, inorganic/organic, organic/inorganic, and organic/organic materials [30]. The “organic” class is related to carbon-based materials, mostly polymers, whereas the “inorganic” class includes metal- or silica-based materials [30]. The choice of material for the core or the shell strongly depends on the end application of the nanomaterial. Moreover, CSNPs can be classified into three types based on their shell properties: hollow-core-shell nanoparticles, core-multishell nanoparticles, and core-porous-shell nanoparticles.

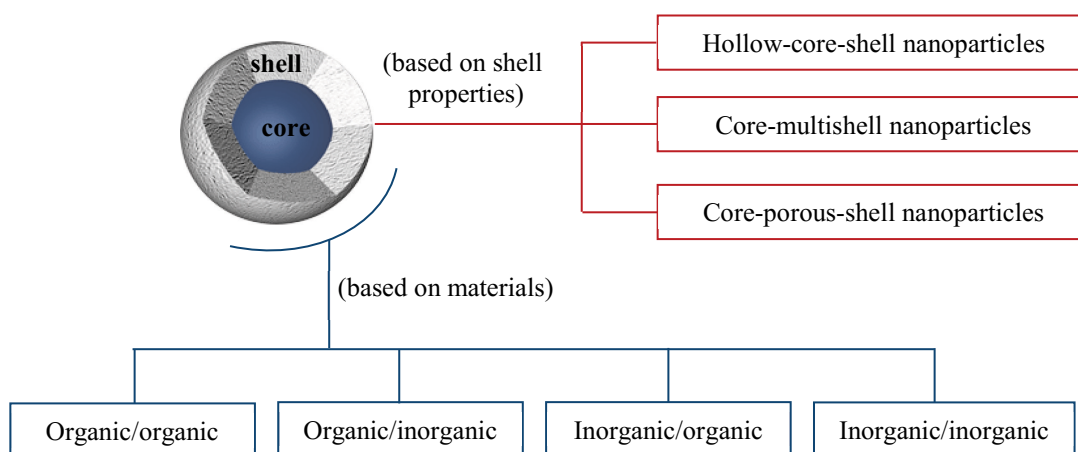


Figure 2.1 General classification of core-shell nanoparticles based on the properties of their shells and material-types, based on Gawande et al. [30].

Core-shell nanoparticles have been receiving increasing attention, owing to their versatility in composition and structure [30] and their broad range of applications, which

include coating, catalysts, optics [31–33], and biomedical applications [1,30,34,35]. Nanoparticles have largely influenced biomedical applications in various fields such as controlled drug delivery and release, targeted drug delivery, bioimaging, and diagnostics [29]. The main advantage of NPs over larger particles is their high surface-to-volume ratio, which allows a more efficient surface modification leading to an enhancement of circulation time and bioavailability [1]. Moreover, the coating of the core can improve many of the core's properties: the cytotoxicity can be reduced, the dispersibility, biocompatibility, thermal stability, and chemical stability can be improved, and the NP can be conjugated to other bioactive molecules [1,36]. These additional advantages make CSNPs an interesting alternative to conventional NPs in bioimaging, and drug delivery [1,30,34–36]. For example, CSNPs are extensively studied for bioimaging application because the core can encapsulate imaging molecules and protect them from photobleaching, and the shell material is responsible for the surface properties such as biocompatibility and conjugation with bioactive materials [1]. Future generations of multifunctional CSNPs will exhibit many new properties that will surely result in new applications with improved performances [29]. A schematic of a multifunctional CSNP for biomedical applications is shown in Figure 2.2.

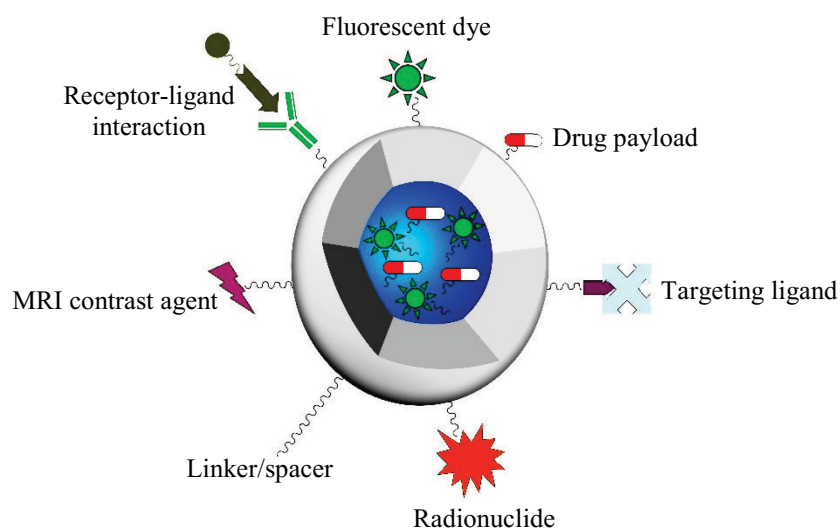


Figure 2.2 Scheme of a multifunctional core-shell nanoparticle for biomedical applications, based on Chatterjee et al. [1].

2.2 Nanoparticles in bioimaging

Early and accurate diagnosis of cancer is the most important factor for the patient's survival, and largely depends on the rapid and sensitive detection of tumor cells. In the last two decades, advancement in nanotechnology have significantly benefited bioscience owing to their wide variety of applications in drug delivery [37], diagnostic sensors [38], and imaging agents [39,40]. Bioimaging techniques have an undeniable effect on improving human health by improving the diagnosis and prevention of diseases. Moreover, *in vivo* imaging has attracted much attention as a tool to better understand living organisms and, in particular, the human body which is an extremely complex system [41,42]. Various bioimaging tools can be used, such as magnetic resonance imaging (MRI), positron emission tomography (PET), ultrasound, computed tomography (CT), and optical imaging [1].

Fluorescence imaging is one of the simplest technologies for bioimaging, and it is widely used in research [43]. Fluorescence microscopy was first reported by Reichert and Heimstädt in 1911, which was a few decades after the development of organic fluorescent molecules [44]. Fluorescent dye molecules were traditionally used for imaging, but they suffer from low brightness, photobleaching, and non-specific targeting [40]. A comprehensive study in the field of bioimaging indicates that the available nanomaterials with the purpose of imaging are promising because fluorescent nanomaterials can overcome limitations of organic fluorescent dyes, such as poor hydrophilicity, rapid photobleaching, and low quantum yield [41]. Several types of nanosystems can be used for bioimaging, such as organic polymers, NPs made from silica and organically modified silica, quantum dots, carbonaceous nanomaterials, and metal-based NPs [45]. Among all available nanomaterials, fluorescent-based NPs are the most interesting ones for *in vivo* bioimaging [41]. Fluorescent-based NPs have the potential to overcome the limitations of fluorescent dye molecules and provide highly sensitive and selective tumor imaging. Thousands of dye molecules can be incorporated into one nanoparticle, leading to a greater brightness of the NP compared to a single dye molecule [40]. Also, the formed shell around the dye molecules can protect these molecules from photobleaching and consequently allow long-duration imaging of tumor cells [40]. Moreover, the modifiable surface of these NPs enables the immobilization of various targeting ligands and consequently leads to selective tumor imaging agents [40].

Fluorescent-based NPs can be fabricated by incorporating fluorescent dyes into the particle's matrix or by immobilizing the dye molecules on the surface of the particles [46]. The doped dyes can be either inorganic or organic [46]. Photobleaching can be considerably reduced by incorporating organic dyes into a particle matrix that enables the depletion of oxygen surrounding the dye [46]. The dye molecules can be either physically encapsulated into the particle matrix or chemically bonded to the particle. Although the former method is much easier to implement and applicable to a wider variety of dyes, the latter method gained more interest because it prevents the dye molecules from leaking out of the particle [46].

2.2.1 Properties of silica nanoparticles

Excellent control over the synthesis of NPs is a prerequisite for their application in biomedical fields [6]. Moreover, NPs that are used for bioimaging need to be non-toxic, selective, small enough to enter cells, and they need to have a good dispersibility in the biological environment. Various kinds of NPs can be used for bioimaging, such as quantum dots [47], carbon nanotubes [48,49], magnetic nanoparticles [50], and SNPs [45]. Among them, SNPs have gained special interest for imaging due to their ease of synthesis [6,40], uniform morphology over a range of particle sizes [7], relatively low cost [8], excellent biocompatibility [6,9,40], hydrophilicity [6], transparent matrix [51], inert nature [51], and many possible surface modifications [9]. The great potential of SNPs in biomedical applications was especially highlighted after the U.S. Food and Drug Administration approved the first in-human clinical trial of ultrasmall SNPs for the real-time fluorescent detection and imaging of melanoma with lymphatic drainage patterns and nodal metastases [52]. These ultrasmall cancer-selective multimodal SNPs, with a diameter of 7 nm, have a unique combination of structural, optical, and biological properties [53,54]. The silica core contains Cy5 dye molecules, and it is coated with methoxy-terminated polyethylene glycol (PEG) chains and further functionalized with cyclic arginine–glycine–aspartic acid peptide ligands and radioiodine [53,54].

In general, SNPs for biomedical applications are classified into two main types: mesoporous SNPs (2-50 nm pore size) and nonporous/solid SNPs (Figure 2.3) [6,40]. Mesoporous SNPs are used as drug delivery vehicle: drugs can be loaded at high concentrations, by either chemical or physical adsorption, and easily released from the

mesopores and nanochannels [6,40]. Mesoporous SNPs are loaded with cargos in the nanochannels and the inner surface of these nanochannels can be modified in order to control the binding affinity with cargo molecules. In order to prevent a premature release of the cargo molecules, gatekeepers are attached to the surface of the mesoporous SNPs [6]. In contrast, nonporous/solid SNPs are mainly used in bioimaging applications to deliver cargos either by encapsulation, conjugation with the silica matrix or binding to the surface of the particles [6]. The cargos are released by degradation of the silica matrix or the chemical linkers [6]. Silica nanoparticles can be accumulated in tumor tissues through either passive or active targeting pathways, and the imaging agents inside the silica particles give the accurate location of nanoparticles in tumor tissues [40].

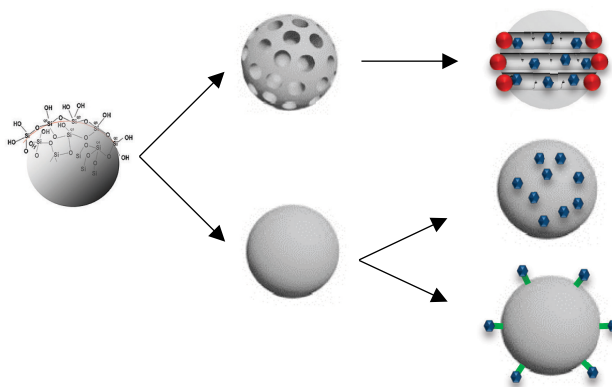


Figure 2.3 Schematic diagram of the (a) mesoporous silica nanoparticles and (b) nonporous silica nanoparticles loaded with cargos, based on Tang et al. [6].

Although nanomaterials that can circulate in the body have great potential in diagnosis and treatment, it is extremely important that these nanomaterials can be eliminated from the body in a reasonable amount of time [55]. Cho et al. monitored the excretion of SNPs in urine and feces on five-week-old male BALB/c mice [56]. They reported that excretion largely depends on particle size and they found that SNPs with diameter around 50 nm, reached their highest concentration in urine after 12 h and in feces after 24 h. Moreover, one week after intravenous injection of SNPs, SNPs were not detected in urine regardless of their size [56]. They studied the excretion of three sizes of SNPs (50, 100, and 200 nm) and reported that smaller particles were present in urine and feces at higher concentrations and were cleared more rapidly [56]. Moreover, it was reported that mesoporous silica nanoparticles could decompose *in vivo* into harmless

silicic acid by-product, which makes these materials attractive for long-term applications [57,58].

2.2.2 Synthesis of silica nanoparticles

Silica nanoparticles can be prepared via a sol-gel process that involves the hydrolysis of a silicon alkoxide precursor followed by the polycondensation of monomers in the presence of an acid or base catalyst in order to form the desired NPs [59,60]. The silicon alkoxide precursor can be, for example, tetramethoxysilane (TMOS) and tetraethoxysilane (TEOS) [61]. During the hydrolysis of TEOS in water, the alkoxide group is replaced by a hydroxyl group (Figure 2.4 A) [62,63]. Consequently, the hydrolyzed TEOS undergoes a polycondensation reaction, leading to either water or ethanol as a by-product (Figure 2.4 Beq. 2-2) [62,63]. Both forms of condensation lead to the formation of siloxane bridges (Si-O-Si), which account for the silica structure [63].

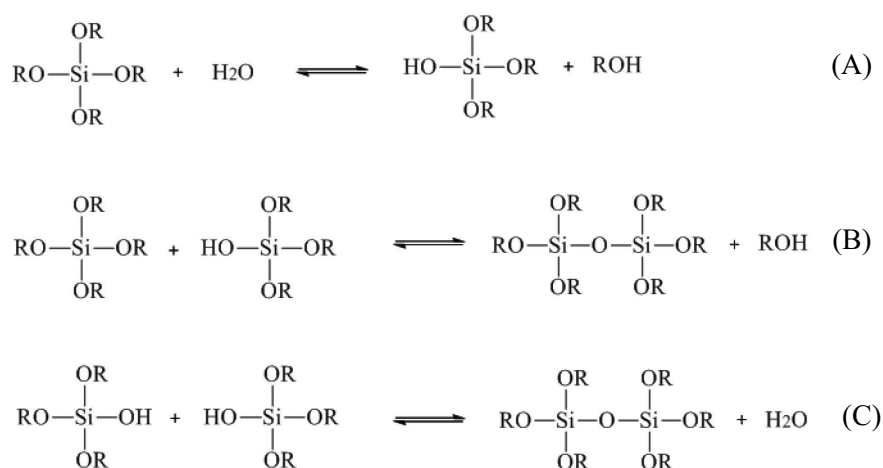


Figure 2.4 Hydrolysis and condensation reactions of the silica precursor.

The formation of silica particles can be divided into two stages, namely nucleation and growth [64]. The growth mechanism of silica has been explained by two models: monomer addition and controlled aggregation [63]. According to the monomer addition model, after the nucleation stage, particle growth takes place on the surface of primary particles by addition of hydrolyzed monomers. In contrast, the aggregation model

elaborates that the nucleation step takes place continuously throughout the reaction and the resulting nuclei aggregate together in order to form dimer, trimer, and larger particles. Eventually, both models lead to the formation of a silica network [63].

Two main approaches have been used for the synthesis of solid SNPs: the Stöber method and reverse microemulsion (Figure 2.5) [51,63,65]. The synthesis of spherical silica particles, with diameters ranging from 50 to 2000 nm, was first reported by Stöber et al. in 1968 [51,66]. This pioneering method involved ammonium hydroxide as a catalyst to hydrolyze and condense the silica precursor in a mixture of ethanol and water.

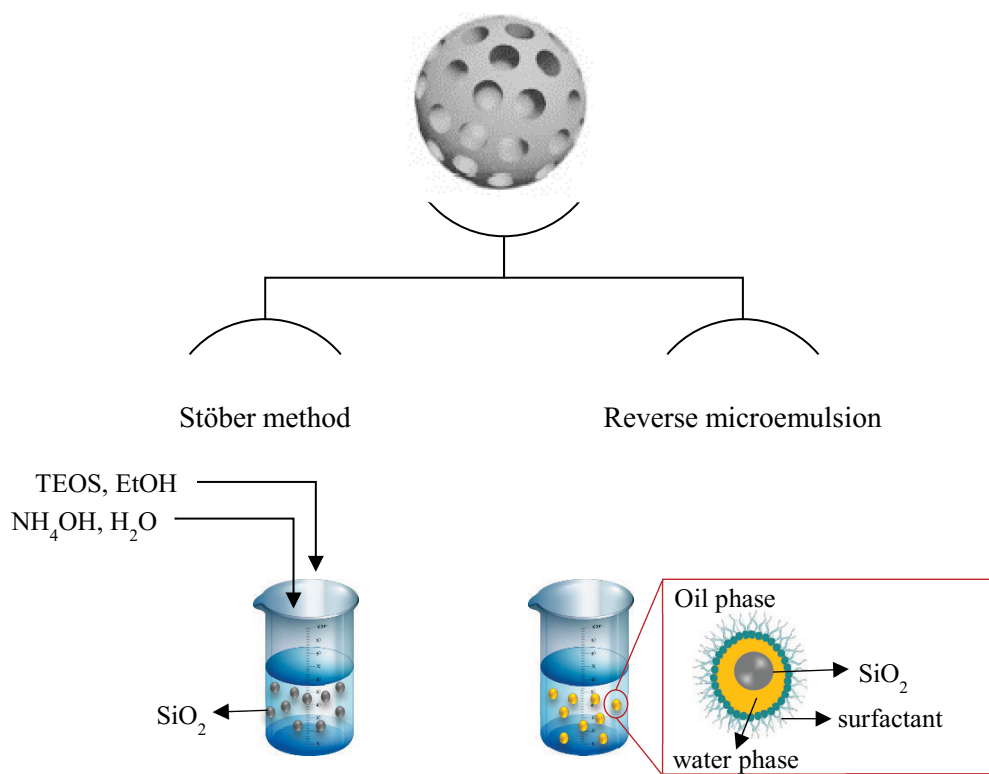


Figure 2.5 Schematic diagram of Stöber method and reverse microemulsion to synthesize silica nanoparticles.

Alternatively, the synthesis of SNPs has been performed by reverse microemulsion, which was reported by Arriagada and Osseo-Asare in 1992 [67]. This synthetic process could, by then, overcome the main limitation of the Stöber method, which was the synthesis of SNPs with uniform size distribution [68]. This method involves the ammonia-catalyzed polymerization of the silica precursor in a water-in-oil

(W/O) microemulsion [59,67]. The reverse microemulsion is transparent: isotropic liquid media consist of nanometer-sized water droplets stabilized by surfactant/co-surfactant molecules, which reduce the interfacial tension between water and oil phases in bulk oil [68,69]. The water droplet serves as a nanoreactor for controlling the kinetics of particle nucleation and growth in SNP synthesis. In this method, therefore, the size and dispersity of the SNPs are limited by the size of the water droplets and can be controlled precisely by the water-to-surfactant molar ratio. The silica precursor cannot be hydrolyzed and then it diffuses into the micelles, which contain water and the catalyst. Consequently, the polycondensation of the hydroxysilicates occur in the micelles only [68]. This method leads to the formation of highly monodisperse and perfectly spherical particles with sizes ranging from 35 to 70 nm [69]. It should be noted that small enhancements in nanotherapeutic penetration can lead to significant improvements in therapeutic effectiveness [70]. Therefore, a precise control of the size, shape, and surface properties of SNPs (Figure 2.6) during the synthesis procedure improves the application of SNPs in biomedical applications [6].

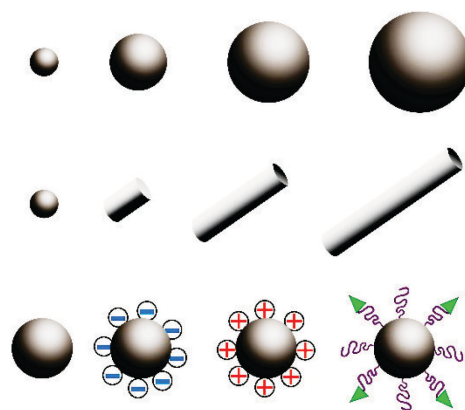


Figure 2.6 Schematic representation of the controlled physicochemical properties of SNPs, based on Tang et al. [6].

2.2.2.1 Size

Particle size plays a key role in biodistribution, blood circulation, tissue penetration, and cellular uptake [71]. Decreasing the size of NPs enhances the delivery by leading to longer circulation times as well as a more rapid transport within tumors.

However, smaller particles possess lower drug and imaging agent payloads [70]. Nanoparticles with diameters below 100 nm have relatively little protein adsorption on their surface, making their blood clearance twice as low as that of the particles with diameters above 200 nm [72].

As already mentioned, SNPs can be prepared by two methods: the Stöber method and reverse microemulsion. The Stöber method was further extended in order to investigate the effect of different parameters on SNP size [73,74]. It was found that the particle size increased by increasing the concentration of the catalyst (ammonium hydroxide) and that of the silica precursor, and by decreasing the amount of water. Moreover, ethanol as a solvent resulted in significantly larger particles than methanol did [74]. Finally, Kim et al. synthesized monodispersed SNPs with excellent control on the size of the particles in a range of diameters from 5 to 450 nm by using the Stöber method [74]. The size of the SNPs can also be manipulated by using the reverse microemulsion approach. The most important factor for controlling the size of the NPs in this method is the micelle size, which is related to the water-to-surfactant ratio. By decreasing the water-to-TritonX-100 molar ratio (R) from 15 to 5, the size of the SNPs increased from 69 to 178 nm [75–77]. Higher values of R result in a larger amount of water available inside the micelle, consequently promoting the nucleation step. Hence, the number of produced nuclei increases and leads to the formation of smaller silica particles [76]. Another important factor is the catalyst concentration, which has a reverse effect on the particle size. By increasing the concentration of ammonium hydroxide, more OH^- ions are provided for TEOS hydrolysis. Therefore, the hydrolysis rate of silica precursor increases and produces more monomer and ethanol, as a by-product. Ethanol can act as a co-surfactant and enhance the intermicellar exchange rate. Enhancing the fluidity of the interface increases the nuclei formation and eventually leads to the formation of smaller silica particles [52]. The concentration of silica precursor and co-surfactant (n-hexanol) has a negligible effect on particle size and the majority of excess TEOS does not participate in hydrolysis and condensation reactions [75].

2.2.2.2 Shape

The shape of NPs can largely effect their blood circulation as well as their tumor penetration behavior [6,71,78,79]. Rod-shaped NPs have shown superior circulation

times (which largely effect the therapeutic efficiency [78]) compared to spherical NPs [80]. Moreover, nanorods seem to perform better than nanosphers in terms of penetration and distribution into tumors and *in vivo* cellular uptake efficiency, owing to the improved transport through pores [70,71].

One of the advantages of silica is its possibility to be fabricated with different morphologies such as spheres and tubes. The synthesis of spherical SNPs has already been explained comprehensively. Silica nanotubes were first synthesized by Nakamura et al. in 1995, according to the Stöber method [81]. Nanotubes were prepared by hydrolysis of TEOS in a mixture of ethanol, ammonia, water, and tartaric acid. Generally, silica nanotubes have been synthesized by using a template as a structure-directing agent, and the selective removal of the template in a post-treatment step such as extraction, chemical reaction, and calcination [82]. Therefore, selecting an appropriate template is a key for a successful template-directed synthesis [82]. Various organic or inorganic templates, can be used for the fabrication of silica nanotubes, such as anodic aluminum oxide [83], multi-walled carbon nanotubes [84], and gel systems [85].

2.2.2.3 Surface property

Biodistribution and the tumor penetrations of NPs largely depend on the surface properties of the NPs [6]. The surface properties of SNPs can be altered, according to the final application, via simple surface modifications [6]. In physiological conditions (pH around 7.4), bare SNPs are negatively charged. Their strong interaction with red blood cell membranes causes hemolysis, making them poorly biocompatible. However, the reason of the hemolytic activity of SNPs is not completely clear [71].

At physiological conditions, the amine groups and methylphosphonate groups have positive and negative charges, respectively [86]. Hence, for example, 3-aminopropyltriethoxysilane (APTES) was used to induce a positive surface charge by bonding chemically to the SNP surface and exposing amine groups [87]. Moreover, 3-(trihydroxysilyl)propyl methylphosphonate can also be immobilized, making the SNP surface negatively charged [86]. The SNPs surface can also be modified with biocompatible polymers, such as PEG, in order to minimize opsonization, which means that plasma proteins (opsonins) tend to cover the surface of SNPs to form a protein corona that can be detected by the reticuloendothelial system, consequently leading to rapid

clearance of the NPs [58,71]. The presence of PEG on the surface of SNPs can reduce protein and cell adsorption onto the SNPs [88]. Moreover, Mansfield et al. reported that the permeation of SNPs through porcine gastric mucosa can be significantly improved by surface modification of the NPs with either poly(2-ethyl-2-oxazoline) (PEOx) or PEG. They also indicated that these two polymers demonstrated comparable abilities to improve the diffusivity of SNPs in mucin dispersions and through the gastric mucosa [27].

2.2.3 Synthesis of fluorescent dye-doped silica nanoparticles

Fluorescent dye-doped SNPs were synthesized for the first time by Blaaderen and Vrij in 1992 [89]. They incorporated fluorescein isothiocyanate (FITC) dye molecules through covalent bonds into SNPs using the Stöber method [89]. For this purpose, APTES was first covalently linked to amine-reactive FITC, and the resulting conjugate was polymerized with TEOS in a mixture of water, ethanol, and ammonia [90]. In general, dye molecules can be incorporated into a silica matrix either by covalent bonding or by non-bonding (i.e. electrostatic interactions) processes by using two synthetic methods: Stöber method and reverse microemulsion (Figure 2.7) [91]. Using the Stöber method for the synthesis of dye-doped SNPs is simple, but the incorporation yield of dye molecules doping in SNPs by non-bonding process is very low and largely depends on the adsorption force between dye and silica precursor. However, the reverse microemulsion method can overcome this limitation and control the concentration of the encapsulated dye molecules in SNPs by using a water-soluble dye [91]. Moreover, the surface modification of SNPs is much easier by reverse microemulsion than by the Stöber method [68,91].

Covalent bonding of the dye molecules with the silicate matrix is preferable because it prevents the dye molecules from leaking out of the silica matrix. For this purpose, dye molecules with functional groups are required to react with a functionalized alkoxide. The modified dye can be further hydrolyzed and condensed with the silica precursor to form dye-doped SNPs [75]. Various succinimide ester- or isothiocyanate-modified dye molecules, such as tetramethylrhodamine, rhodamine B, and Cyanine5, are commercially available, and they easily react with APTES and consequently be covalently bonded to the silica matrix [75]. This emphasizes the limitation of the chosen dye and consequently makes the non-bonding approach interesting [91]. Highly

concentrated fluorescent dye-doped SNPs can be successfully prepared by reverse microemulsion. The hydrophilic fluorophores penetrate into the micelle, in which hydrolysis and condensation of the silica precursor take place, leading to the physical encapsulation of dye molecules into the silica network [91]. It should be noted that polar dye molecules are used in the reverse microemulsion method in order to increase the electrostatic attraction of the dye with a negatively charged silica matrix [92]. For example, inorganic dye molecules such as tris(bipyridine)ruthenium(II) chloride (Ru(bpy)) can simply get entrapped in the silica matrix by using reverse microemulsion [52,93]. The reported leakage of dye molecules that were encapsulated via this method is negligible due to the presence of strong electrostatic attraction [92]. Some photostable organic dye molecules have hydrophobic properties [94]. The incorporation of hydrophobic dye molecules into the hydrophilic structure of a silica matrix requires specific modifications of either the silica or the dye. One simple and effective approach to enhance the solubility of the hydrophobic dye molecules is to link hydrophilic dextran to these dye molecules [75].

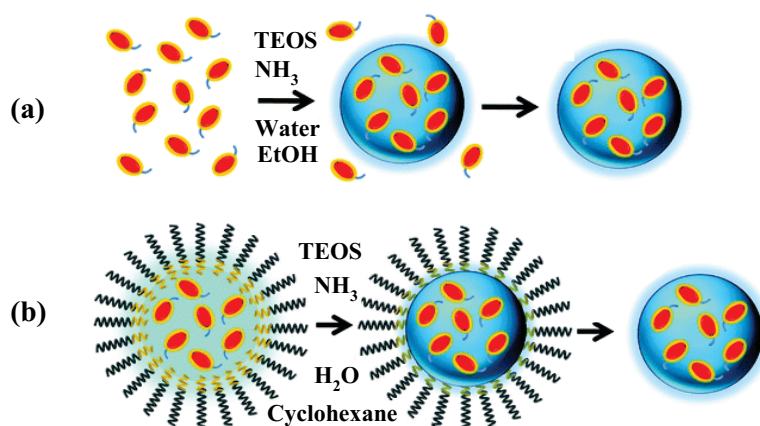


Figure 2.7 Schematic representation of two synthetic approaches to fabricate dye-doped silica nanoparticles: **(a)** Stöber method and **(b)** reverse microemulsion method [5].

Fluorescent-doped SNPs can be accumulated in tumor tissues through two different pathways: either passive or active targeting. The former pathway refers to the potential accumulation of NPs in the absence of targeting ligands [71]. Nanoparticles target tumors by using the enhanced permeability and retention (EPR) effect, which was

first reported by Matsumura et al. in 1986 [40,95]. The EPR effect arises from the rapid growth of tumors, which leads to the formation of new blood vessels in order to supply oxygen and nutrients for further proliferation. These imperfectly formed blood vessels possess leaky epithelia with fenestrations between 200 and 2000 nm depending on the types of tumors and their locations. These fenestrations cause an increase of the permeability of the vessels that surround tumors, and they enable the nanoparticles to extravasate and consequently accumulate in the tumor [71]. The accumulation efficiency largely depends on the physiochemical properties of nanoparticles including size, shape, and surface charge [71]. For example, particles of certain sizes accumulate in tumor sites rather than in normal tissues, owing to the abnormal newly formed blood vessels of tumor tissues [40]. Active targeting has the potential to enhance the accumulation efficiency on NPs at tumor sites through NP surface modification with various types of targeting ligands, such as aptamers, antibodies, peptides, and folic acid, that have selectivity and affinity toward the relevant tissues [40,71]. The imaging agents inside the selective silica particles can give the accurate location of the tumor tissue [40].

2.3 Polymers in biomedical applications

Nanocarriers interact massively with their surrounding environment, such as endothelium vessels, cells, and blood proteins, leading to their rapid removal from the circulation by the mononuclear phagocyte system. In order to address this problem, new research indicate that stealth nanocarriers can be obtained by polymeric coating [96]. “Stealth” is defined as a property of a polymer/particle which allows the latter to avoid clearance by the body and remain in circulation for a longer time. Various polymers have been used in medicines, such as PEG, polysialic acid (PSA), polyglutamic acid (PGA), polylactic and polyglutaric acid (PLGA), polyvinylpyrrolidone (PVP), and polydextrans [97]. Among these polymers, PEG has gained the most interest in delivering proteins, aptamers, and small molecule drugs [97]. It is also widely used as a shell for NPs in biomedical applications that require long circulation times in blood, since PEG reduces the degree of opsonisation [98]. Moreover, PEGylation of SNPs can enhance penetration since the “stealth” properties of PEG can reduce the adhesive interactions of NPs with collagen fibers in the stroma [27]. However, possible interactions of PEG with the immune system and its possible degradation under stress have been reported [21,25].

Recently, specific antibodies against PEG were detected in the serum of patients who had been treated with PEG-asparaginase and PEG-uricase. Based on these findings there is a clear need for alternative materials that can replace PEG without showing similar side effects [97].

Poly(2-methyl-2-oxazoline) (PMeOx) and Poly(2-ethyl-2-oxazoline) (PEtOx) have been proposed for this challenge since they meet several requirements for biomedical applications, such as hydrophilicity, biocompatibility, versatile end group chemistry, chemical stability [26], and a similar “stealth” behavior to that of PEG [27]. Mansfield et al. reported that these two polymers, PEG and POx, have comparable abilities to enhance the diffusivity of SNPs in mucin dispersions and through the gastric mucosa [27]. In addition, POx has some advantages compared to PEG. For example, regarding the synthesis procedure, PEG involves a complex synthetic process and toxic reactants while polymerization of 2-oxazoline is relatively simple [27]. Moreover, PEG suffers from bioaccumulation and can form vacuoles in some organs whereas POx does not bioaccumulate and it degrades under specific conditions [27]. The low drug capacity of PEG chains is another disadvantage since it can only be functionalized by the end group. However, POx can be easily modified with side-chain functionalities and monomers that bear a functional group, possibly affecting its solubility and allowing chemical coupling with targeting moieties [99]. Therefore, considering the limitations of PEG, POx can be a superior alternative in medical applications. This polymer is suitable to be designed as a polymer therapeutics in different types such as polymeric micelle for drug delivery, POx-drug/-protein conjugation, and gene delivery [27].

2.3.1 Poly(2-oxazolines)

Oxazolines are five-membered heterocyclic compounds with an endo-imino ether (-N=C-O-) group. Among the three possible structural isomers of oxazoline, namely: 2-oxazoline, 3-oxazoline, and 4-oxazoline, 2-oxazoline is the most well-known monomer in organic and polymer chemistry [100]. Kagiya et al. reported in 1966 the first cationic ring opening polymerization (CROP) of 2-oxazoline [101,102]. The main driving force for the CROP of 2-oxazoline is not the relief of ring strain as in most ring-opening polymerizations, but it is the isomerization of the imino ether to the more thermodynamically stable amide group [103].

Figure 2.8 shows the mechanism for the CROP of 2-oxazoline, which consists of initiation, propagation, and termination, where an electrophile-like alkylating agent (IX) is used as an initiator. Initiation starts with the nucleophilic attack of the free electron pair of the nitrogen atom of the 2-oxazoline monomer onto an electrophilic initiator, and forming an oxazolinium species. Then, another monomer nucleophilically attacks the oxygen atom of the newly formed oxazolinium species, causing the ring to open by isomerization of the imino group to N-acyl group. In the propagation upon further monomer additions, another monomer nucleophilically attacks the oxygen atom of the oxazolinium to open the ring, while there still is an active propagating group at the chain end. The polymerization is continued until either all the monomers are consumed or a nucleophile (the terminating agent) is added to terminate the reaction [100,104].

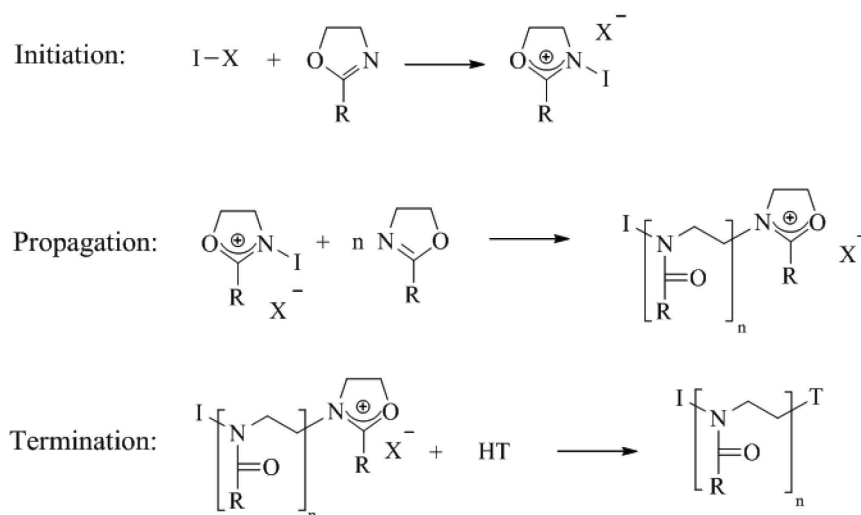


Figure 2.8 General polymerization mechanism of cationic-ring opening polymerization of 2-oxazolines.

The CROP of 2-oxazolines has been accomplished by using various initiators including Lewis acids (such as boron trifluoride diethyl etherate [BF₃-OEt₂]) [105], alkyl esters (tosylates and triflates), alkyl halides (chloride, bromide, iodide), and acetyl halides [24]. It is also important to note that alkyl iodide initiators are usually converted from chlorides or bromides to iodide by using co-initiators such as sodium iodide and potassium iodide [24,106]. Depending on the nature of the initiator, when an initiator generates a stronger nucleophile, polymerization precedes a covalent propagation species owing to the instability of the propagating 2-oxazolinium ion (Figure 2.9). If the

nucleophilicity of the monomer and the counter anion of the initiator are comparable, both mechanisms (cationic or covalent) can coexist [100,102]. Both reaction processes, involving two different types of species (ionic or covalent), lead to well-defined polymer chains with narrow average molecular weight distributions [102,107].

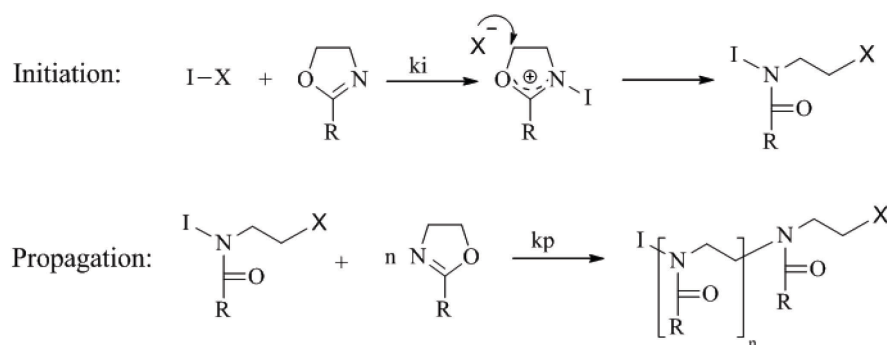


Figure 2.9 Polymerization mechanism of 2-oxazoline containing a covalent propagation species.

The polarity of these polymer chains can easily be modified by changing the length of the 2-oxazoline alkyl group. Hence, hydrophilic polymers are obtained when methyl and ethyl groups are used, and hydrophobic polymers are obtained when longer side chains are used. Generally, the synthesis of well-defined POx with appropriate functional groups and a controlled molecular weight is important for various applications. It should be noted that side-reaction may take place during the polymerization of 2-oxazoline owing to the reactive cationic species. Litte at al. reported in 1975, that a transfer reaction can occur by proton abstraction of the nitrogen atom of the monomer from the R-carbon atom of the propagating species. As shown in Figure 2.10, an uncharged polymer with a C=C double bond and an activated monomer with a positively charged monomer are formed [108]. Once the chain transfer reaction has taken place, the dormant ene-terminated POx chain can act as a nucleophilic species for chain coupling and the molecular weight consequently increases. However, it is less nucleophilic than the monomer and it reacts more slowly [109]. If chain transfer and coupling do not take place, polymerization proceeds in a “controlled/living” manner, which allows the synthesis of copolymers or even more complex architectures for further applications.

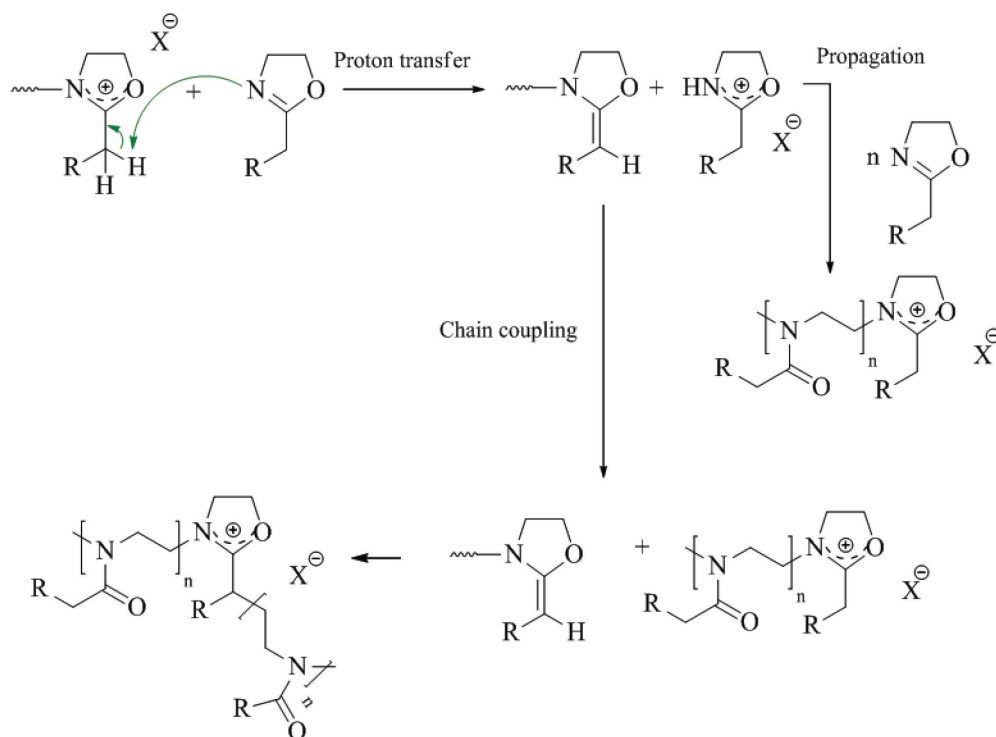


Figure 2.10 Mechanism of chain transfer and chain coupling.

2.3.2 Functionalization of Poly(2-oxazolines)

The functionalization of POx is essential as it allows the development of innovative materials based on this polymer [24]. One of the main advantages of this polymer is that the functional groups can be introduced into the polymer chain by using functional initiators, functional terminating agents, or 2-R-2-oxazolines, where R represents a functional group (Figure 2.11) [24,100]. However, the functional group of the initiator or monomer may interfere with the CROP of 2-R-2-oxazolines and consequently affect the yield and the molecular weight. To address this problem, appropriate protecting groups can be utilized [24]. These protecting groups reduce or remove the nucleophilicity and basicity of the reactive sites by inducing steric hindrance and/or electronic effects. The cationic character of the polymerization process is strongly influenced by the nucleophilic reagents present in the reaction medium such as residual water and by-products of the initiator [24].

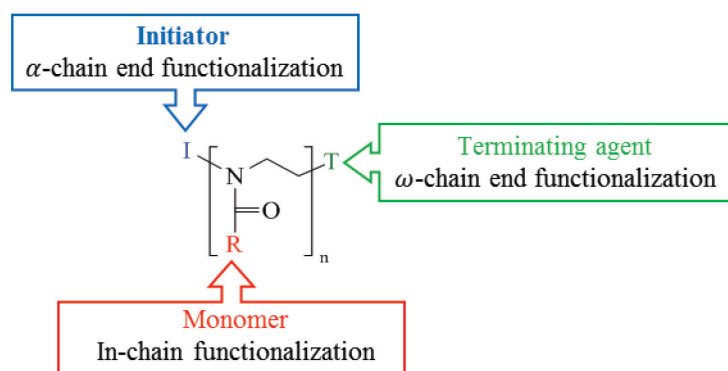


Figure 2.11 Possible ways to synthesize functionalized poly(2-oxazoline)s.

Various initiators have been reported for the CROP of 2-oxazolines [110,111]. In order to synthesize α -chain end-functionalized POx, a wide variety of initiators with protected and unprotected functionalities can be used. Figure 2.12 shows some functionalized initiators, which offer a variety of functionalized POx chains. Initiators with unprotected functionalities which have been reported for the polymerization of 2-oxazolines include propargyl *p*-toluenesulfonate (**I1**) [112,113], 3-butynyl toluene-4-sulfonate (**I2**) [113], 9-(chloromethyl)anthracene (**I3**) [114], and 4-chloromethylstyrene (**I4**) [115]. Most functionalized-POx prepared by these designed initiators were involved in post-polymerization reactions and consequently led to more complex structures. The alkyne-functionalized initiators (**I1** and **I2**) can be used for alkyne-azide “click” reaction [112,113]. The post-polymerization reactions of POx synthesized by **I3** and **I4** were a Diels-Alder reaction and polymerization of the vinyl units, respectively [114,115]. Moreover, initiators with protected functionalities have also been reported, since the initiator functionality is suspected to interfere with the polymerization process. For example, Einzmann et al. synthesized functionalized POx using 2,2-dimethyl-(4-trifluoromethylsulfonyloxymethyl)-1,3-dioxolane (**I5**) as an initiator. The functional polymer chains were deprotected and subsequently used for diacylation with dodecanoyl chloride [116]. Amine-functionalized POx can be prepared by using the bifunctional initiator *N*-(2-(*p*-toluenesulfonyloxy)ethyl)phthalimide **I6**, and by converting the terminal phthalimide group into a primary amine group [111,117].

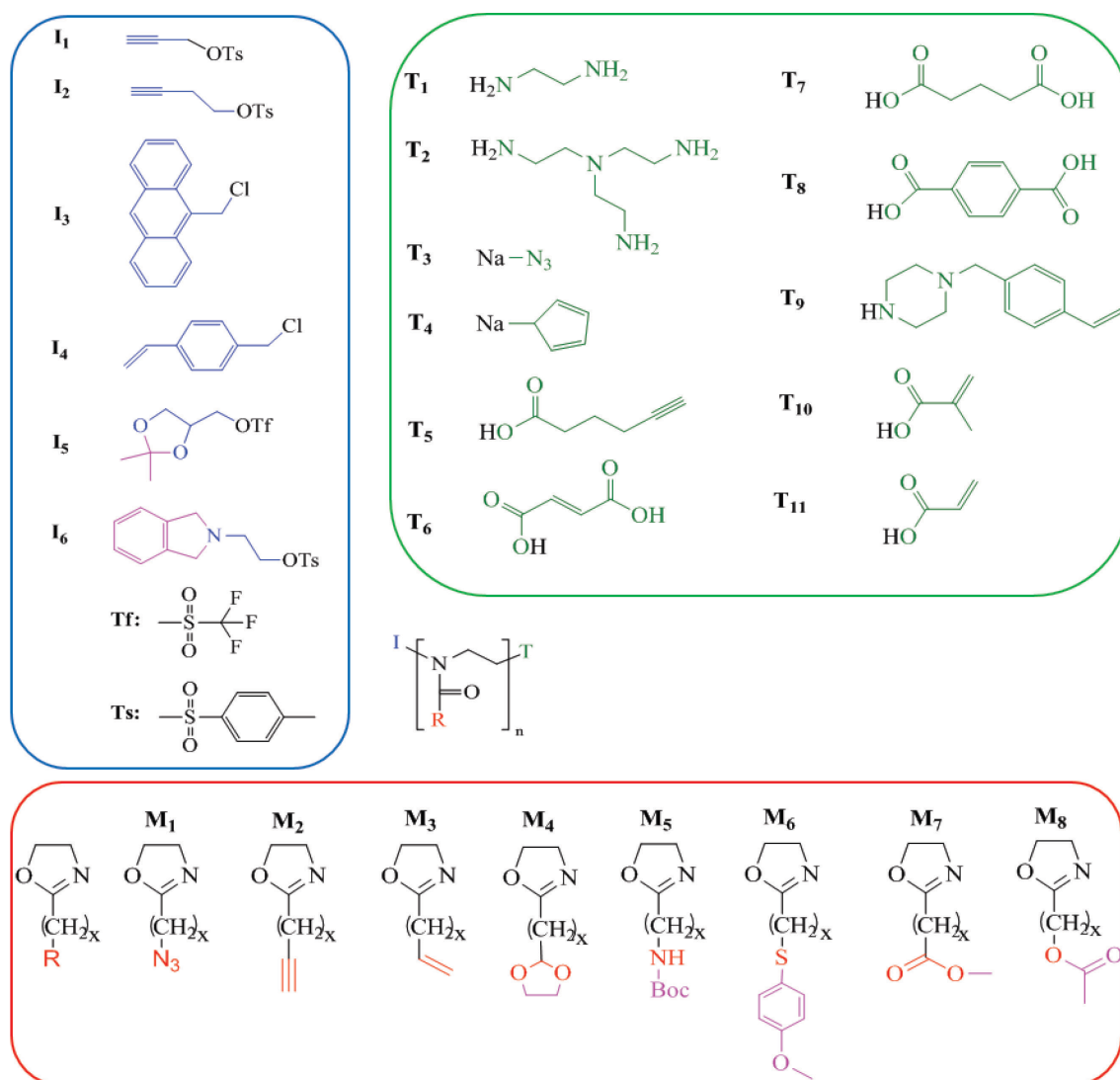


Figure 2.12 Functionalized POx using functionalized initiator (I), monomer (R), or terminating agent (T).

Synthesizing a monomer that bears a reactive group and directly polymerizing the functionalized monomer is the second option to synthesize functionalized POx chains. 2-oxazoline monomers with unprotected functionalities can be prepared and polymerized via CROP of 2-oxazoline monomers that bear various groups such as azide groups (2-(5-azidopentyl)-2-oxazoline, **M1**) [118], alkyne groups (2-(pent-4-ynyl)-2-oxazoline, **M2**) [119], and alkene groups (2-(3-butenyl)-2-oxazoline, **M3**) [120] (Figure 2.12). **M1** and **M2** can be further modified via alkyne-azide “click” chemistry [118,119]. Moreover, the “thio-click” reaction can be performed as a post-modification reaction for **M3** [120]. As with a functionalized initiator, if the monomer that bears a functional group can interfere with the CROP process, the group should be protected to avoid any side-reaction between

the oxazolinium species and the R group in the monomer, R being, among others, an alcohol, carboxylic acid, amine, aldehyde or thiol. 2-Oxazoline monomers with protected aldehyde, such as 2-[3-(1,3)-dioxolan-2-ylpropyl]-2-oxazoline (**M4**) [121], have also been prepared. After polymerization, the 1,3-dioxolan side function can be converted to the corresponding aldehyde, which can react with an amino-oxy group-containing compound in a chemoselective [121]. In addition, POx with pendant amino groups can be synthesized via a protected monomer (2-(N-Boc-5-aminopentyl)-2-oxazoline, **M5** [122]) which, after deprotection, is able to react with various isocyanate compounds such as a fluorescent dye (e.g, fluorescein isothiocyanate, FITC) [122]. 2-Oxazoline monomer with a protected thiol group, 2-(4-methoxybenzylsulfanyl)ethyl-2-oxazoline (**M6**) [123], was synthesized by Cesana et al.. After polymerization and deprotection, pendant thiol groups can react with activated double bonds, including double bonds in maleimide, acrylamide and acrylester, for further modification [123]. 2-Oxazoline monomers were synthesized with ester functionalities (**M7** [124]) and carbomethoxy functionalities (**M8** [125]) in their side chains, which could be converted to hydroxyl groups after deprotection of the polymers [111].

To functionalize the ω -chain end, the CROP of 2-oxazoline can be terminated via the addition of a nucleophilic species that possesses a greater electron-donating capacity than the monomer does. Various terminating agents can be used, their choice depends on the desired end terminal group for the post-polymerization reaction. For example, when a hydroxyl group is required in the polymer chains, a methanolic potassium hydroxide solution or a 5% sodium carbonate aqueous solution can be used as a terminating mixture [97]. Moreover, amino-functionalized POx can be prepared by using ethylenediamine (**T1**) [126] or N,N-bis(2-aminoethyl)ethylenediamine (**T2**) [127]. Clickable functions were introduced by terminating the CROP of 2-oxazoline monomers with sodium azide (**T3**) [114], sodium cyclopentadienide (**T4**) [128], or hexynoic acid (**T5**) [129]. ω -chain end functionalization of POx with carboxylic acid were achieved by using maleic acid (**T6**) [130], glutaric acid (**T7**) [131], or terephthalic acid (**T8**) [131]. N-(4-vinylbenzyl)piperazine (**T9**) can be used as a terminating agent to introduce vinyl group to POx chains, required for the polymerization of vinyl units [115]. Terminating agents such as methacrylic acid (**T10**) and acrylic acid (**T11**) lead to the formation of POx with methacrylic and acrylic end groups [111,131].

2.4 Polymer chemistry for surface modification

Coating material surface with polymers is an efficient way to modify the physicochemical characteristics of these surfaces, as it offers better and more customized mechanical properties than coating with low molecular weight compound does [132]. Various approaches can be employed for the immobilization of thin layers of polymers on solid particles, depending on the required surface properties [133]. As shown in Figure 2.13, surface modification with polymer chains can be fabricated by physisorption or chemisorption [134].

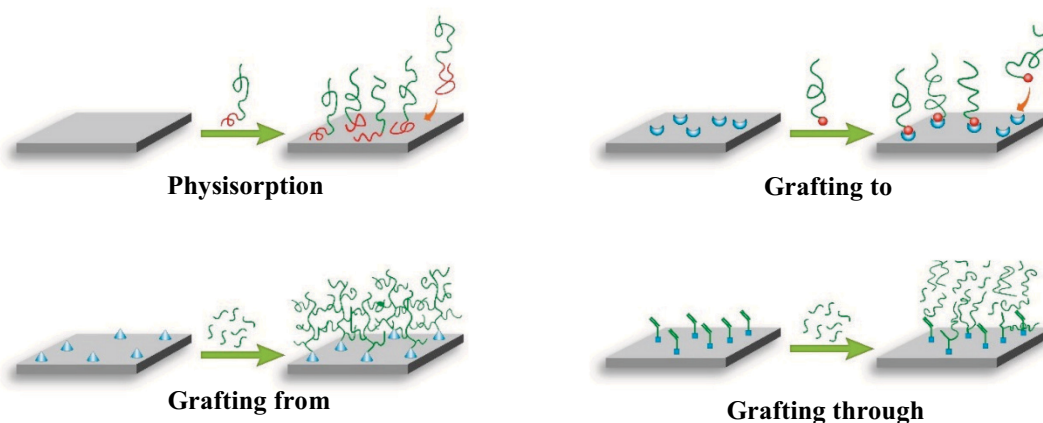


Figure 2.13 Different strategies for the surface modification with a polymer, based on Banerjee et al. [19].

Physisorption involves the adsorption of polymer chains with “sticky” segments, via a noncovalent interaction between the polymer chains and the material surface [132,135]. Via this approach, polymer coatings are typically prepared by means of spin casting or solution dip-coating methods [132]. Because physical adsorption is reversible and the obtained properties are therefore gradually lost over time, this approach is not favored [135]. Chemisorption is more interesting since the polymer chains are covalently linked to the material surface, thereby providing a greater stability of the obtained coating [13,14]. In general, covalently attached polymer layers can be obtained by three main approaches, namely “grafting to”, “grafting from”, and “grafting through” (Figure 2.13) [19]. These methods have their own advantages and disadvantages, which will be explained in detail in subsequent sections.

2.4.1 “Grafting to” approach

The “grafting to” approach involves the chemical reaction of prefabricated functionalized polymer chains with complementary functional groups on the surface of various substrates such as flat plates, fibers, porous structures, and NPs [136]. The major advantages of this approach are its simplicity and the possibility to thoroughly characterize the preformed polymer chains via various methods. Therefore, well-defined polymer chains with a narrow molecular weight distribution can be grafted to material surfaces and lead to the synthesis of well-defined brushes [136]. However, this approach suffers from the relatively low grafting density and thickness of the obtained polymeric layer owing to steric hindrance from previously attached chains on the surface, which hinder the diffusion of additional polymer chains to the reactive sites [135]. In other words, “grafting to” is a self-limiting process [136].

Gold wafers and Silicon (covered with a silicon oxide layer) wafers are two frequently used substrates with the “grafting to” approach [136]. Thiol chemistry is the most widely used way to attach polymer chains that contain thiol (-SH) groups, to gold surfaces [136]. Gold surfaces can be modified in a one-step process if thiol-containing polymer chains are used, such as thiol-functionalized polyethylene glycol (PEG-SH) [137], thiol-functionalized poly(N-isopropylacrylamide) (PNIPAM-SH) [138], and thiol-functionalized polystyrene (PS-SH) [139]. For silicon oxide surfaces, silane chemistry and copper(I)-catalyzed azide-alkyne cycloaddition reaction, “click” chemistry, are widely used for attaching silane-functionalized polymer chains to the surface via a “grafting to” approach by using one- or multi-step processes, (Figure 2.14) [134,136]. However, various multi-step processes can be used if further modification of the surface or the polymer chain is required for obtaining suitable functional groups for the grafting procedure. For example, the reaction between an epoxy-functionalized silica surface, which can be prepared by silanization with 3-glycidoxypropyl trimethoxysilane (GPS), and a carboxy-functionalized polymer [140] or amino-functionalized polymer [141], can be used for the immobilization of polymer chains.

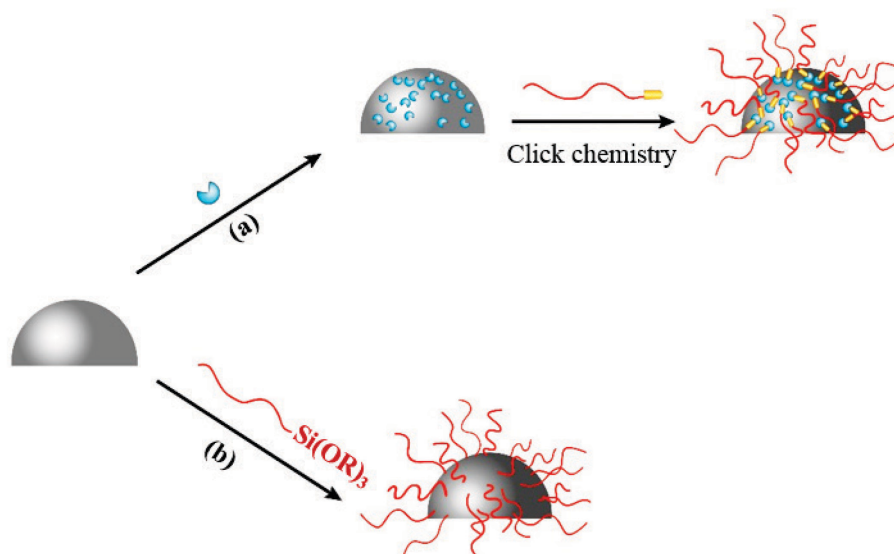


Figure 2.14 Schematic representation of (a) copper(I)-catalyzed azide/alkyne- cycloaddition for NP-surface modification via the click chemistry (b) the silane coupling reaction between hydroxyl groups on the surface of SNPs and silane-functionalized polymer chain, based on Achilleos et al. [134].

“Click” chemistry is a promising method for grafting polymer chains to the particle surface [142–145]. This method is highly efficient and high reaction temperatures can be avoided. In this method, the azide- or alkyne-functionalized polymer chains are grafted to the correspondingly functionalized substrates/particles (Figure 2.14-a) [145]. “Click” chemistry is widely used for the modification of surfaces by polymer chains. For example, Ranjan et al. used “click” chemistry in order to graft alkyne-functionalized polyacrylamide to azide-modified SNPs [144]. Therefore, upon completion of the “click” chemistry reaction, CSNPs were prepared with 0.31 chains/nm² of polyacrylamide [16,144]. The synthesis of fluorescent SNPs with a PEG coating and encapsulated silver clusters using “click” chemistry was reported by Tissandier et al. [146]. Polysiloxane shells with encapsulated silver clusters (Ag@SiO₂ NPs) were prepared by reverse microemulsion and the obtained SNPs were further functionalized with alkyne groups using O-(propargyloxy)-N-(triethoxysilylpropyl)carbamate. Next, azide-functionalized PEG chains were clicked to the alkyne-functionalized SNPs to form hybrid NPs [146]. High grafting densities were obtained by clicking alkyne-functionalized poly(3-hexylthiophene) with azide-functionalized SNPs (0.5 chains/nm²) [147] and by clicking

alkyne-functionalized poly-L-lysine with azide-functionalized SNPs (1.0 chains/nm²) [148].

One of the most efficient methods for the immobilization of polymer chains on the surface of silica-based particles/substrates is the reaction between polymer chains that contain a silane-coupling agent and hydroxyl groups on the silica particle surfaces (Figure 2.14-b) [149]. The major advantages of this method are its high efficiency and its easy process since it does not require prior surface modification of the silica substrates. Huang et al. used a combinatorial approach based on addition-fragmentation chain transfer (RAFT) polymerization and a silane coupling reaction for the fabrication of silica-polymer hybrid particles. Trimethoxysilane-functionalized homopolymers and a series of functional di-, tri-, and tetra-block copolymers were first synthesized by RAFT polymerization using S-methoxycarbonylphenylmethyl S'-trimethoxysilylpropyltrithiocarbonate as a RAFT agent. Then, the obtained silane-functionalized polymers were attached to the surface of SNPs by silane coupling reaction. The grafting density of various polymeric chains on the surface of SNPs found between 0.018 and 0.076 chains/nm² [149]. Moreover, Rahman et al. prepared trimethoxysilane-functionalized polymers from four octadecylated L-phenylalanine-derived polymerizable monomers by using 3-mercaptopropyltrimethoxysilane, as a terminating agent. In the next step, the prepared polymers were immobilized on the surface of SNPs by silane coupling reaction [150].

2.4.2 “Grafting from” approach

The limitations of physisorption and “grafting to” approaches can be avoided in the “grafting-from” approach, which involves surface-initiated polymerization [31,151,152]. More precisely, the “grafting from” approach involves the formation of an initiator layer on the substrate surface followed by polymerization of a monomer directly from the surface. The “grafting from” approach, compared to the “grafting to” approach, presents the advantages of achieving a higher grafting density of the organic shell and providing a better control on the thickness of the polymer brushes [135,144,151]. A greater grafting density was achieved via the “grafting from” approach because the steric barrier to incoming polymers imposed by the *in situ*-grafted chains does not affect the

accessibility of smaller molecules, such as monomers, to the active initiation sites [135]. This approach requires either a bifunctional initiator, with one function to be immobilized on the substrate surface and another function to initiate the polymerization, or an initiator linkage [153,154].

Regarding characterization of the formed polymer chains on the substrate surfaces, the polymer chains are required to be degrafted either by direct cleavage or by dissolution of the substrates. For example, SNPs can be etched by treating with a hydrofluoric acid solution to recover the polymer chains [135]. It should be noted that degrafting by direct cleavage requires the presence of easily cleavable groups. After cleavage/etching, the isolated polymer can be further characterized in order to determine its molecular weight, molecular weight distribution, and composition by using analytical techniques [135]. Although finding an appropriate initiator and degrafting the polymer chains from the substrates make this approach complicated, it is the most promising approach for the synthesis of a dense polymeric shell on NP surfaces [155]. Using silica as a core has several advantages: the surface hydroxyl groups enable the facile attachment of appropriate initiating moieties for the “grafting from” approach, the silica core can act as a sacrificial core for the fabrication of a hollow polymer sphere, and the grafted polymer chains can be characterized [134,156]. The “grafting from” approach leads not only to the formation of CSNPs with high grafting densities but also to the fabrication of hollow polymer spheres with uniform size and good dispersibility in aqueous or organic media by removing the core. The structural integrity of the hollow capsule is obtained by cross-linking the tethered polymer chains. This unique class of materials has gained much interest in the field of medicine owing to the potential to be used as a product encapsulator for controlled release of drugs, dyes, enzymes, etc. [134,156]. For example, Mandal et al. reported the synthesis of hollow polymer microspheres with various shell thicknesses by coating silica particles with poly(benzyl methacrylate) via surface-initiated atom transfer radical polymerization (ATRP). The silica templates were removed by using hydrofluoric acid etching after cross-linking the tethered polymer chains with ethylene glycol dimethacrylate [156].

The choice of a suitable system and technique leads to a better control of the functionality, density, and thickness of the polymer brushes. Various polymerization methods can be used for this approach including anionic polymerization [157], cationic polymerization [158], ring-opening metathesis [159], and living/controlled radical polymerization methods such as ATRP [160,161], nitroxide-mediated polymerization

(NMP) [162], and RAFT polymerization [163,164]. Among these methods, controlled radical polymerization has been shown to be the most effective one for the surface modification of NPs, owing to the versatility of suitable monomers, the mild reaction conditions, and the uniformity of the obtained molecular weight of the polymer chains [154]. Wu et al. comprehensively reviewed the surface-initiated controlled radical polymerization from SNPs [154].

As it was mentioned, greater polymer grafting densities can be achieved by “grafting from” processes than by “grafting to” processes. This can be shown by synthesizing CSNPs using both methods and comparing them. Ranjan et al. synthesized polystyrene-coated SNPs using “grafting to” and “grafting from” approaches. The obtained polymer grafting density increased from 0.29 to 0.68 chains/nm² by replacing the “grafting to” process with a “grafting from” one [142]. Moreover, Rahman et al. fabricated silica-L-phenylalanine composites by several grafting processes. Thermal gravimetric analysis (TGA) results indicate greater mass loss for hybrid particles prepared by surface-initiated polymerization (35.2 %) than by a “grafting to” approach (17.5 %), compared to bare silica particles [150].

2.4.3 “Grafting through” approach

A “grafting through” strategy can also be used for the modification of substrate surfaces with polymer chains. This approach involves the modification of substrate surfaces with a macromonomer that contains polymerizable units, which can be copolymerized with the other monomers in the surrounding medium [15–18]. In other words, the growth of polymer chains is initiated in solution. During the propagation step, a surface-bound monomer unit can be occasionally integrated into the growing polymer chains, leading to a permanent attachment of the polymer chains. Polymer chain growth then proceeds as free or surface-attached units are added to the growing polymer chain [165,166]. In this approach, the synthesis and immobilization of the polymer simultaneously take place in a one-pot system [18]. This makes “grafting through” relatively convenient, although, it requires the synthesis of an appropriate monomer to functionalized the surface [167].

In the “grafting through” approach, an increasing number of polymer chains are attached to the surface during polymerization. This makes an effective barrier to the

penetration of additional polymer chains from the solution and therefore leads to a decrease of the attachment reaction rate. Hence, the attachment process is significantly dominated by the “grafting-to” step, which is the limiting factor. This process provides grafting densities that are close to those obtained by a “grafting to” approach, which are much lower than in surface-initiated polymerization. The most significant difference of this method with the “grafting-to” approach is found after the initiation step, in which the growing polymer chains are still short and only have a few repeating units. Such short chains can penetrate the polymer layer and bind to the reactive surface monomers, leading to further growth of the attached polymer chains [165]. As a consequence, the self-limitation of the attachment process in “grafting through” is not as strict as in “grafting-to” and a slow increase in the grafting density can be observed [15,165].

2.4.4 Other approaches

Apart from the three mentioned well-known methods that have been comprehensively explained in previous sections, a number of other methods have been reported for the modification of particles/substrates. Some of these methods were designed according to the specific properties of polymer chains. Regarding surface modification with POx, Volet et al. synthesized host layers that consist of β -cyclodextrin polymers (P β CD) on the surface of silica particles, which enabled the adsorption of alkyl end-capped PMeOx by a host-guest interaction (Figure 2.15-a). In this case, an alkyl group was introduced into POx chains by using a functionalized initiator, because alkyl groups play an important role due to their affinity toward β -cyclodextrin cavities [21]. Photoimmobilization is another strategy to immobilize polymer chains on a silica surface (Figure 2.15-b). First, a benzophenone unit (photoreactive group) is immobilized on the surface of silica substrate/particle. Benzophenone absorbs UV light around 345 nm; the resulting triplet is biradical in nature and can react with groups in its vicinity [168,169]. This method has been used for the immobilization of a wide variety of polymers, such as POx, chitosan, PEG, and poly(ethyleneimine) [169]. Moreover, Ogoshi et al. reported the synthesis of colloidal POx-silica hybrids in aqueous solution based on the strong hydrogen bonding interactions between amide groups of POx and silanol groups. It should be mentioned that this method leads to the fabrication of colloidal NPs rather than surface modification [170].

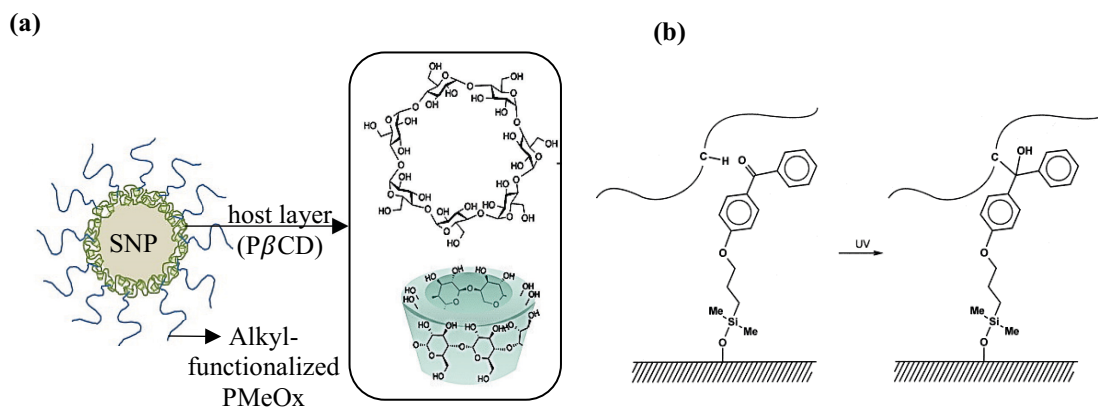


Figure 2.15 Schematic description of (a) SNP coated with β -cyclodextrin polymer (P β CD) as a host layer and alkyl-functionalized PMeOx as a guest layer [21,171], (b) photochemical attachment of POx chains to silica surfaces by illumination of polymer-covered monolayers of a benzophenone derivative [168,169].

Chapter 3. Overview of Project Objectives

The broad objective of the proposed project was to synthesize novel PMeOx-coated SNPs as an alternative system to PEGylated NPs. Two well-known approaches were used to form such hybrid nanoparticles, namely “grafting to” and “grafting from”. Moreover, a new method was introduced, which is the combination of these approaches. A central objective of this project was to synthesize these novel CSNPs with high polymer grafting density. Each method was therefore studied separately, and the obtained results were compared. In order to achieve the general objective of this research, several sub-objectives were formulated as follows:

- The synthesis and characterization of PMeOx-coated SNPs utilizing the “grafting to” approach by using two different methods, namely click chemistry and silane coupling reaction, which required the synthesis of PMeOx chains with appropriate functional groups.
- The development of a protocol for the fabrication of PMeOx-coated SNPs using a surface-initiated polymerization technique.
- The design of a more time-efficient method for the fabrication of PMeOx-coated SNPs through the in situ immobilization and polymerization of MeOx.

Chapter 4. Synthesis of Polyoxazoline-Silica Hybrid Nanoparticles via “Grafting to” Approach*

** Part of this chapter has been published in Journal of Polymer Chemistry, 7 (2016) 1271-1280*

4.1 Introduction

There has recently been an increased interest in the fabrication of core-shell nanoparticles (CSNPs) containing inorganic core and polymeric shells. These hybrid nanoparticles are well-known for designing novel materials with the capability of overcoming the limitations of their inorganic core. Silica nanoparticles (SNPs) are one of the most widely used types of nanoparticles in nanomedicine, and they have excellent biocompatibility and hydrophilicity [6,9]. However, a major challenge is related to their surface properties due to the serum protein adsorption, which may eventually affect the colloidal stability of the particles and their toxicity depending on the serum content [11,12]. This problem can be addressed with the easy surface modifications of SNPs [9]. Poly(2-methyl-2-oxazoline) (PMeOx) can be introduced to the surface of SNPs since it combines properties such as hydrophilicity, biocompatibility, and versatile end group chemistry [21].

Various approaches for the surface modification through polymer chains have been reported including “physisorption”, “grafting to” and “grafting from”, and “grafting through” [31,151,152], which have advantages and disadvantages. Among them, the “grafting to” technique, which is based on the immobilization of the functionalized polymer chains on the surface of the modified particles/substrates [16], has gained much attention due to simplicity and the facile characterization of the pre-fabricated polymer chains [144,151]. However, it suffers from low grafting density, particularly when the molecular weight of the polymer chains increases due to an increase in steric hindrance [172].

The “grafting to” approach is also well-known for immobilizing POx on the surface of silica particles/substrates. There has been a number of studies on introducing various silane groups to POx chains in the termination step (Figure 4.1), including (3-aminopropyl)trimethoxysilane (APTMS) [173], (3-aminopropyl)triethoxysilane

(APTMS) [174], (3-mercaptopropyl)trimethoxysilane (MPTMS) [175], and (4-aminobutyl)dimethylethoxysilane (ABDMMS) [155], which lead to the formation of silane-functionalized POx chains of **FP.1-FP.4**, respectively. Polymer chains can be grafted to the surface through a co-condensation process. Recently, Eckardt et al. also synthesized PEtOx with a triethoxysilane linker. They terminated the polymerization of EtOx with an aqueous NaHCO₃ solution in order to generate a hydroxyl end group, which was further modified with (3-isocyanatopropyl) triethoxysilane (IPTES) to form a silane coupling agent for the PEtOx chains, **FP.5** [35]. These polymers were mainly used for grafting to silicon (e.g. wafer, glass slide) by heating a solution of the silane-modified polymer with the silicon surface [100,174].

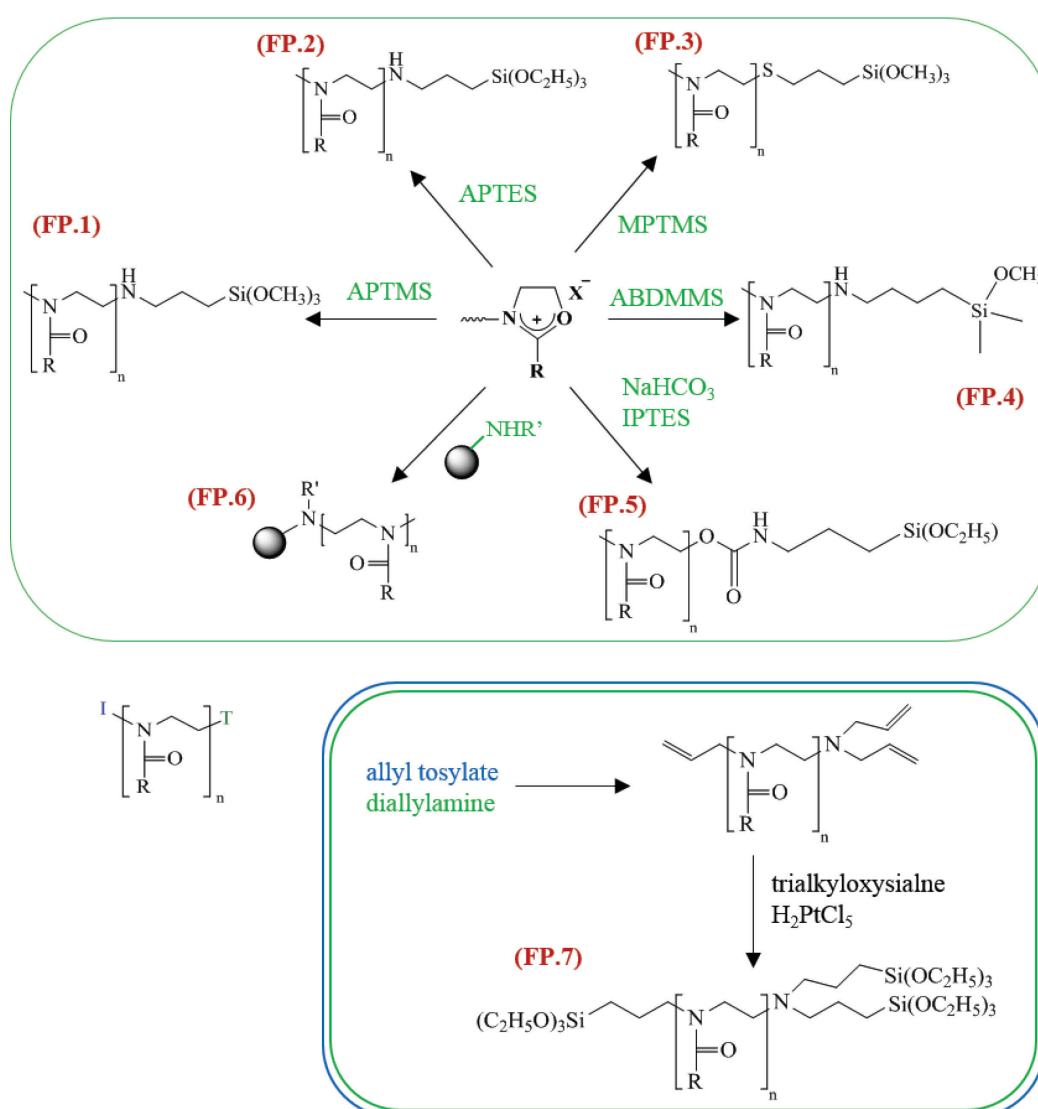


Figure 4.1 Various coupling agents that can be used for the direct termination of the living oxazolinium species and consequently binding them to silica surface (**FP.1-6**), preparation of POx with three silane-functionalized groups (**FP.7**).

Tsubokawa et al. reported an easier method for the direct surface modification of silica surface/substrate with POx, **FP.6**, based on the “grafting to” approach. In this method, CROP polymerization of MeOx was conducted using methyl p-toluenesulfonate (MeOTs) as an initiator; the living oxazolinium species were terminated by amine functionalized SNPs [172]. It is also possible to prepare silane-functionalized POx using the functionalized initiator. POx with three triethoxysilyl groups (**FP.7**) was reported by Chujo et al. using allyl tosylate as an initiator and diallylamine as a terminating agent, followed by the reaction of these double bonds with trimethoxysilane [13,176].

Many contributions also reported the copper(I)-catalyzed azide-alkyne click chemistry reaction (CuAAC) as a promising method for surface modification [142–145]. Therefore, it is necessary to immobilize azide/alkyne functional groups on the surface of the silica particles. There are two strategies for the immobilization of these functional groups on the surface of SNPs: (i) post-synthetic functionalization (grafting) and (ii) direct synthesis (co-condensation) [145]. Figure 4.2-a indicates various synthetic protocols that can be used in order to functionalize SNPs with these two aforementioned groups.

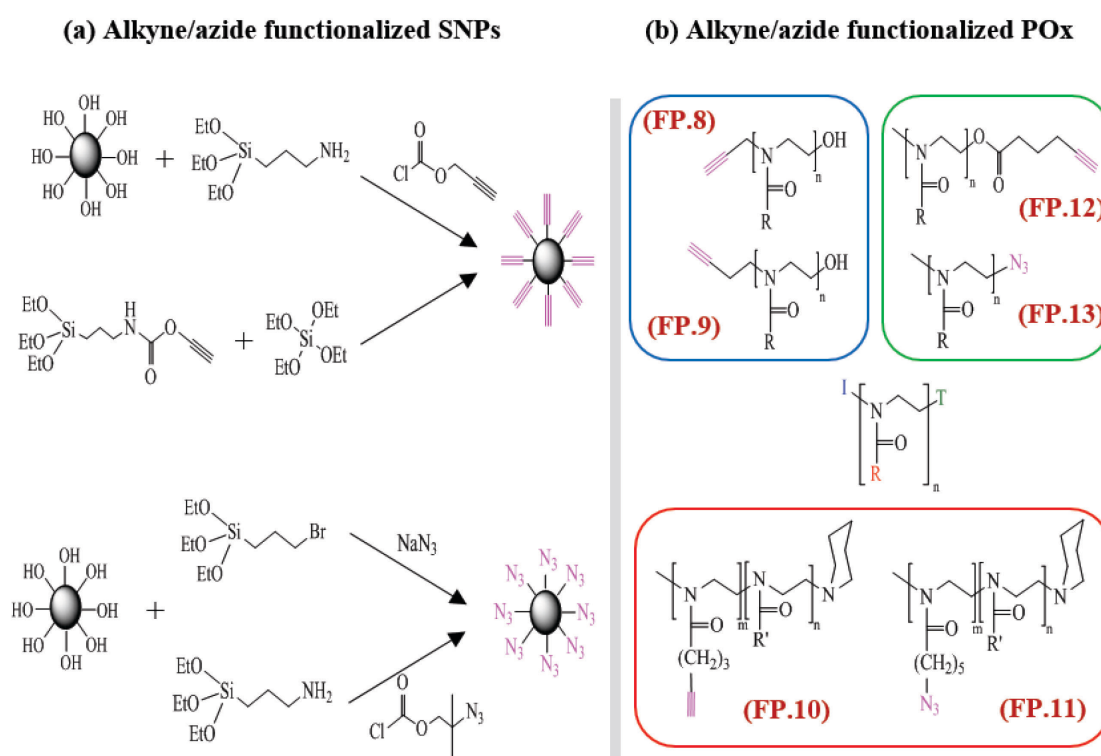


Figure 4.2 Synthesis of (a) alkyne-/azide-functionalized SNPs by grafting or co-condensation approaches [145] (b) various clickable POx.

Various clickable POx chains have been synthesized for click chemistry reaction using a functionalized initiator, monomer, or terminating agent (Figure 4.2-b). The alkyne functional groups can be introduced into the polymer backbone utilizing either functionalized initiators such as propargyl p-toluenesulfonate (**FP.8**) and 3-butynyl toluene-4-sulfonate (**FP.9**) [112,113], or a copolymerizing functionalized monomer such as 2-(pent-4-ynyl)-2-oxazoline (PynOx) with MeOx, EtOx (**FP.10**) [113,119], or the addition of an alkyne-functionalized terminating agent, such as hexynoic acid (**FP.12**) [129]. Moreover, azide-functionalized POx have been reported by either the cationic ring-opening copolymerization of 2-(5-azidopentyl)-2-oxazoline with MeOx (**FP.11**) [118] or terminating the CROP of 2-oxazoline monomers with sodium azide (**FP.13**) [114].

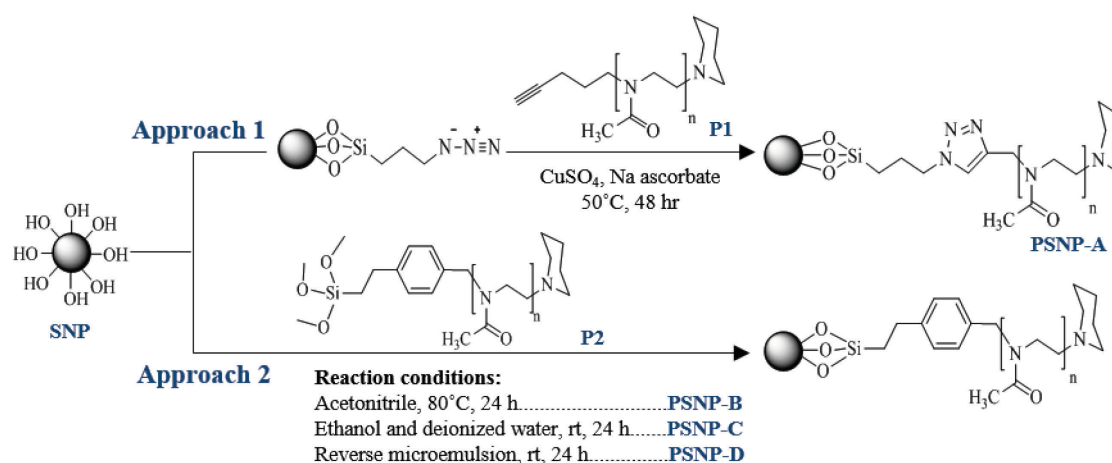


Figure 4.3 Schematic diagram of the formation process of poly(2-methyl-2-oxazoline)-silica nanoparticles (PSNP) by using click chemistry (approach 1) and silane coupling reaction (approach 2) in different reaction conditions.

This chapter describes how these two methods, click chemistry and the silane coupling reaction, were utilized in order to synthesize PMeOx-silica hybrid nanoparticles with the “grafting to” approach (Figure 4.3). For both methods α -telechelic poly(2-methyl-2-oxazolines) were used with alkyne (**P1**) or silane (**P2**) end groups of similar chain lengths and their grafting efficiencies were compared. The latter approach is of particular interest since it led to the development of a novel method for preparing PMeOx-silica hybrid nanoparticles in a water-in-oil (W/O) microemulsion, where the SNPs’ surface modification reactions and the core-shell particle formation proceed simultaneously. This method has advantages including the relatively high grafting density

of polymer chains, time and cost efficiency, and the easy characterization of pre-fabricated polymer chains. Moreover, the ambient reaction condition makes this method superior to other “grafting to” and tandem grafting methods. This method was further used to fabricate and characterize the fluorescent dye-doped SNPs with a PMeOx shell in a one-pot system.

4.2 Results and Discussion

This chapter, which focuses on the synthesis and characterization of the PMeOx-coated SNP via “grafting to” approach and its application in bioimaging, is divided into three parts:

- (i) The synthesis and characterization of PMeOx-silica hybrid nanoparticles based on the “grafting to” approach using either click chemistry or a silane coupling reaction.
- (ii) The preparation of hybrid nanoparticles containing fluorescent dyes in the core, which were further modified with a PMeOx shell for bioimaging applications.
- (iii) The effect of various synthetic parameters on the grafting density of the hybrid nanoparticles that are fabricated with a silane coupling reaction.

4.2.1 Synthesis of the PMeOx-coated SNP through the “grafting to” approach

4.2.1.1 Click coupling between alkyne-functionalized PMeOx and azide-modified SNPs

The click reaction commonly corresponds to the copper-catalyzed azide–alkyne cycloaddition reaction, which provides an efficient method for coupling conjugated macro reagents [177–180]. Therefore, it was expected that the alkyne-functionalized PMeOx could be directly clicked to the azide-functionalized SNPs, leading to the fabrication of hybrid nanoparticles. Figure 4.4 demonstrates the protocol that was used for the fabrication of the PMeOx-coated SNPs via click chemistry.

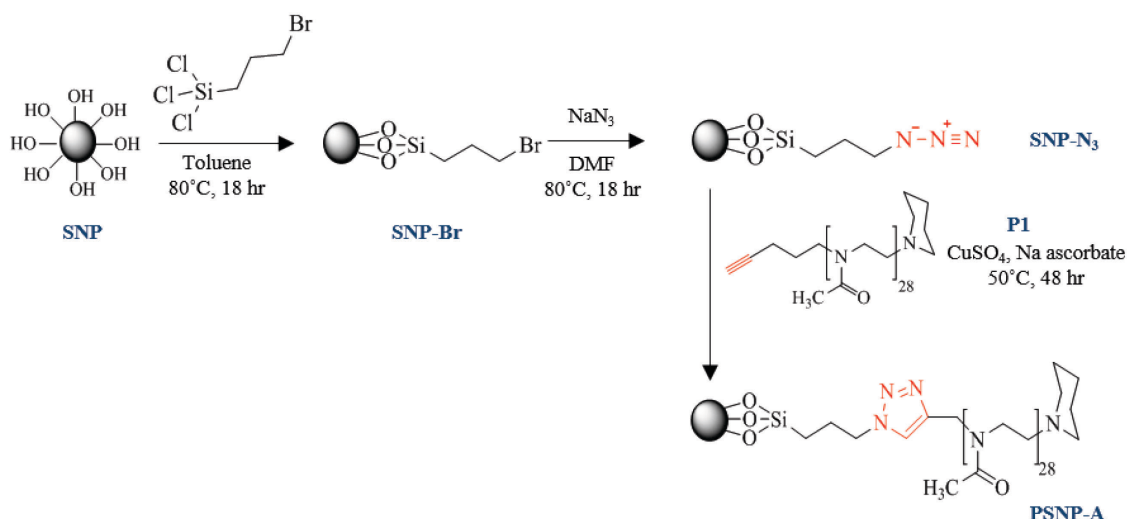


Figure 4.4 Schematic diagram of the formation process of poly(2-methyl-2-oxazoline)-silica nanoparticles using click chemistry.

First, monodispersed SNPs were synthesized as an inorganic core by reverse microemulsion according to a method that was previously reported in the literature [181]. The hydrodynamic diameter of the particle was measured by dynamic light scattering (DLS), and was 43 ± 2 (nm) with a polydispersity index (PDI) of 0.102. Transmission electron microscopy (TEM) images confirmed the spherical shape of SNPs with a narrow particle size distribution (Figure 4.5). The diameters of approximately 100 particles in the TEM images were randomly measured using ImageJ software and the average diameter was 40 ± 4 (nm); this value is consistent with DLS results and the literature [69,182].

Figure 4.6-a shows the fourier transform infrared spectroscopy (FT-IR) spectrum of the synthesized SNPs with characteristic absorption bands arising from the symmetric vibration of Si–O (795 cm^{-1}), asymmetric vibration of Si–OH (935 cm^{-1}), and asymmetric vibration of Si–O (1100 cm^{-1}) [183]. In order to functionalize SNPs with azide groups, 3-bromopropyltrichlorosilane was first used to synthesize **SNP-Br** followed by the substitution of the bromine with an azide group (Figure 4.4) [144]. Elemental analysis proved the presence of bromine (6.3%) in **SNP-Br**, which corresponds to a surface grafting density of 7.5 groups/nm² (Table 4.1). The substitution of bromide with azide was investigated by FT-IR, and the spectra for the modified SNPs are shown in Figure 4.6-a. From the enlarged spectra shown in this figure, the sharp adsorption peak at 2110 cm^{-1} indicated the presence of azide groups on the surface of SNPs [142,184]. The surface

grafting density of 1.5 groups/nm² was calculated for SNP-N₃ based on the presence of nitrogen (0.72%) using elemental analysis.

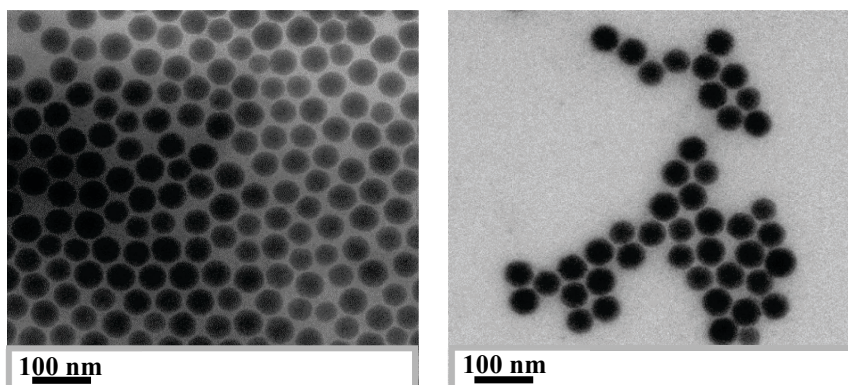


Figure 4.5 TEM images of silica nanoparticles prepared by reverse microemulsion.

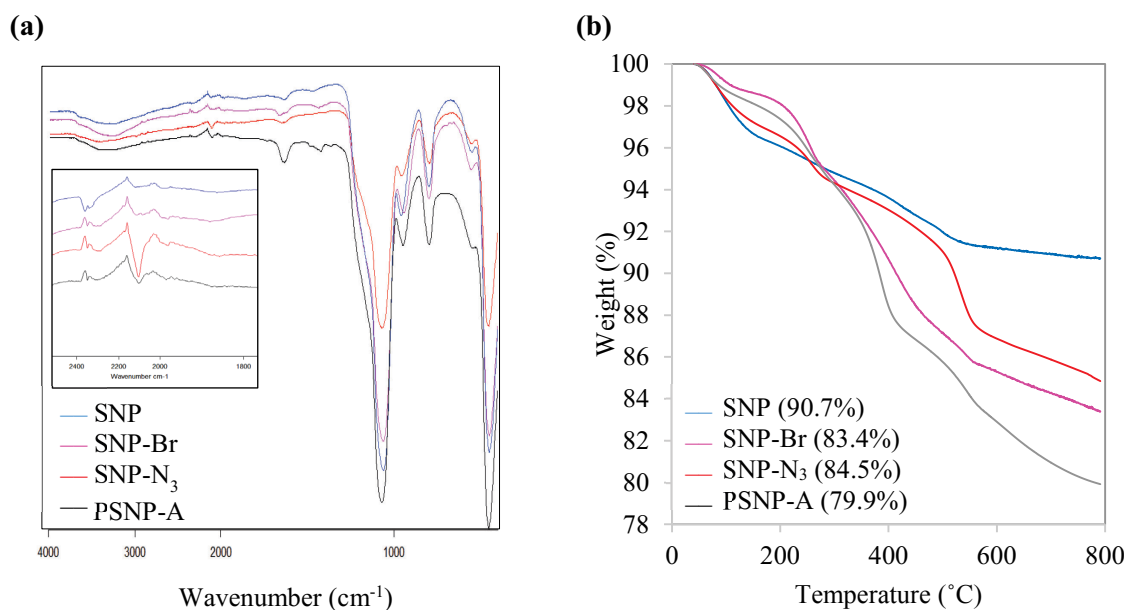


Figure 4.6 (a) FT-IR spectra of SNP, SNP-Br, SNP-N₃, PSNP-A. (b) Thermogravimetric analysis of SNP, SNP-Br, SNP-N₃, PSNP-A.

Thermal gravimetric analysis (TGA) was performed from 40 to 800°C in a nitrogen environment to study the immobilization of functional groups. The mass loss of the bare SNPs and functionalized-SNPs as a function of temperature is presented in Figure 4.6-b. Though the mass loss was investigated from 40 to 800°C, the mass loss up to 120°C

was only related to physically adsorbed water and residual organic solvents. The weight loss of the modified SNPs from 120 to 800°C can be attributed to the thermal decomposition of immobilized ligands on the surface of SNPs [185]. TGA results indicated an additional mass loss of 7.3% and 5.8% for **SNP-Br** and **SNP-N₃**, respectively. The greater mass loss of **SNP-Br** compared to **SNP-N₃** corresponds to the difference in the atomic masses of these two functional groups, and also not complete substitution of bromide with an azide group. Elemental analysis (EA) also confirmed the incomplete substitution of bromide with an azide group, although longer reaction times were used compared to literature [144].

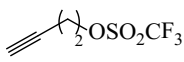
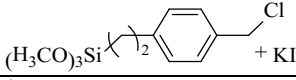
Table 4.1 Elemental analysis of modified SNPs using click chemistry and shell thickness in the synthesized hybrid particle.

Sample	C ^a (%)	N ^a (%)	Br ^a (%)	Surface grafting density ^a (groups/nm ²)	Polymer layer thickness ^b (nm)
SNP-Br	-	-	6.30	7.5	---
SNP-N₃	5.12	0.72	-	1.5	---
PSNP-A	8.67	2	-	0.183	3.6 ± 0.36

^a determined from the elemental analysis; ^b determined by TEM analysis and ImageJ software relative to the pure silica nanoparticles before the “grafting to” reaction.

The presence of excess polymer chains, which is required for the “grafting to” click chemistry, may induce steric repulsion [32] and it is therefore more difficult to approach the azide groups on the surface of SNPs and perform the cycloaddition reaction. Hence, it is important to have better control over the functionality of the polymer chains. Although POx with side alkyne groups have been synthesized [26], the synthesis of POx through an alkyne functionalized initiator may lead to better control over the number of functional groups in the polymer chain. In this study, pent-4-ynyl trifluoromethanesulfonate was first synthesized, which acted as an alkyne-functionalized initiator to initiate the cationic ring opening of MeOx. The synthesized alkyne-functionalized PMeOx (**P1**) was composed of approximately 28 repeat units of 2-methyl-2-oxazoline and showed a molecular weight (M_n) of 3650 g mol⁻¹ with a narrow polydispersity of 1.13 (Table 4.2). ¹H NMR of **P1** is presented in Appendix 10.4. **P1** was subsequently grafted onto **SNP-N₃** using a click reaction to fabricate the PMeOx-coated SNP (**PSNP-A**).

Table 4.2 Analytical data for the polymers **P1** and **P2**.

Polymer	initiator	n ^a	M _n ^b (g mol ⁻¹)	M _w ^b (g mol ⁻¹)	D ^b
P1		28	3650	4130	1.13
P2		29	4480	5555	1.24

^a determined by ¹H NMR end group analysis; ^b determined by size exclusion chromatography (SEC) in DMF with 5 g l⁻¹ LiBr at T=60 °C.

Successful grafting of PMeOx on the SNP was qualitatively confirmed by comparing the FT-IR spectra of **SNP-N₃** and **PSNP-A**. Figure 4.6-a indicates a reduction in the intensity of the azide peak in **PSNP-A** compared to **SNP-N₃** and the appearance of an amide carbonyl peak at 1639 cm⁻¹, which correspond to the amide backbone of the grafted PMeOx chains [186,187]. In addition, TGA confirmed the coupling of polymer chains on the functionalized nanoparticles, as evidenced by an additional 4.6% weight loss. The presence of the grafted PMeOx was also confirmed and quantified by EA, indicating an increase in carbon and nitrogen of 3.55 and 1.28%, respectively (Table 4.1). The surface grafting density of **PSNP-A** was calculated, indicating that 0.18 PMeOx chains were present on the 1 nm² surface area of SNP. Although the click reaction leads to the formation of PMeOx-coated SNP with good grafting density, Ranjan et al. reported greater polymer grafting density for their synthesized hybrid particles, polystyrene-coated SNPs, and polyacrylamide-coated SNPs, using click chemistry [144]. This can be explained by the lower substitution of azide with bromide groups, which emphasizes the effect of functionalization of SNPs and polymer chains in click chemistry.

For further investigation, the morphology of the **PSNP-A** was studied using TEM and the results are presented in Figure 4.7. TEM analysis indicated that **PSNP-A** were not agglomerated. Moreover, comparing the TEM images of **PSNP-A** with azide-functionalized SNPs indicated the formation of a thin polymer layer around the silica nanoparticles and dispersion of the **PSNP-A** in the most common solvent (methanol) for PMeOx.

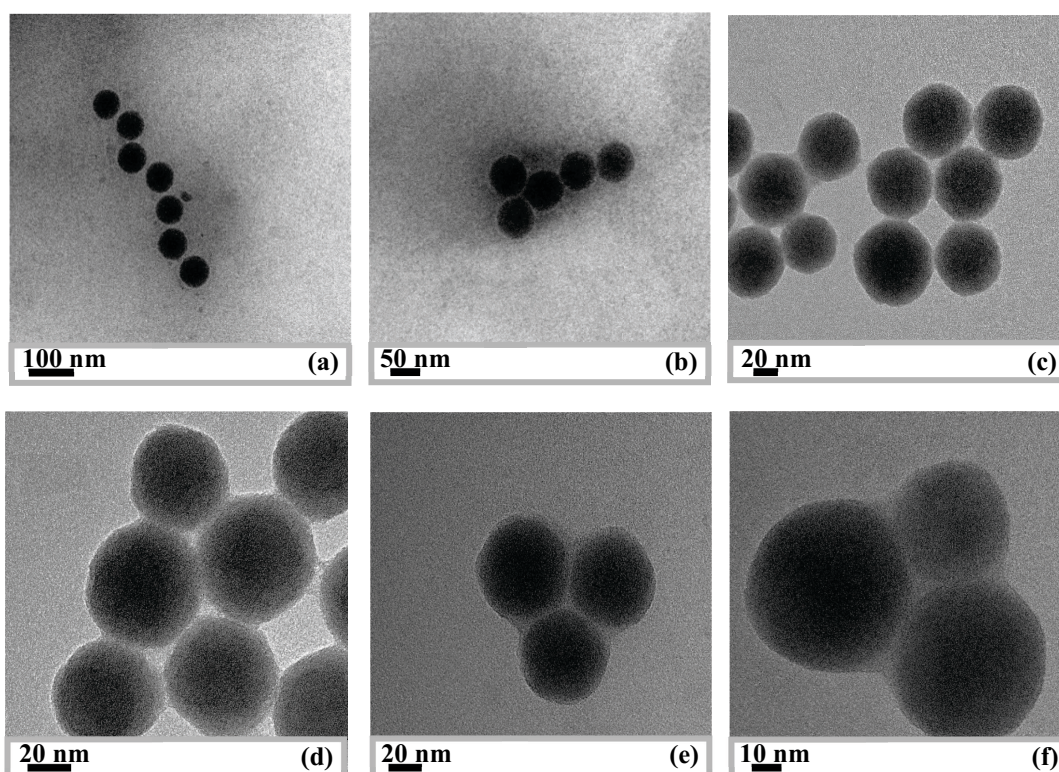


Figure 4.7 TEM image of (a,b) silica-azide nanoparticles, poly(2-methyl-2-oxazoline)-silica nanoparticles (PSNP-A) dispersed in (c,d) methanol and (e,f) isopropanol.

4.2.1.2 Silane coupling reaction between silane agent-functionalized PMeOx and hydroxyl groups on the surface of SNPs

The results from click chemistry help to identify some drawbacks to this approach, such as the dependency of the grafting density of the hybrid particles on the number of available functional groups on the surface of the SNP and in the polymer chain. Moreover, this method suffers from a difficult and costly protocol for removing the copper traces from the product [180]. One approach for enhancing the grafting density is the incorporation a silane coupling agent into a polymer chains; with this method, there is no need for other SNP surface functionalities than the already existing OH-groups. Therefore, PMeOx with trimethoxysilane was prepared, followed by the coupling reaction with the hydroxyl groups on the surface of the SNP, which led to the formation of Si-O-Si bond [66,188]. Although it has been proposed in the literature that either 3-aminopropyltriethoxysilane (APTES) or 3-aminopropyltrimethoxysilane (APTMS) can be introduced as a terminating agent for POx [173,174], and the synthesized

trimethoxysilane-functionalized polymer can be coupled to the surface of the SNP, it should be noted that it is still not easy to achieve 100% chain-end functionality. Thus, the use of a bifunctional initiator that contains a silane agent, which can be grafted onto the surface of the bare SNP and could initiate cationic ring opening polymerization of MeOx, was expected to be more effective.

For this purpose, ((chloromethyl)phenylethyl)trimethoxysilane (CTMS) was used as an initiator. Since the chloride group has low reactivity, even at long polymerization times and high temperatures, the addition of a co-initiator (potassium iodide, KI) can enhance the monomer conversion by the exchange of the chloride anion with the iodide one that has a lower nucleophilicity [106]. The result of $^1\text{H-NMR}$ indicates that CTMS accompanied by KI is a good initiator for the polymerization of MeOx. This polymerization led to the well-defined polymer **P2** with a controlled molecular weight of 4480 g mol^{-1} and a low polydispersity of 1.24 (Table 4.2). $^1\text{H NMR}$ of **P2** is presented in Appendix 10.4.

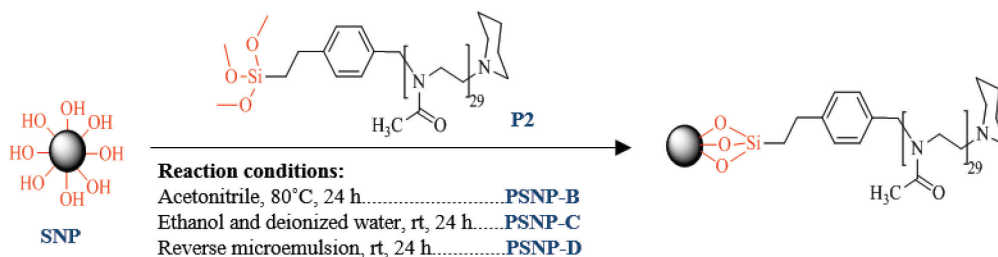


Figure 4.8 Schematic diagram of the formation process of poly(2-methyl-2-oxazoline) silica nanoparticles using silane coupling reaction in various reaction conditions.

In order to investigate the efficiency of silane-functionalized polymer chains **PSNP-B** was prepared in anhydrous acetonitrile at 80°C for 24 h. Generally, the FT-IR and TGA results of PSNP prepared using coupling reaction with different protocols, which are shown in Figure 4.9. In Figure 4.9-a, it is evident that the successful coupling reaction of polymer chains on the surface of SNPs occurred for **PSNP-B** due to the presence of characteristic peaks at 1639 and 1419 cm^{-1} , which were observed due to the stretching band of the amide carbonyl of POx and CH from CH_3 , respectively [186,187,189]. This finding is also in agreement with the TGA results since a greater mass loss was observed for **PSNP-B** than for neat SNPs (Figure 4.9-b).

The grafting densities of composite particles were calculated based on elemental analysis and are summarized in Table 4.3. The **PSNP-B** composite nanoparticles exhibited higher grafting density than **PSNP-A**, and this is consistent with the theoretical expectations. In addition, the grafting density that was obtained for **PSNP-B** is greater than the results of PS-coated SNPs using click chemistry (0.29 groups/nm²) that were reported by Ranhan et al., and it is comparable to the tandem method that was used for the preparation of the same composite material (0.51 groups/nm²) [142].

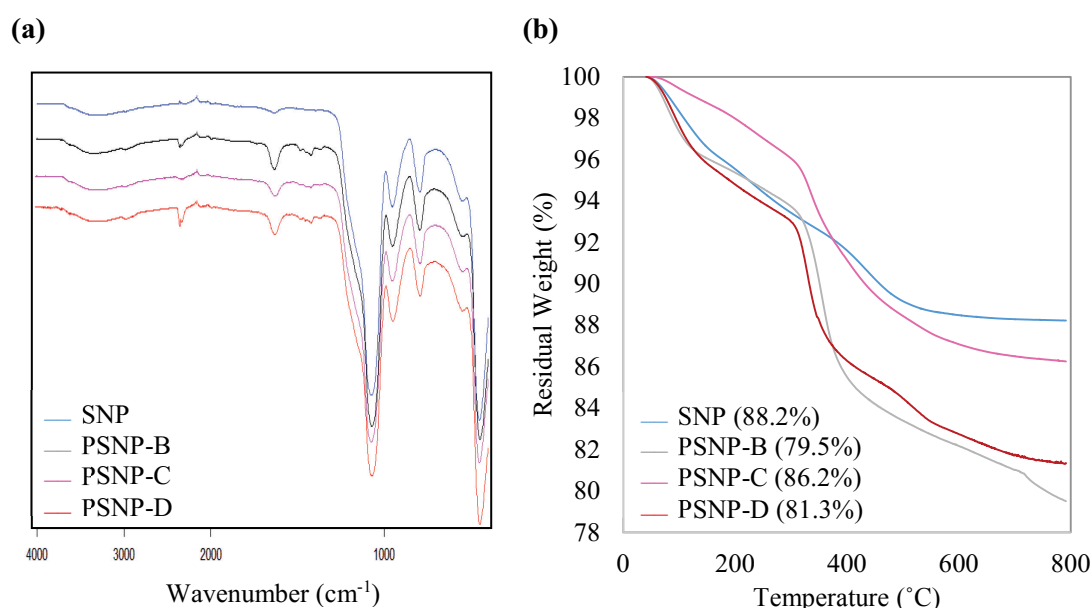


Figure 4.9 (a) FT-IR spectra of SNP, **PSNP-B**, **PSNP-C**, and **PSNP-D** **(b)** Thermogravimetric analysis of SNP, **PSNP-B**, **PSNP-C**, and **PSNP-D**.

Table 4.3 Elemental analysis of modified SNPs using silane coupling reaction and shell thickness in the synthesized hybrid particle.

Sample	C ^a (%)	N ^a (%)	Surface grafting density ^a (groups/nm ²)	Polymer layer thickness ^b (nm)
PSNP-B	9.51	1.66	0.459	4.37 ± 1.06
PSNP-C	6.67	1.07	0.301	nd
PSNP-D	7.66	1.47	0.353	nd

^a determined from the elemental analysis; ^b determined by TEM analysis and ImageJ software relative to the pure silica nanoparticles before the “grafting to” reaction.

Mild reaction condition were used to synthesize composite nanoparticles. **PSNP-C** and **PSNP-D** were prepared in the 25%/75% v/v mixture of ethanol and deionized-

water at room temperature and W/O microemulsion, respectively. These reaction conditions were reported in the literature for the fabrication of amine-functionalized SNPs using APTMS or APTES [164,190,191]. It was used as an attempt to immobilize **P2** on the surface of SNP. W/O microemulsion was previously reported as a successful method for silica coating of polymeric nanoparticles [192] in addition to coating SNPs with polyethylene glycol (PEG) using click chemistry [146]. In both prepared PSNPs, **PSNP-C** and **PSNP-D**, the coupling of polymer chains successfully occurred, which was confirmed by the appearance of an amide peak in FT-IR and the additional mass loss of 2 and 6.9% for **PSNP-C** and **PSNP-D**, respectively (Figure 4.9). These results were also consistent with EA by comparing the %C in these samples (Table 4.3).

The lower grafting density of **PSNP-C** (0.301 chains/nm²) and **PSNP-D** (0.353 chains/nm²) compared to **PSNP-B** (0.459 chains/nm²) can be explained by the mobility of polymeric chains in the solution since the polymeric chains can easily move and diffuse to the surface of a particle at high temperatures. This is also consistent with the result that Huang et al. obtained while optimizing the reaction conditions for synthesizing a composite particle using the “grafting to” approach [32]. Moreover, combining reverse microemulsion and the silane coupling reaction of functionalized polymers as a synthetic strategy for surface modification seems to be more promising than the coupling reaction in a mixture of ethanol and water in a basic environment. Although the silane agent in polymer chains can be hydrolyzed in the presence of water to make the polymer chain completely water soluble, the steric repulsion between PMeOx chains can also prevent the chains from approaching the surface of the SNP. This problem could be partly solved by reducing the reaction volume using W/O microemulsion. In this case, PMeOx chains are not soluble in an oil phase, cyclohexane, and since they are hydrophilic they diffuse into the aqueous phase and their trimethoxysilane end also will be hydrolyzed in the presence of water, which make them completely hydrophilic. SNPs have already been synthesized and entrapped inside the aqueous phase; these polymer chains diffuse into water droplets and have the possibility to be condensed on the surface of SNPs (Figure 4.10).

By using W/O microemulsion the reaction volume, aqueous phase, decreased significantly. As a result, the concentration of polymer chains increased and had a greater chance of approaching the SNPs and co-condensing on the surface of particles without a high temperature requirement. The obtained grafting density of **PSNP-D** is comparable with **PSNP-B**, which indicates the successful coupling of polymer chains on SNPs at

ambient conditions by limiting the reaction volume. Moreover, the combining method reduces the amount of time required and the cost by shortening the reaction time. This method required less solvent for washing nanoparticles. Comparing the grafting density of PSNPs that were prepared by a coupling reaction and click chemistry, indicated that although click chemistry corresponds to an efficient and selective reaction between azide and alkynes [142], this method depends largely on the quantity and efficiency of the functionalized SNPs and alkyne-functionalized polymer chains. A coupling reaction can overcome this since in this method there is no need to functionalize the surface of the SNP.

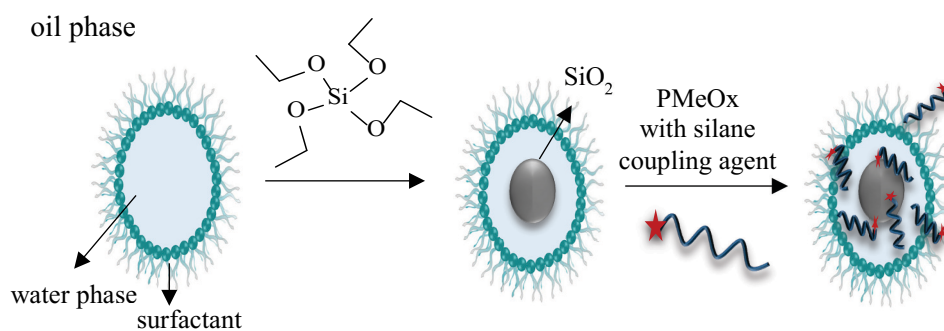


Figure 4.10 Schematic strategy for the synthesis of PMeOx-silica hybrid nanoparticles using water in oil micro emulsion (**PSNP-D**).

From the particle size that was obtained by TEM analysis using ImageJ software (Figure 4.11), the polymer shell thickness for the PMeOx-grafted nanoparticle with the lowest grafting density **PSNP-A**, with 3.6 ± 0.36 nm and for PMeOx-grafted nanoparticle with the highest grafting density, **PSNP-B**, with 4.37 ± 1.06 nm. These values are in agreement with a PMeOx (degree of polymerization = 30) that was grafted to a mica surface by Rehfeldt and colleagues [173] who measured a polymer layer thickness of 2.44-3.97 nm (~ 3.2 nm on average) in the dry state by ellipsometry. The radius of gyration for the PMeOx with 30 repeat units can be estimated at ~ 2.25 nm and the end-to-end distance is approximately ~ 5.50 nm. The larger experimental values that were observed relative to the calculated radius of gyration are not surprising since higher grafting densities led to more extended polymer conformation on the surface [173].

However, some entanglement of free polymer to the polymer shell cannot be completely ruled out, even after extensive washing.

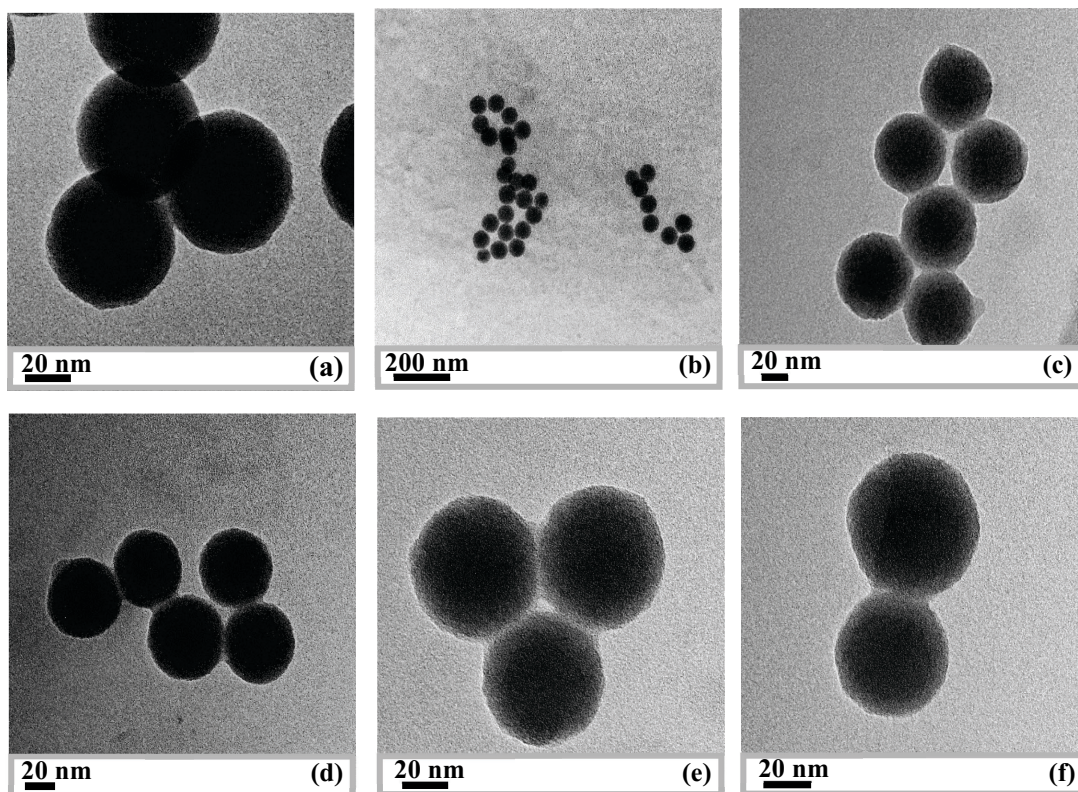


Figure 4.11 TEM images of (a,b) silica nanoparticles, poly(2-methyl-2-oxazoline)-silica nanoparticles (**PSNP-B**) dispersed in (c,d) methanol and (e,f) isopropanol.

4.2.2 Synthesis of fluorescent-dye doped SNP-coated with PMeOx

The reverse microemulsion not only provides an efficient method for synthesizing monodispersed SNPs, it also allows for doping of fluorescent dye molecules into the particle either by the physical encapsulation or covalent bonding of the dye with the silica matrix [146,181,182,193]. Moreover, reverse microemulsion can be used to synthesize hybrid nanoparticles with silane functionalized polymers [194]. Therefore, it was expected that hybrid nanoparticles containing an inorganic-core with fluorescence dye molecules and PMeOx shells could be synthesized in a one-pot system. For this purpose, SNPs were first labeled with fluorescence dye molecules using different approaches, such as covalent binding or electrostatic interaction, which can be used for bioimaging, diagnosis, and therapeutic applications (Figure 4.12).

In this study, two fluorescence dye doped SNPs were prepared, namely **SNP-Ru(bpy)** and **SNP-FITC**, which contained tris(bipyridine)ruthenium(II) chloride (Ru(bpy)) and fluorescein isothiocyanate (FITC), respectively. **SNP-Ru(bpy)** was prepared by encapsulating Ru(bpy) dye molecules inside the silica matrix using reverse microemulsion according to a previously reported study in the literature [181,182,193]. The electrostatic interaction between positively charged Ru(bpy) and the negatively charged silica shell prevents leakage of the dye from the silica matrix [195]. For the synthesis of **SNP-FITC**, FITC was first chemically bonded to the (3-aminopropyl)trimethoxysilane (APTMS) through the amino group in APTMS and the isothiocyanate group in FITC. In the next step, the fluorescent silicon alkoxide precursors were added to the W/O microemulsion in order to react with tetraethyl orthosilicate (TEOS) and form the fluorescent silica nanoparticles [146].

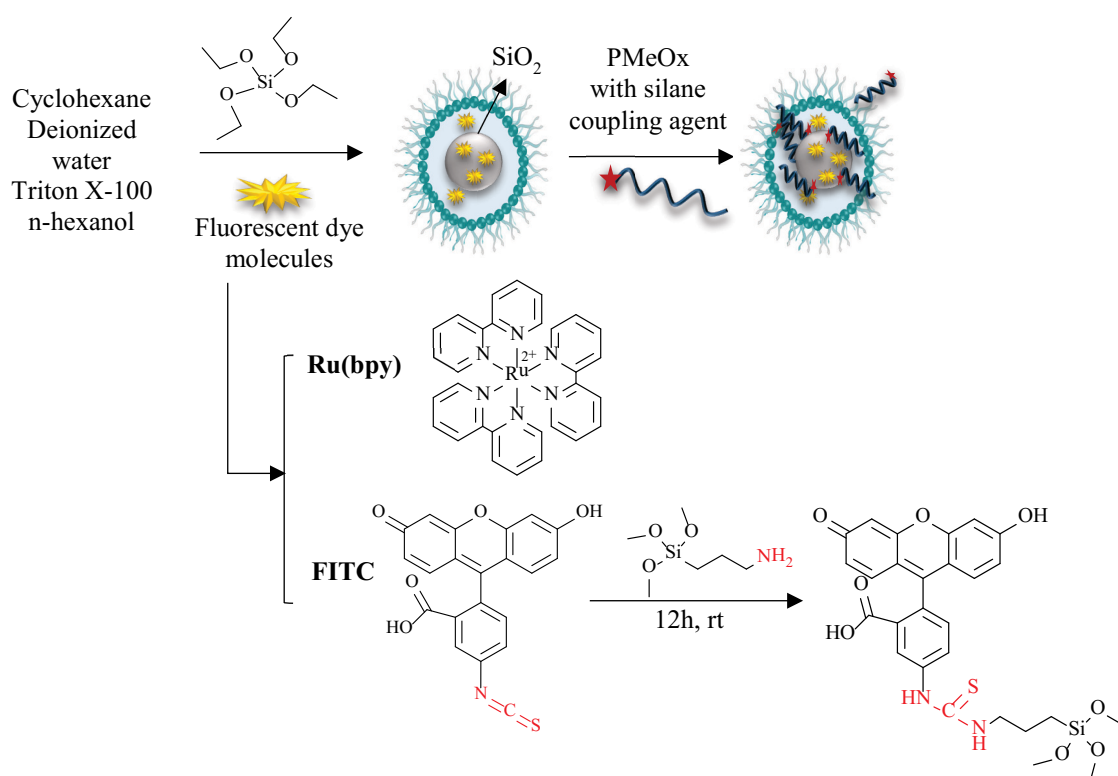


Figure 4.12 Schematic diagram for the formation process of poly(2-methyl-2-oxazoline) dye-doped silica nanoparticles in one-pot system by using reverse microemulsion method.

UV-Vis spectroscopy was used to prove the presence of fluorescent dye molecules inside the silica matrix by the appearance of absorption peaks at 452 and 482 nm for **SNP-Ru(bpy)** and **SNP-FITC**, respectively. Moreover, the FT-IR spectrum of **SNP-Ru(bpy)**

indicated the successful encapsulation of the Ru(bpy) dye molecules in SNPs by the appearance of a strong characteristic peak of the C-H bend of the pyridine ring in Ru(bpy) at 766 cm^{-1} (Figure 4.13-a). The FT-IR spectrum of **SNP-FITC** also illustrated an additional band at 1633 cm^{-1} compared to neat SNPs, which was assigned to the stretching modes of the aromatic C=C in the FITC molecule [196]. The presence of the FITC dye in the silica matrix, which was confirmed with UV-Vis, and the absence of the band relative to vibrational mode of the free dye, N=C=S at 2100 cm^{-1} , may indicate the coupling of dye with silica matrix [196,197].

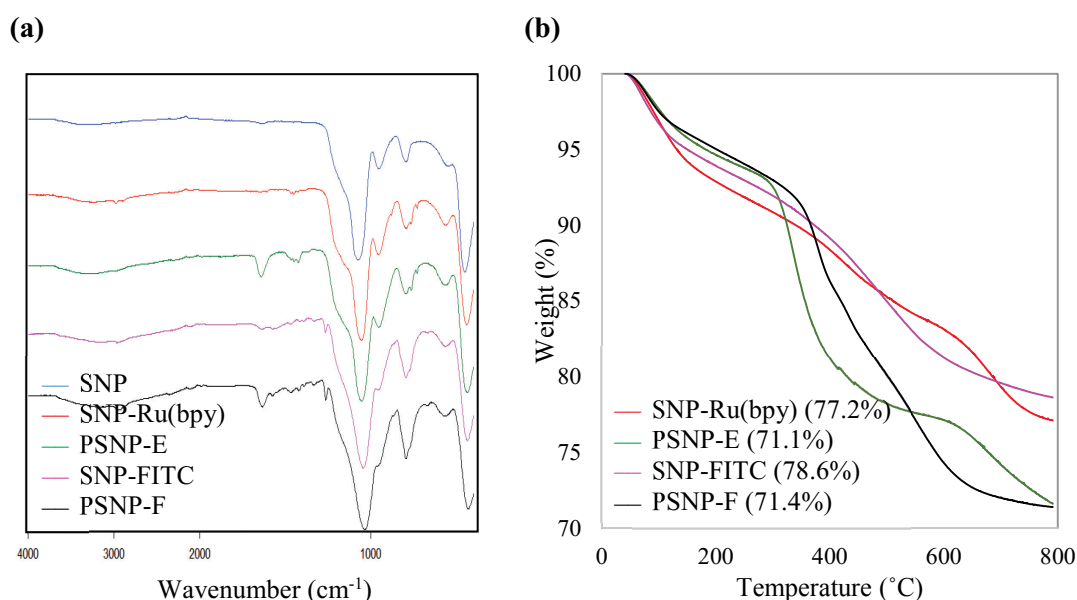


Figure 4.13 (a) FT-IR spectra of **SNP**, **SNP-Ru(bpy)**, **PSNP-E**, **SNP-FITC**, and **PSNP-F** **(b)** TGA of **SNP**, **SNP-Ru(bpy)**, **PSNP-E**, **SNP-FITC**, and **PSNP-F**.

The surfaces of **SNP-Ru(bpy)** and **SNP-FITC** were further modified with PMeOx to fabricate **PSNP-E** and **PSNP-F**, respectively. The successful silane coupling reaction of polymer chains on the surface of **SNP-Ru(bpy)** and **SNP-FITC** was confirmed by the presence of peaks for the stretching band of the amide carbonyl of PMeOx and CH from CH_3 at 1639 and 1419 cm^{-1} , respectively [186,187,189]. TGA results were also in good agreement with the FT-IR since a greater mass loss of 6.1% and 7.2% was observed for **PSNP-E** and **PSNP-F**, respectively, compared to their core particles (Figure 4.13-b). The additional mass loss of hybrid nanoparticles confirmed the coupling of polymer chains to the surface of nanoparticles since the physically adsorbed

polymer chains were washed with three washing cycles with ethanol, methanol, and deionized water.

Figure 4.14 shows TEM images of the SNPs containing Ru(bpy) and FITC. In both cases, NPs appear to be spherical, and the size of the particles was measured by using ImageJ software and summarized in Table 4.4. The results indicated a narrower particle size distribution for **SNP-Ru(bpy)** compared to **SNP-FITC**, which is in excellent agreement with DLS results. Regarding the polymer coating of the fluorescent NPs, TEM images clearly indicate the formation of polymeric shell around the particles. The shell thickness was measured to be around 2.3 and 1.1 nm for **PSNP-E** and **PSNP-F**, respectively. The thinner shell in **PSNP-F** can be explained owing to the increased error from greater particle size distribution of the **SNP-FITC**.

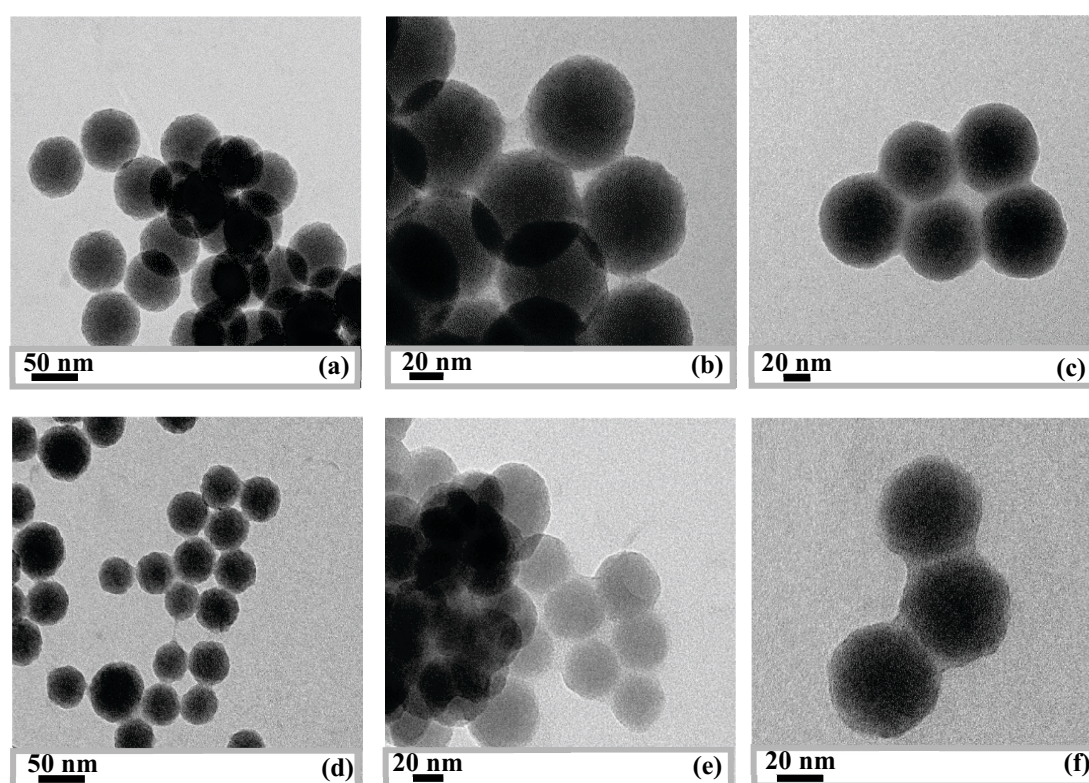


Figure 4.14 TEM images of **SNP-Ru(bpy)** (a), **PSNP-E** dispersed in methanol (b) and isopropanol (c) **SNP-FITC** (d), **PSNP-F** dispersed in methanol (e) and isopropanol (f).

The concentrations of the Ru(bpy) and FITC doped in SNP and PSNP were calculated using UV-Vis spectroscopy with calibration curves of these two dye molecules (Appendix 10.5), and summarized in Table 4.4. As expected, the concentration of FITC

doped in SNP with and without polymeric shell remained without any significant change, since these dyes were chemically bonded to the silica matrix and it is not possible to easily leak out of the NP. In **PSNP-E**, the characteristic peak of Ru(bpy) dye appeared, which confirms that Ru(bpy) dyes remained in the silica matrix although a part of them might leak out from the SNP (Figure 4.13-a). The concentration of the dye molecule increased significantly once a polymeric shell was formed around the NPs (Table 4.4). This polymeric shell could protect the dyes inside the silica matrix from leakage since they were merely physically encapsulated inside the silica matrix and it is possible to leak out during the washing process. This also highlighted the effect of the washing process since in the third wash the concentration of Ru(bpy) dyes was almost the same in SNPs and PSNPs, while in the fifth washing step lower concentrations of Ru(bpy) in SNPs were measured compared to PSNPs.

Table 4.4 Particle size and concentration of dyes inside silica matrix before and after the formation of the polymeric shell.

Particle code	Diameter ^a (nm)	PDI ^a	Diameter ^b (nm)	Shell thickness ^b (nm)	c _{dye} ^c ($\mu\text{mol mL}^{-1}$)
SNP-Ru(bpy)	57 ± 0.3	0.12	61.7 ± 1.5	-	0.093
PSNP-E	-	-	64.05 ± 1.5	2.35	0.154
SNP-FITC	69.48 ± 2.7	0.41	50.1 ± 2.9	-	0.254
PSNP-F	-	-	51.2 ± 3.1	1.1	0.256

^a measured by DLS; ^b determined based on TEM images using ImageJ software; ^c calculated based on the calibration curve of the pure dyes for 0.5 mg/mL of NPs in solution.

4.2.3 Study the effect of different synthesis parameters on grafting density

The synthesis and characterization of a PMeOx–silica hybrid nanoparticles using the “grafting to” method was based on click chemistry and silane coupling reactions reported in previous sections. Although in both cases polymer chains were successfully grafted onto the surface of SNPs, the silane coupling reaction led to a higher grafting density (0.30 to 0.45 chains/nm²) compared to the click chemistry (**PSNP-A** with 0.183 chains/nm²). Among the silane grafting processes, the highest grafting densities were obtained by coupling polymer chains in anhydrous acetonitrile at a high temperature (80 °C) to the surface of SNPs (**PSNP-B**). This was most likely due to the increasing mobility of polymeric chains in the solvent. Moreover, the synthesis of a hybrid nanoparticle in

reverse microemulsion (**PSNP-D**) also indicated promising results and it has the advantages of being time and solvent-efficient and may be of special interest when grafting temperature-sensitive moieties to the silica nanoparticle surface. Hence, the effect of various synthetic parameters such as reaction time, temperature, and feed ratio were studied on the grafting density of trimethoxysilane functionalized polymer chains of these two hybrid nanoparticles.

4.2.3.1 The effect of synthetic parameters on grafting density of the PSNP-B

As discussed, **PSNP-B** was prepared with alkoxy silane-hydroxyl coupling reaction in anhydrous acetonitrile at 80°C for 24 h. In order to study the effect of the reaction temperature on grafting density of polymer chains, the first set of hybrid nanoparticles was prepared at different temperatures while other reaction conditions remained constant. Therefore, four samples including **PSNP-B-1**, **PSNP-B-2**, **PSNP-B-3**, and **PSNP-B-4** were prepared in acetonitrile at 40, 70, 100, and 120°C, respectively. Figure 4.15-a indicates the FT-IR spectra of the prepared samples and confirms the formation of polymer shell in all trials by the appearance of two characteristic peaks of PMeOx containing a stretching band of the amide carbonyl of PMeOx and CH from CH₃ at 1639 and 1419 cm⁻¹, respectively [186,187,189]. Moreover, TGA was performed to investigate the immobilization of polymer chains. The mass loss of the bare SNP and hybrid nanoparticles as a function of temperature is presented in Figure 4.15-b. The amount of grafted polymer, Γ_{PMeOx} , in the synthesized hybrid nanoparticles was calculated based on their mass loss by using eq. 7-1.

Table 4.5 summarizes the effect of the reaction temperature on mass loss and the value of Γ_{PMeOx} . The amount of grafted polymer was increased by increasing temperature, which indicates that the co-condensation reaction depended largely on the reaction temperature. This could be expected, since the mobility of polymeric chains was accelerated by increasing the temperature so that they could easily diffuse to the surface of SNP and meet hydroxyl groups and consequently the amount of grafted polymer increased. Huang et al. reported the same behaviour when they optimized the azide-alkyne cyclohexane click reaction to modify SNP by functionalized polymer chains. However, the authors observed a maximal temperature (at 90°C) and they believe that

beyond this point the reactive sites on the SNPs were shielded by grafted polymer chains [32].

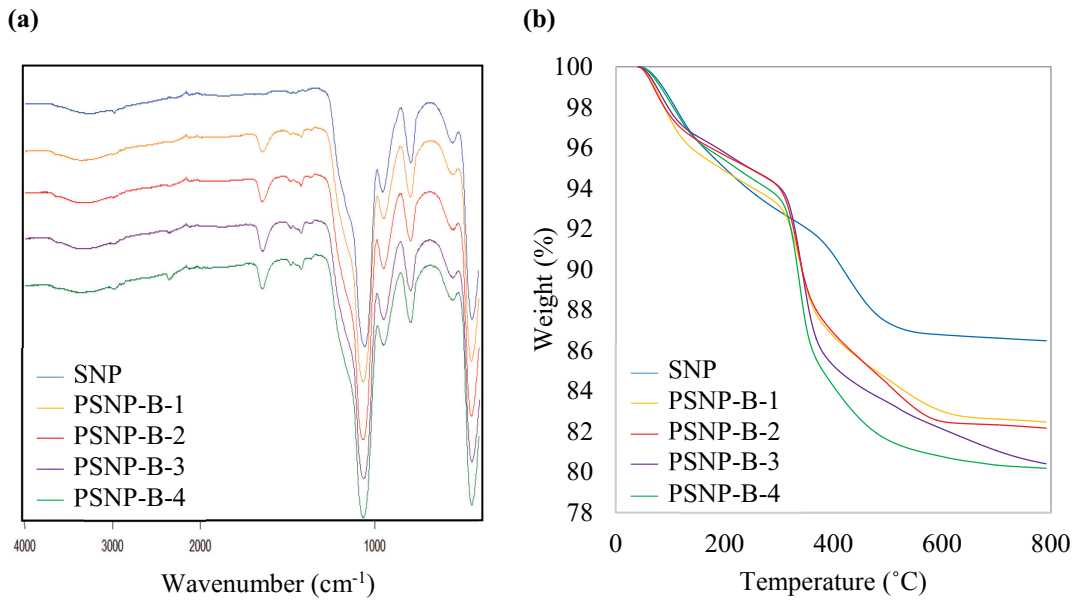


Figure 4.15 (a) FT-IR spectra of bare SNP, PSNP-B-1, PSNP-B-2, PSNP-B-3, and PSNP-B-4 **(b)** TGA of bare SNP, PSNP-B-1, PSNP-B-2, PSNP-B-3, and PSNP-B-4.

Table 4.5 Analytical data from the PSNP-B by varying the reaction temperature, time, and feed ratio.

Particle code	Reaction temperature (°C)	Reaction time (h)	Feed ratio P/SNP	Mass loss ^a (%)	Γ_{PMeOx} ^b (mg m ⁻²)
PSNP-B-1	40	24	2	13.04	0.76
PSNP-B-2	70	24	2	13.72	0.89
PSNP-B-3	100	24	2	14.99	1.14
PSNP-B-4	120	24	2	15.81	1.30
PSNP-B-5	80	2	2	13.2	0.61
PSNP-B-6	80	5	2	13.7	0.72
PSNP-B-7	80	15	2	14.1	0.79
PSNP-B-8	80	48	2	14.24	0.82
PSNP-B-9	80	24	1	13.51	0.86
PSNP-B-10	80	24	2	14.40	1.03
PSNP-B-11	80	24	4	16.00	1.34
PSNP-B-12	80	24	8	16.46	1.44

^a mass loss data determined from the TGA from 150 to 650°C; ^b calculated from the mass loss data using eq. 7-1.

The second set of hybrid nanoparticles was prepared in anhydrous acetonitrile at 80 °C in order to study the effect of reaction times (from 2 to 48 h) on the amount of grafted polymer. Figure 4.16 illustrates the FT-IR spectra and TGA analysis of the hybrid particles, which confirmed the high rate of co-condensation reaction since the hybrid particles were formed after 2 h. Moreover, in the first stage there was no clear steric repulsion between polymer chains owing to the low grafting density. The amount of grafted polymer increased by increasing the reaction time from 2 to 15 h, which indicates that after 2 h polymer chains required a longer time to approach the hydroxyl group on the surface of SNPs due to the steric repulsion between polymeric chains. After 15 h, the surface of SNPs was almost covered by grafted polymers and the trimethoxy silane and hydroxyl group could not approach each other anymore. Hence the Γ_{PMeOx} value remained constant after 15 h. Huang et al. reported a similar trend [32].

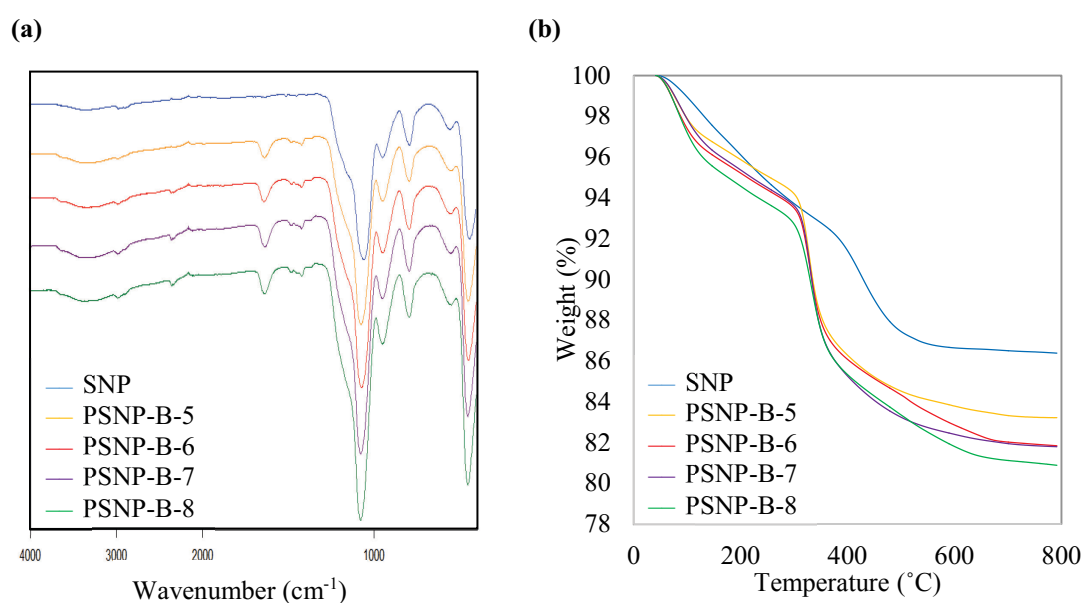


Figure 4.16 (a) FT-IR spectra of bare SNP, PSNP-B-5, PSNP-B-6, PSNP-B-7, and PSNP-B-8
(b) TGA of bare SNP, PSNP-B-5, PSNP-B-6, PSNP-B-7, and PSNP-B-8.

The last set of experiments was conducted to investigate the effect of the **P2/SNP** feed ratio on the amount of grafted polymer. Hence, the last set of samples was prepared at a different ratio mass of trimethoxysilane-functionalized PMeOx to mass of SNP. Figure 4.17-a confirms the successful formation of PMeOx coated SNP in all trials by the appearance of the peaks of PMeOx. Moreover, TGA confirmed the coupling of the

polymer chain to the surface of the nanoparticle, as evidenced by an additional weight loss compared to bare SNPs. It should be noted that the Γ_{PMeOx} value first increased significantly by increasing the concentration of polymer chains (Table 4.5), indicating the significantly increased probability of the silane coupling reaction. Huang et al. reported a similar effect of polymer concentration [32]. Beyond the mass ratio of 4 only a limited increase in Γ_{PMeOx} value could be observed, which suggests the prominent effect of steric repulsion. The above results indicate that this method is promising for the synthesis of PMeOx-coated SNPs and could be generalized to the fabrication of hybrid nanoparticles containing silica as a core and various polymers as a shell.

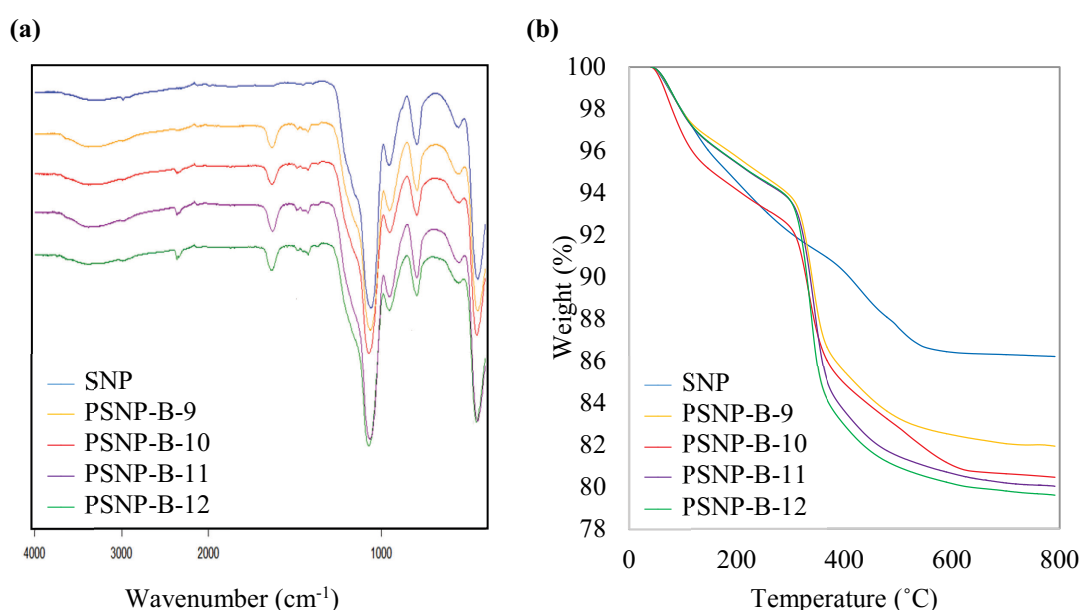


Figure 4.17 (a) FT-IR spectra of bare SNP, PSNP-B-9, PSNP-B-10, PSNP-B-11, and PSNP-B-12 **(b)** TGA of bare SNP, PSNP-B-9, PSNP-B-10, PSNP-B-11, and PSNP-B-12.

4.2.3.2 The effect of synthetic parameters on grafting density of the PSNP-D

For hybrid nanoparticles prepared with reverse microemulsion method, PSNP-D, the effect of two synthetic parameters, reaction time and feed ratio, were studied on grafting density. The first series of hybrid nanoparticles, namely PSNP-D-1, PSNP-D-2, PSNP-D-3, and PSNP-D-4, was synthesized at different reaction times of 2, 16, 24, and 48 h, respectively. The grafting of polymer chains on the surface of SNPs investigated by FT-IR and TGA (Figure 4.18). The results indicated that 2 h is not sufficient for the grafting of PMeOx chains on the SNPs' surface while in PSNP-B-5 hybrid nanoparticle

was formed after 2 h. This could be expected since the mobility of polymeric chains was accelerated at high temperature and increase the probability of the co-condensation reaction. However, polymer chains in mild reaction condition like reverse microemulsion require longer time, at least 15 h, to diffuse into the aqueous phase and grafted on the surface of particles. Moreover, the Γ_{PMeOx} value did not significantly change by increasing the reaction time (Table 4.6), which indicated that in mild reaction condition the steric repulsion became more pronounced and therefore it was not easy for PMeOx chains to approach the hydroxyl groups of the silica surface.

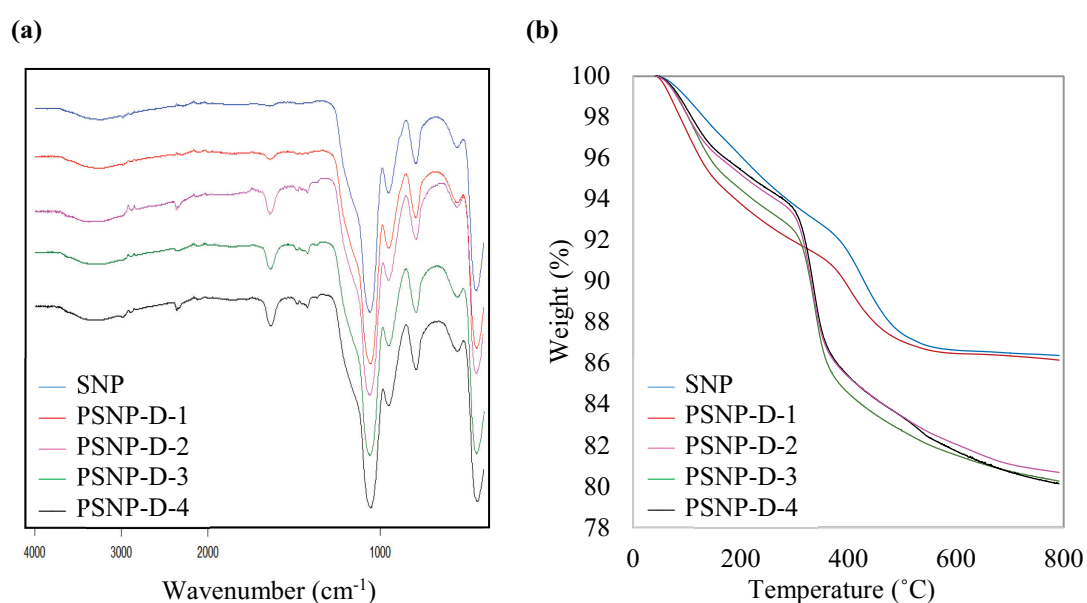


Figure 4.18 (a) FT-IR spectra of bare SNP, PSNP-D-1, PSNP-D-2, PSNP-D-3, and PSNP-D-4 (b) TGA of bare SNP, PSNP-D-1, PSNP-D-2, PSNP-D-3, and PSNP-D-4.

Table 4.6 Analytical data from the PSNP-D by varying reaction time and feed ratio.

Particle code	Reaction temperature (°C)	Reaction time (h)	Feed ratio P/SNP	Mass loss ^a (%)	Γ_{PMeOx} ^b (mg m ⁻²)
PSNP-D-1	25	2	2	8.44	0.09
PSNP-D-2	25	16	2	14.77	1.25
PSNP-D-3	25	24	2	14.58	1.21
PSNP-D-4	25	48	2	15.32	1.36
PSNP-D-5	25	24	0.5	14.71	1.14
PSNP-D-6	25	24	1	15.14	1.22
PSNP-D-7	25	24	2	14.87	1.17
PSNP-D-8	25	24	3.5	15.01	1.20

^a mass loss data determined from the TGA from 150 to 500°C; ^b calculated from the mass loss data using eq. 7-1.

The second set of samples was prepared to investigate the effect of feed ratio on the amount of grafted polymer in hybrid nanoparticles. Figure 4.19 shows the FT-IR spectra and TGA of the prepared hybrid nanoparticles and Table 4.6 summarizes the mass loss and Γ_{PMeOx} value of each samples. The results shows that in reverse microemulsion method the ratio mass of trimethoxysilane-functionalized PMeOx to mass of SNP also did not have a considerable effect on the amount of grafted polymer. However, in **PSNP-B** a significant effect of feed ratio was observed. In general, although reverse microemulsion approach is really promising and easy for synthesis of PMeOx-coated SNPs, it is not easy to improve the surface modification of hybrid nanoparticles prepared by this method.

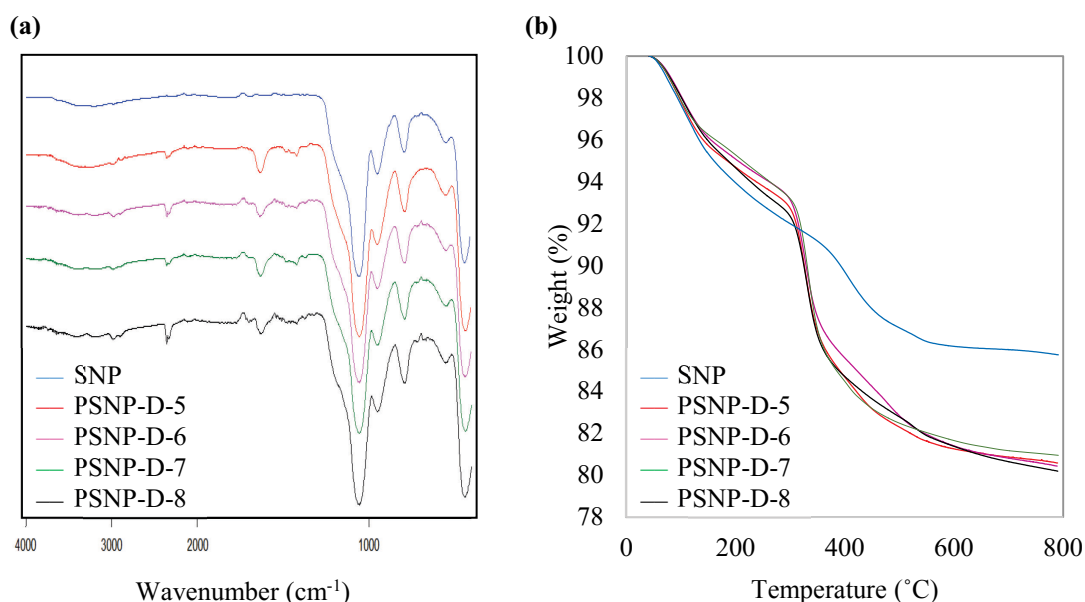


Figure 4.19 (a) FT-IR spectra of bare SNP, PSNP-D-5, PSNP-D-6, PSNP-D-7, and PSNP-D-8 (b) TGA of bare SNP, PSNP-D-5, PSNP-D-6, PSNP-D-7, and PSNP-D-8.

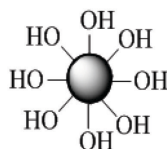
4.3 Conclusion

PMeOx-silica hybrid nanoparticles were prepared using the “grafting to” method based on click chemistry and silane coupling reactions. In both cases polymer chains were successfully grafted onto the surface of SNPs; however, a silane coupling reaction led to a greater grafting density than click chemistry. In silane coupling reaction, PMeOx with trimethoxysilane was first synthesized using a functionalized initiator that was accompanied by a co-initiator, followed by the condensation of the hydrolyzed coupling

agent with hydroxyl groups on the surface of SNPs using various reaction conditions. For a given process, the grafting density is enhanced by coupling polymer chains in an anhydrous solvent at a high temperature due to the increasing mobility of polymeric chains in the solvent, which leads to a higher polymer density. A combining method was also developed with reverse microemulsion and a silane coupling reaction to graft polymer chains onto the surface of SNPs, which did not require an extra step for washing SNPs or a high temperature to achieve greater grafting density. This method was applied to graft polymer chains on SNPs, which led to a high grafting density at ambient conditions by limiting the reaction volume. Moreover, this efficient method of surface modification has the advantages of being time and solvent efficient. This method was also utilized as an effective method for the synthesis of fluorescent dye-doped silica nanoparticles coated with a PMeOx shell in a one-pot system for bioimaging applications. The effects of synthetic parameters were investigated for the grafting density of the hybrid nanoparticles that were prepared by silane coupling reaction.

4.4 Experimental

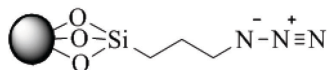
4.4.1 Synthesis of silica nanoparticles (SNPs)



The W/O microemulsion were prepared by first mixing cyclohexane (7.5 mL), n-hexanol (1.8 mL), and Triton X-100 (1.77 mL). The mixture stirred for 5 min followed by the addition of deionized water (0.5 mL). The mixture stirred for another 15 min and then silica precursor, TEOS (0.1 mL), was added to it. After 30 min, the silica polymerization reaction was initiated by adding 60 μ l of NH_4OH . The reaction was allowed to continue for 24 h at room temperature. Once the polymerization was completed, the synthesized nanoparticles were isolated from microemulsion with acetone and collected by centrifugation at 4500 rpm for 15 min. The synthesized SNPs were washed at least three times with ethanol to remove surfactant and other impurities. The synthesized particles were air dried and weighted for the yield, which was about 20 mg. The specific surface area of the SNPs calculated from the linear part of the Brunauer-

Emmett-Teller (BET) plot reached $69.7 \text{ m}^2 \text{ g}^{-1}$. The diameter of particles was measured via DLS, which was $43 \pm 2 \text{ (nm)}$ with a PDI of 0.102, and TEM, which was $40 \pm 4 \text{ (nm)}$.

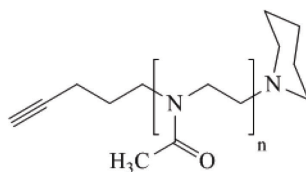
4.4.2 Synthesis of azide-modified silica nanoparticles (SNP-N₃)



Generally, synthesis of azide-modified SNPs (SNP-N₃) has two parts containing functionalization of silica nanoparticles with 3-bromopropyltrichlorosilane (SNP-Br) followed by the substitution of the bromine with azide group while it was reacted with Sodium azide [144]. Synthesized SNPs (1 g) were dried in vacuum oven at 70°C for 24 h in order to reduce the aqueous contents on the surface of the particles. These particles were washed at least three times with anhydrous toluene. Then, these cleaned nanoparticles (1 g) were dispersed in 20 mL of fresh anhydrous toluene in an argon environment in a two necked-round bottom flask. After 1 h sonication, the flask was moved to an oil bath at 80°C and 25 mL of fresh anhydrous toluene was added. The flask was sonicated for 10 min and moved back to the oil bath. 5 mL of 3-bromopropyltrichlorosilane in 15 mL of toluene was added dropwise. The reaction was stirred for 24 h at 80°C. Then the functionalized SNPs were collected by centrifugation. The synthesized nanoparticles were washed five times with toluene and two times with DMF without any drying process.

The functionalized SNPs, which were collected from the last step, were immediately used for the next step and dispersed in 20 mL of DMF under argon in a two necked-round bottom flask. The flask was moved to the oil bath at 80°C for 10 min. Followed by the addition of 80 mL fresh DMF and 2 g of NaN₃. The bromine groups were then converted to azide groups by nucleophilic substitution reaction with NaN₃ in DMF. The reaction was stirred for another 24 h at 80°C. The azide-modified SNPs were recovered by centrifugation at 4500 rpm for 90 min. The particles were washed, by the cycle of centrifugation and re-dispersion, at least three times with water and ethanol. Synthesized particles were characterized by DLS, FT-IR, TGA, and EA. EA indicated that the SNP-N₃ contained 1.5 azide groups per nm² on the surface.

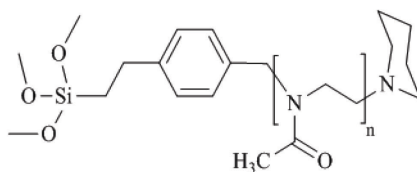
4.4.3 Synthesis of alkyne-functionalized PMeOx (P1)



First Pent-4-ynyl trifluoromethanesulfonate was synthesized, which act as an alkyne-functionalized initiator [238]. Therefore, a solution of 2 g (21.4 mmol, 1 eq.) 4-Penty-1-ol and 1.68 mL (20.76 mmol, 0.97 eq.) pyridine in 15 mL anhydrous dichloromethane (DCM) were added to a cold solution (0°C) of 4.68 mL (27.8 mmol, 1.3 eq.) trifluoromethanesulfonic anhydride in 15 mL DCM. The mixture is stirred at 0°C for 30 minutes under argon atmosphere. The organic phase was washed three times with 15 mL water and consequently a pure and colorless liquid of pent-4-ynyl trifluoromethanesulfonate were obtained after distillation and dried with MgSO₄. ¹H-NMR (500 MHz, CDCl₃): δ (ppm) = 1.99-2.03 (m, *J* = 4.6 Hz, 3H, CH₂-CH₂-C≡CH), 2.38 (dt, *J* = 4 Hz, 2H, CH₂-CH₂-CH₂), 4.67 (t, *J* = 8 Hz, 2H, CH₂-CH₂-O). ¹³C-NMR (500 MHz, CDCl₃): δ (ppm) = 14.4, 27.9, 70.1, 75.6, 81.1, 117.5.

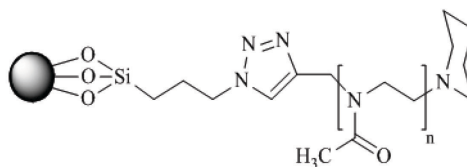
All the polymerizations were carried out in a Schlenk tube under an inert atmosphere (argon) using freshly distilled and dried solvents. To a solution of 141 μl of pent-4-ynyl trifluoromethanesulfonate (0.59 mmol, 1 eq.) in acetonitrile (5 mL), 1.5 mL of 2-methyl-2-oxazoline (17.61 mmol, 30 eq.) was added. The reaction mixture was stirred at 120°C for 5 h. At room temperature, 175 μl of piperidine (1.76 mmol, 3 eq.), which acts as a terminating agent, was added and the reaction mixture was stirred overnight. The solvent and remaining excess of piperidine were removed at reduced pressure. The mixture was diluted with chloroform and precipitated in cold diethyl ether. The product, **P1**, was recovered by centrifugation and dried in vacuum for 24 h. The yield was 93%. ¹H-NMR (500 MHz, CDCl₃, δ): 1.78 (m, 2H, CH₂-CH₂-CH₂), 2.14 (m, 90H, CH₃, MeOX), 2.46 (brs, 2H, C-CH₂-CH₂), 3.47 (m, 120H, CH₂-CH₂, backbone). SEC was used to calculate molecular weight ($\overline{M}_n = 3653 \text{ g mol}^{-1}$) and dispersity (*D* = 1.13).

4.4.4 Synthesis of trimethoxysilane-functionalized PMeOx (P2)



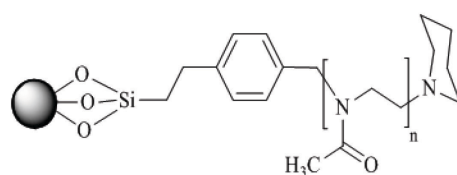
The mixture of 64.4 μl of ((chloromethyl)phenylethyl)trimethoxysilane (CTMS) (0.26 mmol, 1 eq.) and 87 mg of KI (0.53 mmol, 2 eq.) in acetonitrile (5 mL) was sonicated for 1 h in order to the exchange of the chloride anion with iodide anion. Then 670 μl 2-methyl-2-oxazoline (7.87 mmol, 30 eq.) was added to the mixture and the glass tube was heated at the desired temperature (120°C). After 5 h, the mixture cooled down to reach the room temperature and 78.9 μl of piperidine (0.79 mmol, 3 eq.) was added and the reaction mixture was stirred overnight. The solvent and remaining excess of piperidine were removed at reduced pressure. The mixture was diluted with chloroform and precipitated in cold diethyl ether. The product was recovered by centrifugation and dried in vacuum for 24 h. The yield was 89%; however, it is not accurate owing to the presence of KI in the product. It should be noted that the dialysis of the product is not possible owing to the presence of trimethoxysilane groups in the polymer chains. $^1\text{H-NMR}$ (500 MHz, CDCl_3 , δ): 0.98 (brs, 2H, Si- CH_2 - CH_2), 2.15 (m, 93H, CH_3 , MeOx), 2.74 (brs, 2H, CH_2 - CH_2 -C), 3.47 (m, 120H, CH_2 - CH_2 , backbone), 3.57 (s, 9H, Si-O- CH_3), 4.50 (m, 2H, C- CH_2 -N). SEC was used to calculate molecular weight ($\overline{M}_n = 4480 \text{ g mol}^{-1}$) and dispersity ($D = 1.24$). The low D may not be achievable since trimethoxysilane in **P2** is highly reactive and could react in the presence of water/moisture, which may lead to the appearance of a bimodal distribution with a higher polydispersity.

4.4.5 Click coupling between alkyne-functionalized PMeOx and azide-modified SNPs (PSNP-A)



0.2 g (0.05 mmol) of Alkyne-functionalized PMeOx (**P1**) were added to 15 mL of Dimethyl sulfoxide (DMSO) in a round-bottomed flask and stirred for 30 min. 0.05 g of azide-modified SNPs was added and the mixture was sonicated for 1 h. A solution of 0.005 g (0.031 mmol) CuSO₄ in 1 mL of deionized water was added to the prepared mixture. Followed by the addition of a solution contains 0.015 g (0.75 mmol) of sodium ascorbate in 1 mL deionized water. The mixture was heated for 48 h at 50°C. The polymer-shell silica nanoparticles (**PSNP-A**) were recovered by centrifugation at 4500 rpm for 30 min and washed two times with ethanol and two times with deionized water in order to remove unreacted polymers and other impurities. Finally the hybrid particles were dried in vacuum for 24 h and characterized by FT-IR, TGA, TEM, and EA.

4.4.6 Coupling reaction between silane agent PMeOx and SNPs (**PSNP-B**, **PSNP-C**, and **PSNP-D**)



Silane-functionalized PMeOx were grafted on the SNPs through the reaction between silanol groups on the surface of SNPs and alkoxy silane-functionalized polymer to form PSNPs. A series of samples were prepared at different reaction conditions. The last letter in the PSNP abbreviation (B, C, D) refers to different reaction conditions used for coupling **P2** to the surface of SNPs. The composite particles were characterized using FT-IR, TGA, TEM, and EA.

Synthesized SNPs (0.05 g), which were dried in vacuum oven at 70°C for 24 h, dispersed in 15 mL of anhydrous acetonitrile under argon atmosphere. The mixture was sonicated for at least 1 h, followed by the addition of **P2** (0.1 g). The mixture was heated at 80°C for 24 h under vigorous stirring in order to prevent undesirable coupling. After the coupling reaction, composite particles were washed one time with acetonitrile and at least two times with deionized water and then dried under vacuum at room temperature. The hybrid particles synthesized by the aforementioned procedure named **PSNP-B**.

PSNP-C prepared by dispersing SNPs (0.05 g) and polymer chains, **P2** (0.1 g), to the solution contains 25%/75% ethanol and deionized water (2.5 mL ethanol and 7.5 mL

deionized water) and ammonium hydroxide was added to reach the pH of 10, in which methoxy silane groups have almost high hydrolysis and condensation rates [198]. The prepared mixture stirred at room temperature for 24 h and consequently hybrid particles were recovered by centrifugation followed by washing process containing two times with deionized-water and one time with ethanol.

PMeOx coating of SNPs in **PSNP-D** was performed through the formation of a water-in-cyclohexane reverse microemulsion. In other words, reverse microemulsion method for preparation of SNPs and grafting of polymer chains on the surface of SNPs were combined and taken place in the microemulsion, which led to the formation of PSNP. Hence, W/O microemulsion were prepared as it was discussed above and after 24 h, **P2** (0.04 g) were added to the emulsion and stirred for 24 h. Then, acetone was added to disrupt the reverse microemulsion, and the polymer-coated SNPs were collected by centrifugation. The hybrid particles were washed two times with ethanol and one time with deionized-water. This method has two main advantages including shortening the synthesis procedure and less wasting of solvents required for washing process.

4.4.7 Synthesis of Ru(bpy)-doped silica nanoparticles (SNP-Ru(bpy))

Ru(bpy)-doped Silica Nanoparticles (**SNP-Ru(bpy)**) were synthesized using W/O microemulsion method according to a previously reported in the literature [181,182,193]. The reverse microemulsion were prepared by mixing cyclohexane (7.5 mL), n-hexanol (1.8 mL), Triton X-100 (1.77 mL), 0.48 mL of Ru(bpy) dye solution (20 mM in deionized water), and TEOS (0.1 mL). The silica polymerization reaction was initiated by adding 60 μ L of NH_4OH . The reaction was allowed to continue for 24 h at room temperature in dark to prevent photobleaching. Once the polymerization was completed, the synthesized nanoparticles were isolated from microemulsion with acetone and collected by centrifugation. The synthesized **SNP-Ru(bpy)** were washed, by the cycle of centrifugation and re-dispersion, at least three times with ethanol and one time with deionized water to remove all impurities. The synthesized particles were air dried.

4.4.8 Synthesis of PMeOx coated SNP-Ru(bpy) via reverse microemulsion (PSNP-E)

PMeOx coating of **SNP-Ru(bpy)** was performed in the prepared reverse microemulsion. In other words, preparation of SNPs and grafting of polymer chains on the surface of SNPs were combined and taken place in the microemulsion, which led to the formation of **PSNP-E**. Hence, W/O microemulsion were prepared as it was discussed above and after 24 h, PMeOx (0.04 g, n=25) were added to the emulsion and stirred for another 24 h. Then, acetone was added to disrupt the reverse microemulsion, and the polymer-coated **SNP-Ru(bpy)** were collected by centrifugation. The hybrid particles were washed two times with ethanol and one time with methanol.

4.4.9 Synthesis of FITC-doped silica nanoparticles (SNP-FITC)

The **SNP-FITC** was prepared based on Tissandier et al., [146]. Hence, the fluorescence solution was first prepared by dissolution of dye molecules, fluorescein isothiocyanate (FITC, 3 mg), in (3-Aminopropyl)trimethoxysilane (APTMS, 40 μ l). The solution was stirred for 12 h at room temperature in dark under argon environment. Then reverse microemulsion was prepared by mixing cyclohexane (9.6 mL), n-hexanol (2.3 mL), Triton X-100 (2.3 mL), and water (0.6 mL). The emulsion was stirred for 5 min and consequently the prepared fluorescence solution and TEOS (0.13 mL) were added to the flask. After 30 min, TEOS (0.03 mL) was added to the microemulsion followed by 24 h stirring at room temperature in dark. The microemulsion was broken as it was discussed earlier.

4.4.10 Synthesis of PMeOx coated SNP-FITC via reverse microemulsion (PSNP-F)

To the above microemulsion PMeOx (0.04 g, n=23) was added followed by 24 h stirring. Then the polymer-coated **SNP-FITC** were collected by centrifugation. The hybrid particles were washed two times with ethanol and one time with methanol.

Chapter 5. Synthesis of Polyoxazoline-Silica Hybrid Nanoparticles via “Grafting from” Approach*

** Part of this chapter has been published in Journal of Polymer Chemistry, 7 (2016) 5157-5168*

5.1 Introduction

The surface modification of inorganic nanoparticles such as silica with a polymeric shell has recently attracted enormous attention. This attention is owed to their tunable surface properties, which makes them promising candidates in the biomedical application for diagnostics and drug delivery [1,30,34,35]. The stability and grafting density of the tethered polymer layer are two main factors that need to be considered during the synthesis of such hybrid nanoparticles. Among various approaches that can be used for surface modification, the “grafting from” approach is the most promising, as it leads to great stability of the polymer chains due to covalent binding of the polymeric modifiers onto the inorganic particles and a high grafting density. This approach is mainly based on the immobilization of initiators on the surface of the substrate followed by the polymerization of the monomer from the surface and various polymerization methods that can be used for controlled surface-initiated polymerization [154,188]. Compared to the “grafting to” and “grafting through” approaches, in which the steric barrier to incoming polymers is imposed by the grafted chains, the “grafting from” approach does not affect the accessibility of smaller molecules such as monomers to the active initiation sites, leading to a high grafting density [13,199]. Moreover, by using the “grafting from” approach a larger thickness of the fabricated polymer layer can be achieved compared to the “grafting to” approach [151]. Among various polymers used for biomedical application, poly(2-oxazoline) (POx) is one of the most promising polymers that can be used for the surface modification of the particles due to its biocompatibility, tunable solubility, and chemical functionality [104,200,201]. Hence, hybrid nanoparticles that contain a silica core and a water-soluble poly(2-methyl-2-oxazoline) (PMeOx) shell could be a promising candidate in bioscience [23–25].

Despite the fact that “grafting from” is the most promising approach for surface modification, surprisingly, surface-initiated polymerization has not been extensively explored for the modification of silica particles with POx chains. In 1994 Yoshinga et al.

first reported the cationic graft-polymerization of 2-methyl-2-oxazoline on polymer coated silica particles. The p-nitro benzenesulfonate group was immobilized on the surface of polystyrene-coated silica particles, which can initiate the CROP of MeOx. The results indicated the dragging out of the grafted polymer due to the lack of cross-linking in the copolymer layer. Therefore, trimethoxysilane-terminated poly(maleic anhydride-styrene) were used to address this problem; however, the polymerization did not proceed in the propagation [202]. Later, in 2008, Ueda et al. reported the synthesis of graft-polymerization of MeOx from the surface of SNPs in a solvent-free dry-system and solution system. As an initiator, 3-iodopropyltrimethoxysilane was used, which immobilized on the surface of SNPs at a high temperature (250°C) in the solvent-free dry-system. The introduced iodopropyl groups initiated the CROP of MeOx. Their results indicate that the solvent-free dry-system is the more promising method compared to solution system since in solution system only a 0.5% conversion was obtained after a 2 h polymerization time, while the conversion significantly increased to 98.8% in the solvent-free dry-system. However, no further characterizations of the polymer chains and grafting density were reported [203].

There are also few contributions focusing on coating silica surfaces with POx via the “grafting from” approach by using silane-functionalized initiators including tosylate initiator [204], 1-bromopropyltrichlorosilane [205], and 3-iodopropyltrimethoxysilane [206] for different applications. Although they confirm the polymerization of the 2-oxazoline monomers on the surfaces via transmission electron microscopy (TEM) and scanning electron microscope (SEM), in all of these reports the lack of polymer chain characterization could be clearly seen. Surface-initiated living cationic polymerization of 2-oxazoline on different substrates have been greatly investigated. For example, polymerization of 2-ethyl-2-oxazoline (EtOx) was carried out from flat gold surfaces and gold NPs by Jordan et al., in which a self-assembled monolayer of 11-hydroxyundecanethiolate was formed on the gold surface followed by the substitution of hydroxyl group into the triflate group in the presence of a medium stream of trifluoromethanesulfonic anhydride, and consequently the polymerization of the monomer [188,207]. Bayramgolu et al. also reported the surface-initiated polymerization of MeOx from bromide-functionalized methacrylate-based cross-linked microspheres [208]. The surface-initiated polymerization of 2-isopropenyl-2-oxazoline (IPOx) was also carried out on glassy carbon by Zhang et al. in 2009 [209]. The IPOx monomer contains two polymerizable groups, namely the 2-oxazoline ring for CROP and a vinyl group for

either living anionic or radical polymerization. First, poly(2-isopropenyl-2-oxazoline) brushes were formed on the surface of glassy carbon by self-initiated photografting and photopolymerization of IPOx with UV-light. This was followed by submerging the substrate in a solution of methyl trifluoromethane sulfonate (MeOTf) in acetonitrile and then into a solution of 2-oxazoline monomer in acetonitrile [209]. In 2012, they reported the surface-initiated polymerization of IPOx on 3-aminopropyltrimethoxysilane-modified silicon substrates [210].

This chapter mainly focuses on the synthesis of PMeOx-coated SNPs via the “grafting from” approach. An appropriate initiator was first immobilized on the surface of SNPs followed by CROP of 2-methyl-2-oxazoline from the particle’s surface (Figure 5.1). The versatility of this method was further investigated by terminating the polymer chains with different functional groups such as amine moieties, which can be subsequently used to modify the particle surface with fluorescent probes such as fluorescein (FITC) or targeting molecules such as folic acid (FA). Finally, the formation of SNPs containing fluorescent dyes in the silica core coated with hydrophilic polymer chains (PMeOx) was studied.

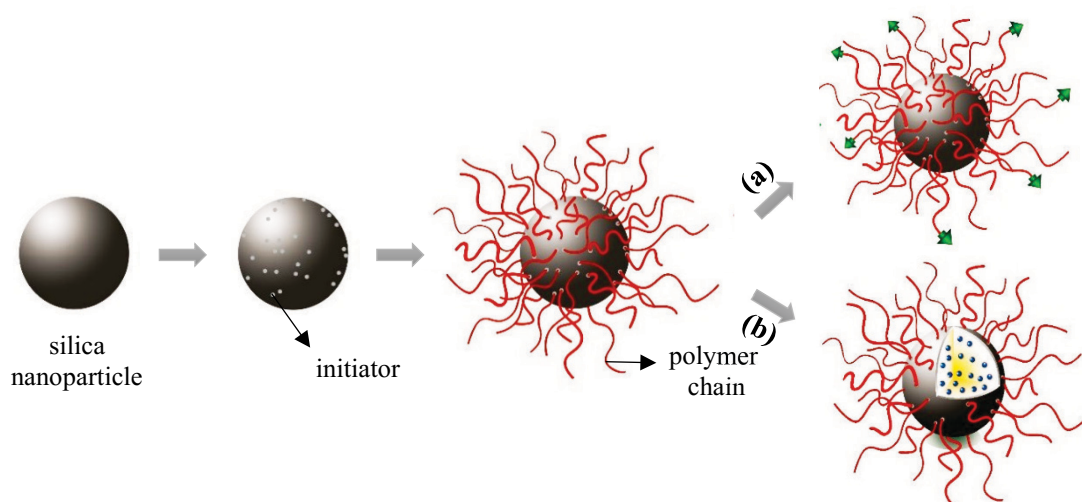


Figure 5.1 Schematic strategy for the synthesis of PMeOx-coated SNPs using “grafting-from” approach followed by further functionalization of the hybrid nanoparticle via (a) the functionalization of the polymer chains or (b) doping fluorescent dye molecules in the core of the hybrid nanoparticle.

5.2 Results and discussion

The preparation of polymer-coated NPs with high grafting densities can be achieved by using the “grafting from” approach [154,157–164,211–213]. This method requires a bifunctional initiator, with one function to immobilize on the surface of SNPs and another function to initiate the polymerization [153]. Moreover, it is well-known that the initiator characteristics can strongly affect the polymerization mechanism of 2-oxazoline in order to induce homogeneous growth of the polymer chains [159]. In this chapter, surface-initiated polymerization of MeOx is investigated by using two different initiators.

5.2.1 Synthesis of the PMeOx-coated SNP via “grafting from” approach using 4-(bromomethyl)benzoic acid as an initiator

One approach for fabrication of PMeOx-coated SNPs is the immobilization of 4-(bromomethyl)benzoic acid (BMBA) as an initiator on the surface of SNPs. Hence, it requires to be immobilized on the surface of SNPs to form **SNP-BMBA**. The synthesis of **SNP-BMBA** contains a two-step reaction: (i) amino modification of SNPs with (3-aminopropyl)triethoxysilane (APTES) via a silane coupling reaction to form **SNP-NH₂**; (ii) introduction of benzyl bromide to the surface of the amine-functionalized silica core (Figure 5.2).

The successful immobilization of BMBA on the surface of SNPs was investigated by FT-IR and TGA, which are shown in Figure 5.3. The FT-IR spectrum of the neat SNPs shows three characteristic absorption bands arising from the symmetric vibration of Si–O, asymmetric vibration of Si–OH, and asymmetric vibration of Si–O at 795, 935, and 1100 cm^{-1} , respectively [183]. The adsorption peak at 1690 cm^{-1} , which can be clearly seen in the enlarged spectra of Figure 5.3-a, indicated the characteristic vibrations of the carbonyl (C=O stretching) groups of the BMBA molecule in **SNP-BMBA**. Moreover, TGA analysis showed a mass loss of 12.7%, 16.7%, and 17.3% for SNPs, **SNP-NH₂**, and **SNP-BMBA**, respectively. The additional mass loss of the modified SNPs compared to neat SNPs verify the successful modification step of the silica surface.

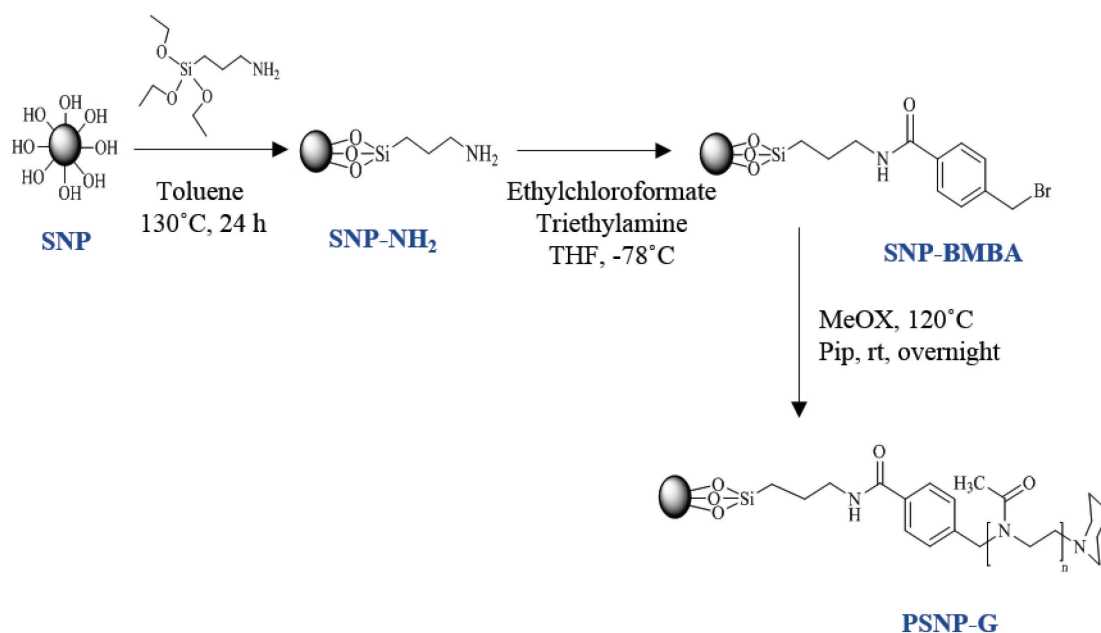


Figure 5.2 Reaction scheme for the synthesis of poly(2-methyl-2-oxazoline)-silica hybrid nanoparticles by means of surface-initiated cationic ring opening polymerization using 4-(bromomethyl)benzoic acid (BMBA) as an initiator.

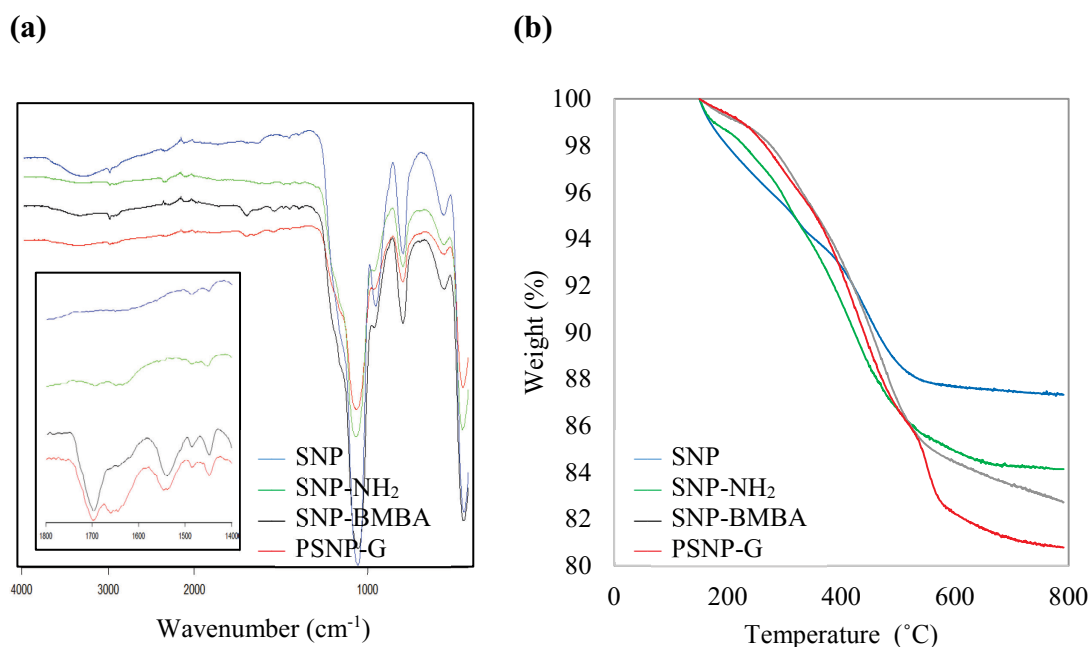


Figure 5.3 (a) FT-IR spectra of SNP, SNP-NH₂, SNP-BMBA, and PSNP-G (b) TGA of SNP, SNP-NH₂, SNP-BMBA, and PSNP-G.

The benzyl bromide groups on the surface of silica core were used to initiate the CROP of MeOx. The FT-IR spectra of **PSNP-G** indicates the appearance of a small peak at 1639 cm^{-1} corresponding to the stretch band of the amide backbone of the grafted PMeOx [186,187], and TGA illustrates an additional mass loss of 2% for **PSNP-G** compared to **SNP-BMBA**. However, the intensity of the FT-IR peak and the mass loss suggest that the polymerization of MeOx was not taken place appropriately, which can be explained due to the low concentration of the immobilized initiator on the surface of core. Considering, the essential effect of the initiator concentration immobilized on the surface of SNPs on grafting density of the polymer chains, this protocol suffers from the difficulty and low-efficiency of the multi-step synthesis. To be more precise, the amino modification of SNPs via silane coupling reaction is a very-well known procedure [86,214] and the TGA results (Figure 5.3-b) also indicated the successful immobilization of amine groups on the surface of SNPs. Therefore, the unsuccessful polymerization of MeOx may arise from the insufficient introduction of benzyl bromide to the surface of the amine-functionalized silica core.

5.2.2 Synthesis of the PMeOx-coated SNP via “grafting from” approach using ((chloromethyl)phenylethyl)trimethoxysilane as an initiator

The grafting density of the hybrid particles prepared by the “grafting from” approach depends largely on the number of initiators on the surface of SNPs; however, it should be noted that all the initiators cannot initiate the polymerization. The obtained results from the former part identify the dependency of the grafting density in hybrid particles on the number of available functional groups immobilized on the surface of SNPs. Since different steps of modification are required, it is not easy to achieve a high grafting density in the hybrid particles. Hence, one method to enhance the number of initiators on the particle surface, is through the direct incorporation of an appropriate initiator on the surface of the SNPs by using a silane agent that contains already an initiator group, which can be directly grafted on the surface of bare silica NPs and also could initiate a cationic ring opening polymerization of 2-methyl-2-oxazoline (MeOx). For this purpose, ((chloromethyl)phenylethyl)trimethoxysilane (CTMS) was used as an initiator. Since benzyl chloride groups have a low reactivity even at longer polymerization times and high temperatures, the addition of a co-initiator (potassium iodide, KI) can

enhance the monomer conversion by the exchange of the chloride anion with the one that has a lower nucleophilicity [106]. This part is divided into three sections:

- (i) Synthesis and characterization of polyoxazoline-silica hybrid nanoparticles and the study of the effect of reaction time and monomer concentration on the grafting density of the synthesized hybrid nanoparticles.
- (ii) Immobilization of fluorescein isothiocyanate (FITC) and/or folic acid (FA) on the surface of the functionalized-hybrid nanoparticles as a fluorescent imaging labeling and targeting ligand in biomedical applications, respectively (Figure 5.4).
- (iii) The preparation of hybrid nanoparticles containing a fluorescent dye molecules in the SNP core modified with a dense PMeOx shell.

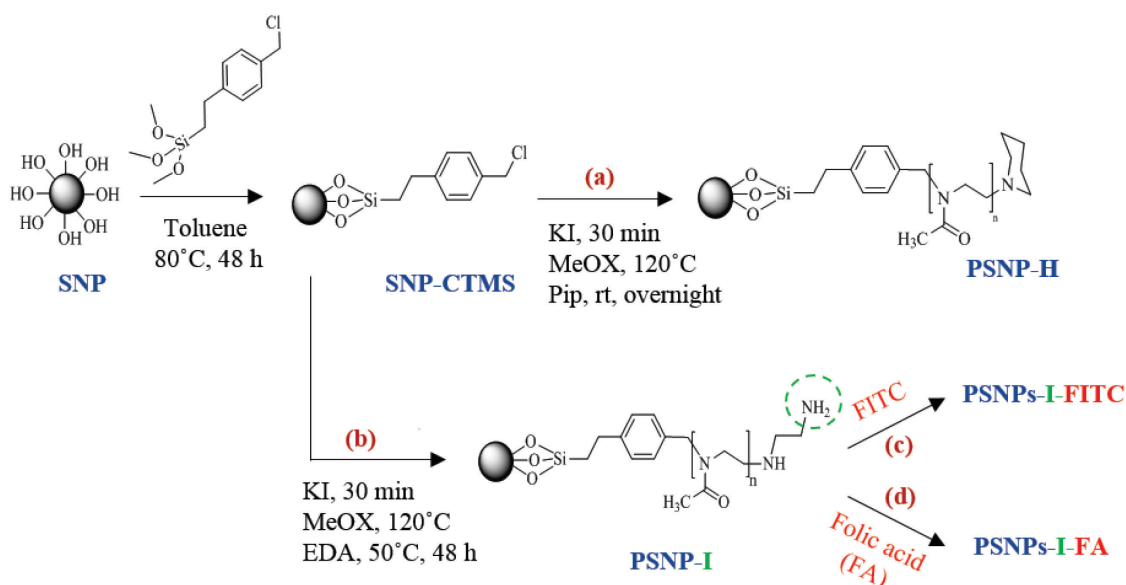


Figure 5.4 Synthesis of poly(2-methyl-2-oxazoline)-silica hybrid nanoparticles, **(a)** by means of surface-initiated cationic ring-opening polymerization using((chloromethyl)phenylethyl)trimethoxysilane (CTMS) as an initiator, **(b)** using different terminating agents for subsequent particle modification with **(c)** fluorescein (FITC) and **(d)** folic acid (FA).

5.2.2.1 Immobilization of CTM on the surface of SNPs

Silica nanoparticles (SNPs) were first synthesized as an inorganic core using reverse microemulsion. The diameter of the synthesized particles were measured by DLS, which was 57 ± 3 (nm) with a PDI of 0.09. The obtained particle sizes were in good

agreement with TEM measurements where the diameter of about 50 particles in TEM images were randomly calculated via ImageJ software and averaged to be about 53 ± 2 (nm). SNPs were initially modified with CTMS via a silane coupling reaction between hydroxyl groups on the surface of the particles and trimethoxysilane of the CTMS. The elimination of the unreacted free CTMS from the grafted silica was carried out by a series of centrifugations and the dispersion of the nanoparticles in anhydrous toluene. At least three series of washing process were necessary for complete elimination of unreacted CTMS since the UV-Vis spectrum of the supernatant in the third centrifugation indicated the absence of absorption at a wavelength of 220 nm. The successful modification of SNPs was verified by comparing the FT-IR spectra of SNP and **SNP-CTMS** (Figure 5.5-a). The immobilization of CTMS on the surface of SNPs was confirmed by the presence of two additional characteristic peaks at 1627 and 713 cm^{-1} corresponding to the stretching of the C=C [215] and C-Cl [216], respectively.

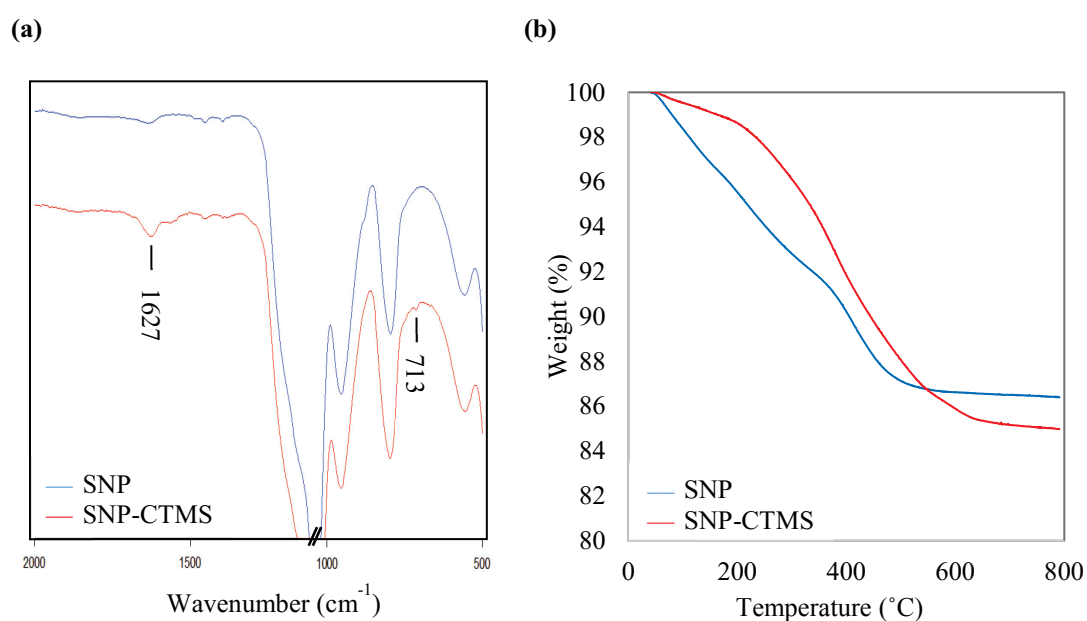


Figure 5.5 (a) FT-IR spectra of the SNP and **SNP-CTMS** **(b)** TGA of SNP and **SNP-CTMS**.

TGA was performed in a nitrogen environment to investigate the mass loss of bare SNP and **SNP-CTMS** as a function of temperature. The immobilization of CTMS on the surface of SNPs was confirmed by indicating an additional mass loss of 1.4% (Figure 5.5-b). Moreover, the surface grafting density of the 4 groups/ nm^2 (0.47 mmol of initiator/g of silica) was calculated for **SNP-CTMS** based on the presence of chlorine (1.43%) using

elemental analysis. Regarding the size and morphology of the nanoparticles, TEM image indicated the morphology of the **SNP-CTMS** remained without any aggregation similar to the bare SNPs and their sizes were calculated around 54.2 ± 1.2 nm (Figure 5.6).

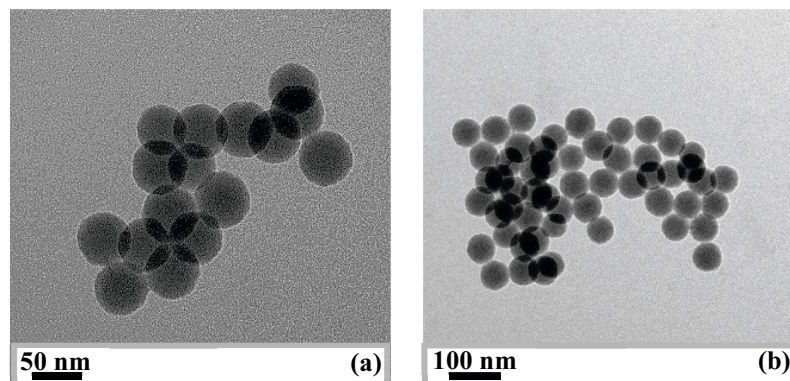


Figure 5.6 TEM images of (a,b) **SNP-CTMS**.

The synthetic strategy for the fabrication of PMeOx-coated SNPs is shown in Figure 5.4. The benzyl chloride groups of the covalently attached CTMS on the nanoparticle surface were used to initiate the cationic ring opening polymerization of MeOx, however, the addition of potassium iodide (KI) is necessary to increase the reactivity of the initiator [106]. Consequently, two series of hybrid nanoparticles (**PSNP-H**) were synthesized and characterized to investigate the effect of two important synthesis parameters, polymerization time and monomer/initiator ratio concentration, on grafting density of the synthesized PMeOx-coated SNPs, respectively.

5.2.2.2 Reaction time effect

The effect of polymerization time on grafting density was investigated by performing the polymerization of MeOx from the surface of the nanoparticles (**SNP-CTMS**) for various reaction times. Therefore, three samples of **PSNP-H-1**, **PSNP-H-2**, and **PSNP-H-3** were prepared at different polymerization times of 1, 3, and 7 h, respectively. Figure 5.7-a illustrates the FT-IR spectra of SNPs, **PSNP-H-1**, **PSNP-H-2**, and **PSNP-H-3**. The FT-IR spectra of all the trials performed exhibited the successful polymerization of MeOx and the formation of the hybrid nanoparticles due to the

appearance of an amide carboxyl peak (1622 cm^{-1}), which corresponds to the carbonyl stretching mode of the amide backbone of the grafted PMeOx chain and the peak at around 1430 cm^{-1} , which is assigned to CH_x deformation mode of PMeOx [210] (Figure 5.7-a). TEM was used to support the hypothesis of formation of a homogenous and dense polymeric shell. In hybrid nanoparticles, the silica core appeared darker than the grafted polymeric shell due to the difference in density. Figure 5.8 shows the TEM image of **PSNP-H-1**, **PSNP-H-2**, and **PSNP-H-3**. The polymeric shell can be clearly identified for the hybrid nanoparticles, and the particle sizes calculated by ImageJ software suggest a controlled growth of the grafted polymer chains. Therefore, it can be reasonably assumed that well-defined hybrid nanoparticles consisting of a silica core surrounded by a dense polymer layer have been synthesized. The polymeric shell thickness can be calculated by comparing the particles size before and after the polymerization of MeOx (Table 5.1). The identification of the polymeric shell in TEM images of the hybrid nanoparticles with a low polymer content is not obvious due to the low DP_n of the grafted PMeOx and collapsing of the polymer chains in the vicinity of the silica surface upon drying [217]. In contrast, the polymeric shell is clearly identified for the hybrid nanoparticles with a high grafting density such as **PSNP-H-3** (Figure 5.8).

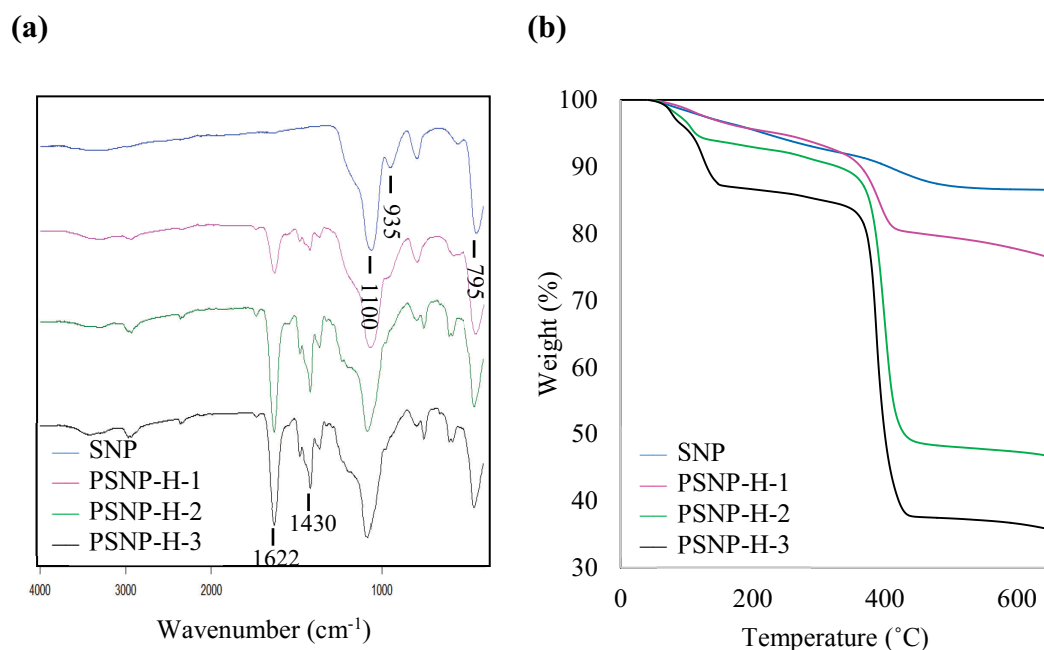


Figure 5.7 (a) FT-IR spectra of SNP, **PSNP-H-1**, **PSNP-H-2**, and **PSNP-H-3** **(b)** TGA of SNP, **PSNP-H-1**, **PSNP-H-2**, and **PSNP-H-3**.

TGA was performed to study the grafting density of the hybrid nanoparticles. The mass loss of the bare SNPs and three trials of **PSNP-H** as a function of temperature is presented in Figure 5.7-b. The mass loss between 40 and 150°C can be attributed to the solvents that are not completely eliminated after the drying process [153]. However, the weight loss between 150 to 500°C in the case of PSNPs corresponds to the decomposition of the PMeOx layer. TGA results indicated an additional mass loss of 22.3, 52.6, and 63.4 % for **PSNP-H-1**, **PSNP-H-2**, and **PSNP-H-3**, respectively. This suggests an increase in polymer content by increasing the reaction time. The grafted polymer chains were not physically adsorbed but chemically bonded to the silica surface since there is no free initiator in the polymerization mixture and MeOx has the only possibility to be polymerized from the surface of the particles. The results of elemental analysis for these three samples are listed in Table 5.2. As it was expected, the content of carbon and nitrogen increased significantly with increasing the polymerization time. Moreover, **PSNP-H-1** indicated that after 1 h, MeOx could polymerize from the surface of SNPs using CTMS as an initiator; however, Ueda et al. reported very low conversion in the solution system by using iodopropyl group as an initiator on the surface of SNPs [203].

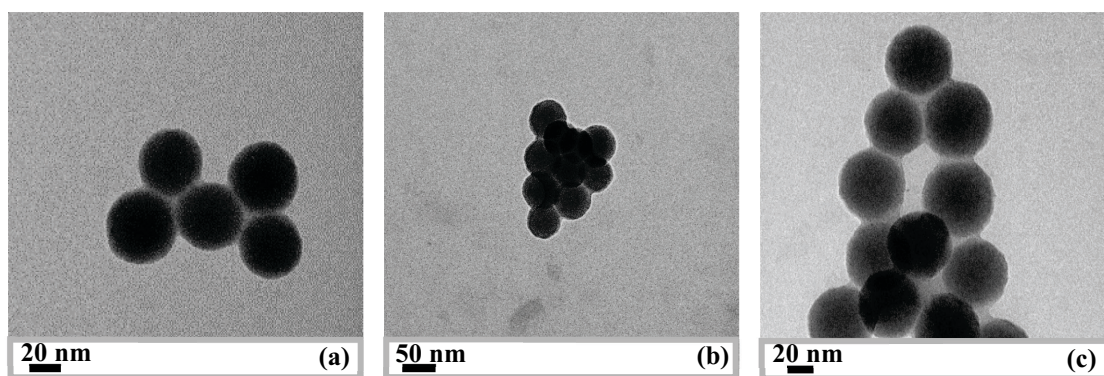


Figure 5.8 TEM images of (a) **PSNP-H-1**, (b) **PSNP-H-2**, and (c) **PSNP-H-3**.

In order to gain information regarding the molecular weight of the grafted PMeOx, sodium hydroxide solution was used to etch the silica core from the polymeric shell. Complete etching of the SNPs was confirmed by the disappearance of the three main characteristic peaks of SNPs at 1100, 935, and 795 cm^{-1} . Subsequently, the polymeric chains were further analyzed with size exclusion chromatography (SEC)

(Table 5.2). The results showed that the polymerization of the PMeOx proceeded in a controlled manner, showing increasing molecular weights with the increase in reaction time, as determined by SEC. This was consistent with literature results for the effect of reaction time on the chain length of the grafted polymer on the surface of the inorganic core [218]. The molecular weight distribution of the grafted polymer remained relatively low ($\bar{D} < 1.24$) with monomodal distribution, indicating a living polymerization process with excellent control over molecular weight during the polymerization. The amount of polymer immobilized on the SNP surface, Γ_{PMeOx} , was calculated based on TGA results using eq. 7-1 and the results are summarized in Table 5.2. It is obvious that a longer polymerization time led to higher polymer contents. The amount of polymer per SNP surface area increased from 1.42 to 12.66 mg m⁻² when the reaction time increased from 1 to 7 h.

Table 5.1 Shell thickness of the PMeOx-coated SNPs by varying time reaction and monomer/initiator ratio concentration.

Particle code	Polymerization time (h)	[CTMS]:[MeOx]	Surface grafting density ^a (groups/nm ²)	Polymeric layer thickness ^b (nm)
PSNP-H-1	1	excess MeOx	1.47	1.33 ± 0.5
PSNP-H-2	3	excess MeOx	1.49	2.8 ± 0.7
PSNP-H-3	7	excess MeOx	1.43	2.6 ± 0.3
PSNP-H-4	24	1:5	0.51	0.41 ± 0.4
PSNP-H-5	24	1:20	0.48	1.39 ± 0.4
PSNP-H-6	24	1:40	1.23	3.05 ± 0.6

^a determined from elemental analysis; ^b determined from the particle size before and after grafting using TEM and ImageJ software.

Table 5.2 Analytical data from PMeOx grafted from the silica nanoparticles surface.

Particle code	M_n^a (g mol ⁻¹)	M_w^a (g mol ⁻¹)	\bar{D}^a	Mass loss ^b (%)	Γ_{PMeOx}^c (mg m ⁻²)	C ^d (%)	N ^d (%)
PSNP-H-1	2398	2542	1.06	22.32	1.42	24.07	3.94
PSNP-H-2	4255	5106	1.20	52.65	10.43	31.54	7.63
PSNP-H-3	6473	8030	1.24	63.41	12.66	36.83	9.23
PSNP-H-4	2327	2443	1.05	14.43	0.33	14.23	2.87
PSNP-H-5	3811	4344	1.14	31.54	4.08	16.22	3.01
PSNP-H-6	5207	6404	1.23	41.51	5.99	31.82	8.50

^a determined by size exclusion chromatography (SEC) in DMF with 5 g L⁻¹ LiBr at T=60°C; ^b mass loss data determined from the TGA; ^c calculated from the mass loss data using eq. 7-1; ^d determined from the elemental analysis of modified SNPs.

5.2.2.3 Monomer concentration effect

The monomer/initiator ratio concentration has been reported to be a very important parameter that can greatly affect the grafting density in the “grafting from” approach [217]. Therefore, the effect of the monomer/initiator ratio concentration was investigated by preparing three hybrid nanoparticles, **PSNP-H-4**, **PSNP-H-5**, and **PSNP-H-6**, with ratios of initiator: MeOx of 1:5, 1:20, and 1:40, respectively (Table 1). The FT-IR spectra indicate the presence of two characteristic bonds of PMeOx at 1622 and 1430 cm^{-1} in all three synthesized hybrid nanoparticles (Figure 5.9-a). It is evident that TGA results are in excellent agreement with FT-IR since the formation of the polymer shell was confirmed by showing greater mass loss for hybrid nanoparticles compared to bare SNPs (Figure 5.9-b). Data of the thermal analysis are given in Table 5.2. As it was expected, the mass loss that was attributed to decomposition of the organic polymer shell increased correspondingly from 14.43 to 41.15% by increasing the monomer concentration from **PSNP-H-4** to **PSNP-H-6**. The observed trend can be associated with a larger polymer amount per particle surface area, Γ_{PMeOx} , of the polymeric shell by increasing the monomer/initiator ratio concentration in the synthesis protocol. The elemental analysis results were also in good agreement with TGA results by indicating proportional increase in carbon and nitrogen content by increasing the monomer concentration (Table 5.2). Table 2 summarizes the M_n of the PMeOx grafted on the surface of SNPs, which indicates that this parameter increases proportionally by increasing the monomer concentration, and leads to the formation of longer polymeric chains. However, D_s of the grafted polymer chains are still narrow with values of 1.06 to 1.23, and SEC data confirm the monomodal molar mass distribution. Figure 5.10 represents TEM image of **PSNP-H-4**, **PSNP-H-5**, and **PSNP-H-6**. Consequently, the thickness of the polymeric shell increased from 0.41 to 3.05 nm by increasing the monomer concentration (Table 5.1).

In conclusion, a greater grafting density with better control can be achieved by using the “grafting-from” approach. The grafting densities were calculated based on the carbon content determined by elemental analysis and gave values of 1.43–1.49 groups/ nm^2 for **PSNP-H-1** to **PSNP-H-3** and 1.23 groups/ nm^2 for **PSNP-H-6**. It is interesting to note that the grafting density was only around 0.5 groups/ nm^2 at lower ratio of initiator:monomer of 1:5 (**PSNP-H-4**) and 1:20 (**PSNP-H-5**) most likely due incomplete exchange of chloride by iodide. The results indicate that the obtained grafting

densities from the “grafting-from” approach are at least three times higher than the best result obtained by the “grafting-to” method, where values of 0.183 to 0.459 groups/nm² were obtained.

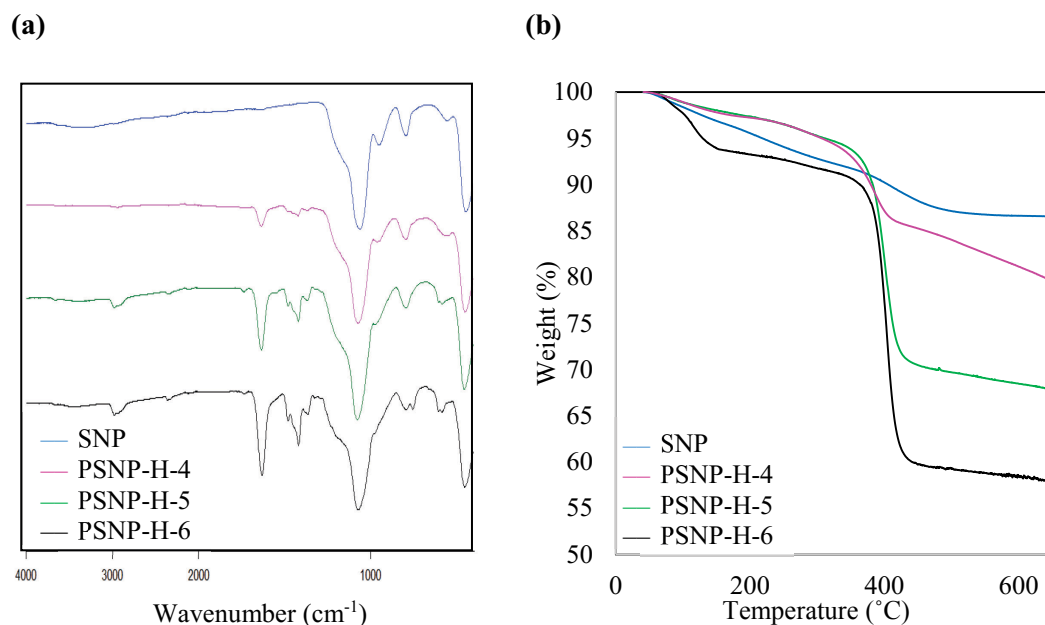


Figure 5.9 (a) FT-IR spectra of SNP, PSNP-H-4, PSNP-H-5, and PSNP-H-6 **(b)** TGA of SNP, PSNP-H-4, PSNP-H-5, and PSNP-H-6.

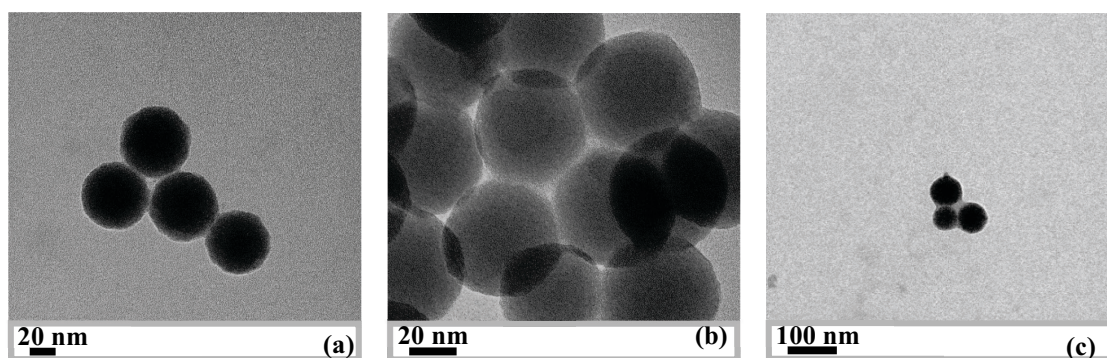


Figure 5.10 TEM images of (a) PSNP-H-4, (b) PSNP-H-5, and (c) PSNP-H-6.

5.2.2.4 Conjugation of folate and/or FITC to polymer-grafted-Silica nanoparticles

One of the main advantages of the living cationic polymerization of 2-oxazolines is the possibility to be chemically functionalized [219]. Therefore, different terminating

agents can be used to functionalize the surface of the synthesized hybrid nanoparticles. In this study, the surface of the hybrid nanoparticles were functionalized with amine groups, which subsequently were reacted with fluorescein isothiocyanate (FITC) as a fluorescence imaging molecule or cancer-targeting ligands such as folic acid (FA) (Figure 5.11) [220]. The amine-functionalized PSNPs were prepared by the “grafting from” method using ethylene diamine (EDA) as a terminating agent (**PSNP-I**). The presence of amine groups on the surface of hybrid nanoparticles was confirmed by the ninhydrin test since ninhydrin can react with a terminal primary amine on the particles surface and produce a purple-blue complex (Ruthemann’s purple). Moreover, the UV-Vis spectroscopy indicated an absorption peak of the formed complex at 588 nm (Figure 5.12) [221,222]. It should be noted that the formation of the complex is not due to the unreacted EDA since the prepared sample was dialyzed against water for 48 h. Moreover, the pre-test was carried out to confirm the removal of the free EDA by dispersing the **PSNP-I** in ethanol followed by centrifugation and consequently the purple complex was not observed in the supernatant. Figure 5.11 outlines the reaction pathway for the bioconjugation of FA and FITC on the surface of the hybrid nanoparticles in order to fabricate **PSNP-I-FA** and **PSNP-I-FITC**, respectively.

The successful conjugation of **PSNP-I** with FITC and FA molecules was confirmed by comparing the UV-Vis absorption spectra of **PSNP-I** with **PSNP-I-FA** and **PSNP-I-FITC**, which indicates additional peaks at 482 and 360 nm, respectively (Figure 5.13). The concentration of the FA and FITC can be determined by the UV-Vis analysis. Therefore, the absorbance of a series of standard solutions containing FITC and FA at different known concentrations, encompassing the sample concentrations, were measured in PBS buffer and DMSO, respectively. The calibration graphs were prepared (Appendix 10.5) and further used to calculate the concentration of FITC and FA conjugated on the surface of the aminated-hybrid nanoparticle. According to the calibration curves, 0.632 ± 0.066 and $0.1005 \pm 0.003 \mu\text{mol mL}^{-1}$ of FITC and FA were conjugated on the surface of 1 mg mL^{-1} of **PSNP-I**. It was found that the concentration of the conjugated FITC is greater than folate, which can be explained due to the higher reactivity of isothiocyanate group in FITC than the carboxylic acid group in FA.

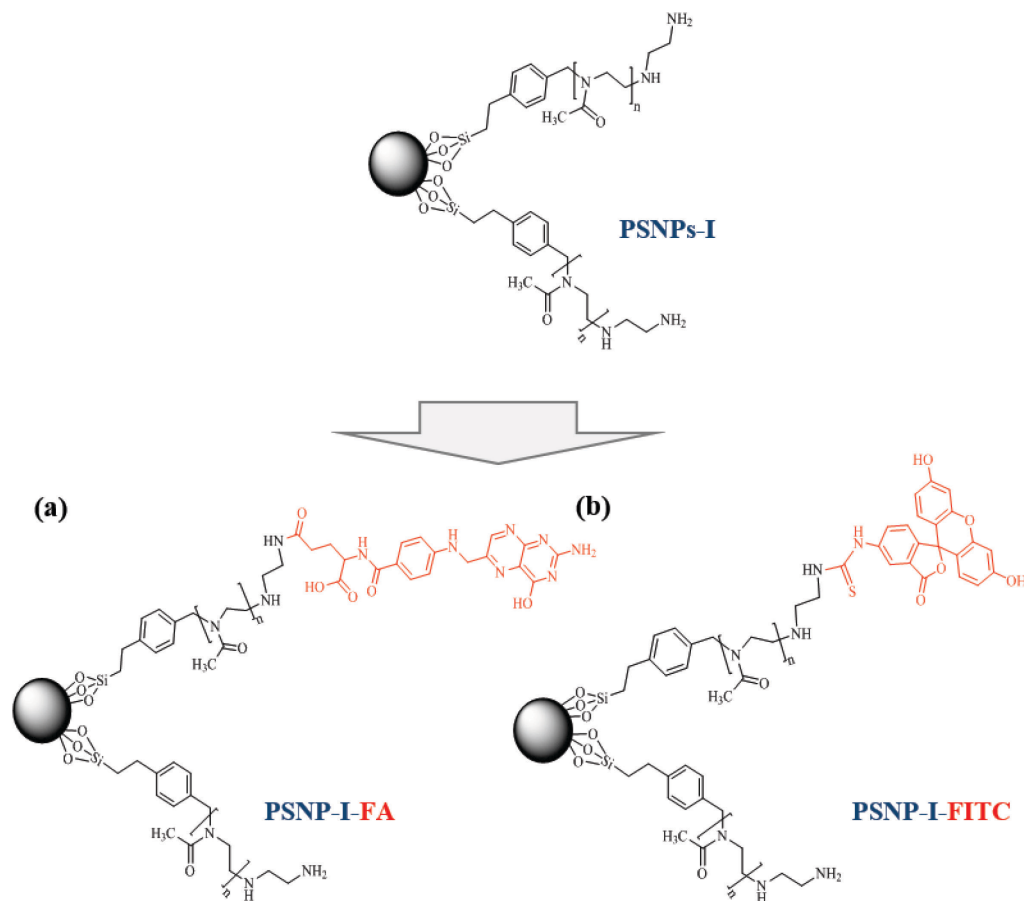


Figure 5.11 Schematic representation of the modification sequence of PMeOx-silica hybrid nanoparticles functionalized with amine groups (**PSNP-I**) conjugated with: **(a)** folic acid, **PSNP-I-FA**, and **(b)** fluorescein isothiocyanate, **PSNP-I-FITC**.

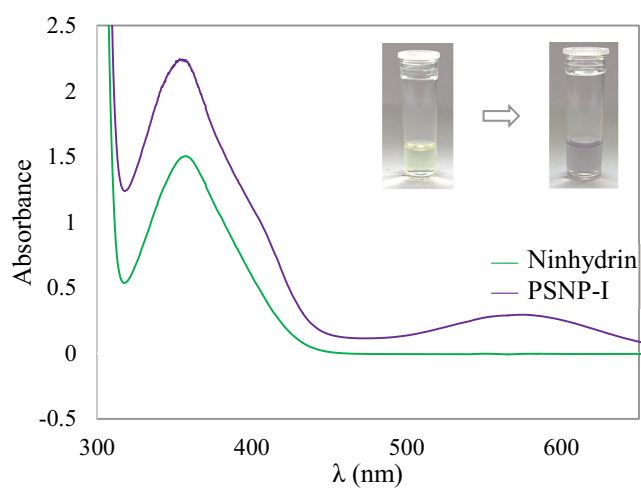


Figure 5.12 UV-Vis absorption spectra of ninhydrin and **PSNP-I**.

Although FA modification of SNPs makes the nanoparticles selective for cancerous cells due to the overexpression of folate receptors on the surface of cancerous cells [223], FA molecules can aggregate at high concentration and consequently inhibit binding to the folate receptors [224,225]. In order to address this problem and achieve greater efficiency of interactions between FA-modified nanoparticles and the cell-surface receptors, low concentration of FA on the surface of particles is required [225]. As an example, Destito et al. synthesized FA-modified particles with FA concentration of $10 \mu\text{mol L}^{-1}$ and reported that these particles are effectively targeted to the folate receptors [225]. Therefore, the concentration of FA on the surface of **PSNP-I-FA** is sufficient and no further concentration is required.

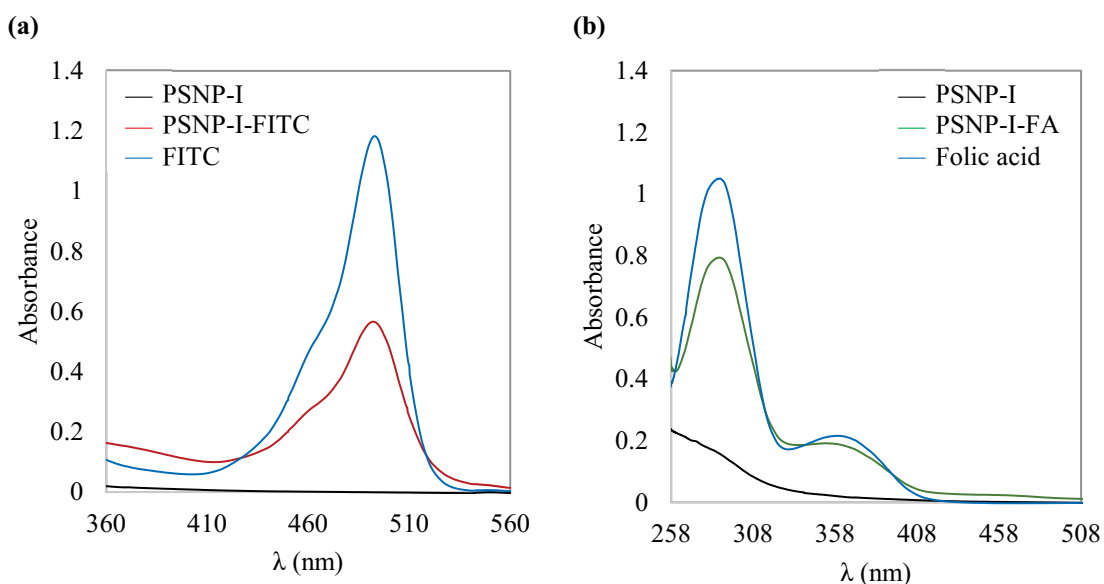


Figure 5.13 UV-Vis absorption spectra of (a) **PSNP-I**, **PSNP-I-FITC**, and bare FITC (b) **PSNP-I**, **PSNP-I-FA**, and pure FA.

To further verify the presence of FITC or FA on the surface of **PSNP-I**, FT-IR spectroscopy analysis was performed. Figure 5.14 illustrates a comparison between the FT-IR spectra of **PSNP-I**, **PSNP-I-FITC**, and **PSNP-I-FA**. As was already mentioned, the formation of a PMeOx shell on the surface of SNPs leads to the appearance of a characteristic peak of amide at around 1622 cm^{-1} as well as a broad peak owing to the CH_3 group at 1430 cm^{-1} . In FT-IR spectrum of **PSNP-I-FITC**, no peak appeared at 2100 cm^{-1} , which was assigned to the $\text{N}=\text{C}=\text{S}$ vibrational mode of the free FITC molecules [196]. In contrast, the UV-Vis indicated the presence of the FITC dye on the surface of

hybrid nanoparticles. These two analysis methods suggest the formation of the thiourea bond and successful conjugation of FITC with the amine group on the surface of hybrid nanoparticles, while the signal of the thiourea bond cannot be easily detected due to the overlapping with the amide peak in the polymer chains. As shown in the enlarged spectra of Figure 5.14, a broad peak was observed at around 1510 cm^{-1} for **PSNP-I-FA**, which corresponds to the absorption band of the benzene loop backbone of folate [226,227]. Moreover, the peak assigned for carbonyl stretching of amides with pure folic acid appear at 1610 cm^{-1} [228]. Altogether, the results of the UV-Vis analysis and FT-IR spectroscopy confirmed the presence of conjugated FA and FITC on **PSNP-I-FA** and **PSNP-I-FITC**, respectively.

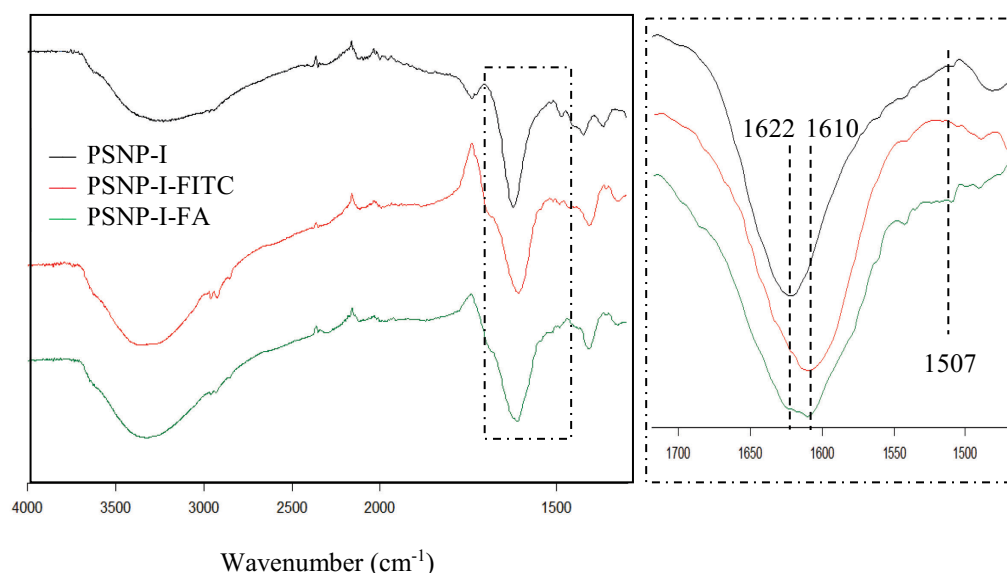


Figure 5.14 FT-IR spectra of **PSNP-I**, **PSNP-I-FITC**, and **PSNP-I-FA**.

5.2.2.5 Synthesis of dye-encapsulated silica nanoparticle coated with a PMeOx shell

Fluorescent dye molecules can be either encapsulated inside the silica matrix or immobilized on the surface of the nanoparticle. The encapsulation approach has attracted more interest due to greater brightness when a larger number of the dye molecules are captured inside a silica matrix [65,229]. Moreover, the synthesized silica shell can protect the dye from photobleaching [93]. Hence, the synthesis of hybrid nanoparticles that contain fluorescent dye inside the NPs is more preferable than that of nanoparticles with

dyes chemically bonded on the surface such as **PSNP-I-FITC**. As mentioned in the previous chapter, tris(bipyridine)ruthenium(II) chloride (Ru(bpy)) can be easily encapsulated inside the SNPs through the electrostatic interaction during the synthesis of NPs using reverse microemulsion [195]. Figure 5.15 illustrates the strategy for synthesis of Ru(bpy)-doped SNPs coated with PMeOx via the “grafting from” approach (**PSNP-J**).

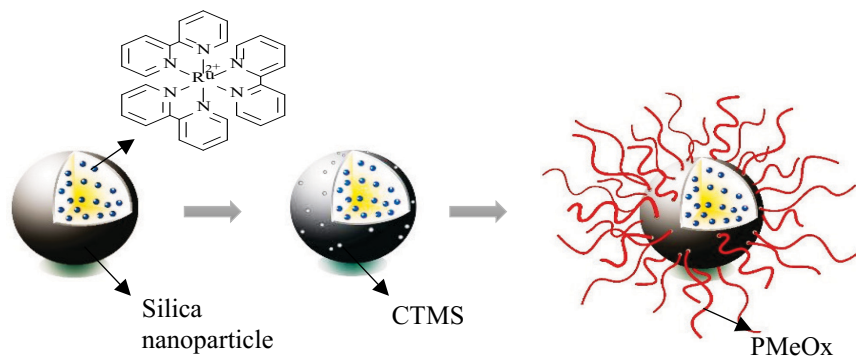


Figure 5.15 Schematic strategy for the synthesis of Ru(bpy)-doped SNPs coated with PMeOx using the “grafting-from” approach.

The FT-IR was used to prove the presence of Ru(bpy) dye molecules inside the SNPs by the appearance of a strong peak at 766 cm^{-1} , which is associated with the characteristic absorbance peak of the C-H bend of the ring in Ru(bpy) (Figure 5.16-a). The aforementioned characteristic peak was appearing both before and after the polymerization of MeOx, which confirms that Ru(bpy) dyes do not leak out from the SNPs; however they are not chemically bonded to the silica matrix. This hypothesis can be further confirmed by calculating the concentration of dye in **SNP-Ru(bpy)** and **PSNP-J**. Therefore, the calibration graph was prepared for Ru(bpy) dye (Appendix 10.5) and further used to calculate the concentration of Ru(bpy) encapsulated inside the SNPs. According to the calibration curves, 0.145 ± 0.024 and $0.135 \pm 0.001\ \mu\text{mol mL}^{-1}$ of Ru(bpy) was found in $1\ \text{mg mL}^{-1}$ of **SNP-Ru(bpy)** and **PSNP-J**, respectively. The synthesis of different layers around the NPs during surface modification of the **SNP-Ru(bpy)** can explain the reason of preventing dye leaking in the NPs. It should be noted that the formation of PMeOx was confirmed by the presence of two peaks in the FT-IR spectrum of **PSNP-J** followed by indicating an additional mass loss of 34.2 % using TGA (Figure 5.16-b).

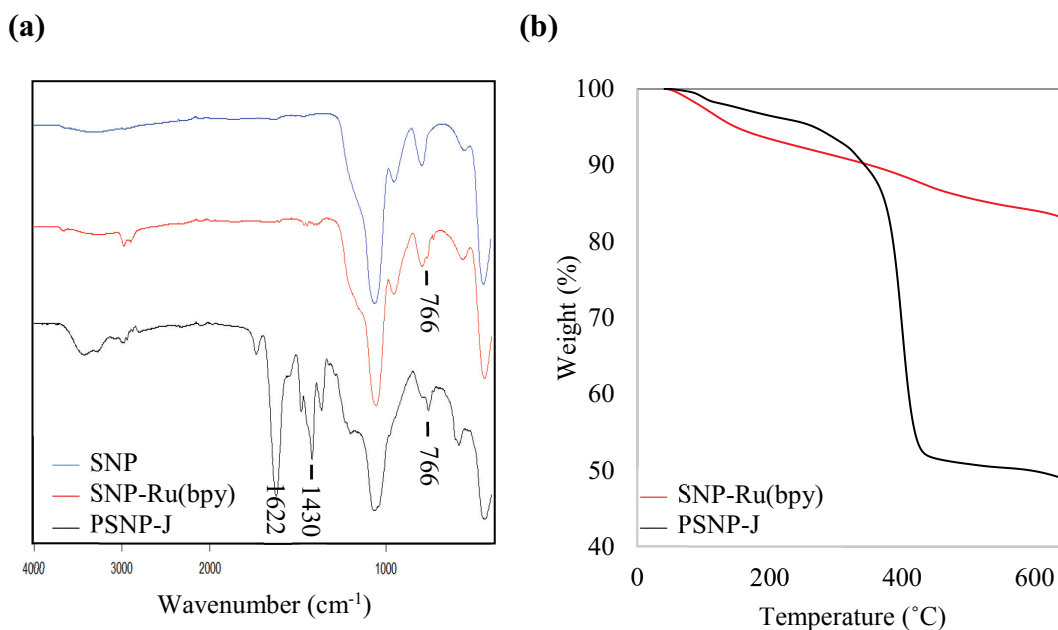


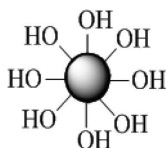
Figure 5.16 (a) FT-IR spectra of SNP, SNP-Ru(bpy), and PSNP-J **(b)** TGA of SNP-Ru(bpy), and PSNP-J.

5.3 Conclusion

The surface-initiated polymerization of MeOx from the surface of SNPs was investigated by using two different initiators, BMBA and CTMS. The possibility to directly immobilize CTMS on the surface of SNPs, via silane coupling reaction, leads to the synthesis of well-defined PMeOx-silica hybrid nanoparticles. The fabricated hybrid nanoparticles via the “grafting from” approach indicates greater grafting density compared to ones prepared with the “grafting to” approach, which was reported in the previous chapter. Moreover, this approach is flexible and enables control over the molecular weight of the grafted PMeOx by altering the polymerization time and the monomer/initiator ratio in the reaction. This method could afford the functionalization of the hybrid nanoparticles using a different terminating agent such as amine groups, which were subsequently conjugated with biomolecules such as fluorescein isothiocyanate (FITC) and folic acid (FA), acting as a fluorescence imaging molecule and cancer-targeting ligands, respectively. This versatile and effective method can be further extended to enable the synthesis of core-shell nanoparticles containing fluorescent dye encapsulated inside the SNPs coated with PMeOx with a high grafting density for biomedical application.

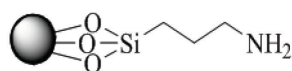
5.4 Experimental

5.4.1 Synthesis of silica nanoparticles (SNPs)



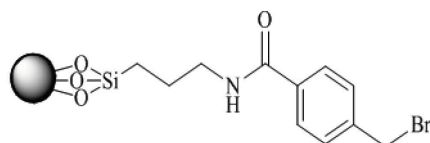
Monodisperse SNPs were synthesized using the W/O microemulsion method [181,230]. The reverse microemulsion was prepared by mixing cyclohexane (7.5 mL), n-hexanol (1.8 mL), Triton X-100 (1.77 mL), deionized water (0.5 mL), and TEOS (0.1 mL). After 15 min, 60 μ l of NH_4OH was added to the emulsion to initiate the silica polymerization. The reaction was stirred for 24 h at room temperature. The synthesized silica nanoparticles were isolated from microemulsion by the addition of the excess amount of acetone and collected by centrifugation at 4500 rpm for 15 min. The synthesized samples were washed by at least three times with ethanol to remove the surfactant and other impurities and then were air dried and weighted for the yield (around 20 mg).

5.4.2 Synthesis of amino-modified SNP (SNP-NH₂)



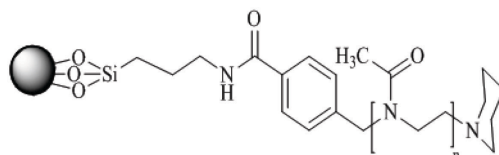
The amino-modification of the prepared SNPs was carried out according to the method reported by Gao et al., [231]. First, SNPs were dried in a vacuum oven at 70 °C for 48 h in order to reduce the aqueous contents on the surface of the particles. Dried SNPs (40 mg) were dispersed in 10 mL of anhydrous toluene in a three-necked round bottom flask under argon. The mixture was sonicated for at least for 30 min. Then excess amount of (3-Aminopropyl)triethoxysilane, APTES 1.1 mL, was added to the flask and the mixture was refluxed at 130 °C for 24 h under argon. The prepared SNPs-NH₂ were washed at least three times with ethanol to remove the unreacted APTES and were dried under vacuum at room temperature.

5.4.3 Synthesis of bromide-modified SNP (SNP-BMBA)



4-(Bromomethyl)benzoic acid (0.297 g, 1.38 mmol), ethylchloroformate (132 μ L, 1.38 mmol), and trimethylamine (TEA) (192 μ L, 1.38 mmol) were dissolved in THF (50 mL). The solution was purged with Argon and cooled down in acetone-liquid nitrogen bath (-78°C) for 40 min. In the next step, amino-functionalized SNPs (40 mg) were added to the solution at -10°C and the reaction was allowed to proceed for 48 h [214]. The product (SNPs-BMBA) were precipitated in hexane and collected by centrifugation (4500 rpm, 15 min). The particles were washed at least three times with acetone and were dried under vacuum at room temperature.

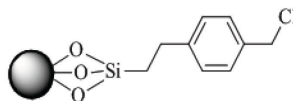
5.4.4 Preparation of PSNP-G via “grafting from” approach



The **PSNP-G** were prepared based on the cationic ring opening polymerization of 2-methyl-2-oxazoline using **SNP-BMBA** as a nanoreactor to initiate the polymerization. Therefore, 50 mg of **SNP-BMBA** was dispersed in anhydrous acetonitrile (7.5 mL) by sonication for 30 min. Then, excess amount of 2-methyl-2-oxazoline (1 mL, 11.75 mmol) was added to the glass tube followed by stirring the reaction mixture in an oil bath at 120°C for 5 h. Then, the mixture was cooled down to reach the room temperature and 300 μ L of piperidine (3.02 mmol) was added as a terminating agent and the reaction mixture was stirred overnight at room temperature. The solvent and the remaining excess of piperidine were removed at reduced pressure. The mixture was diluted with chloroform and precipitated in cold diethyl ether.

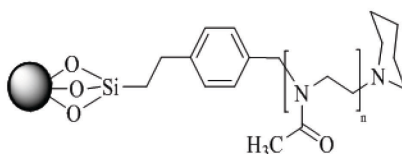
Consequently, the product was collected by centrifugation and dried under vacuum for 24 h.

5.4.5 Synthesis of chloride-modified SNP (SNP-CTMS)



Synthesized SNPs were dried in a vacuum oven at 70 °C for 48 h in order to reduce the aqueous contents on the surface of the particles. Dried SNPs were modified with (chloromethyl)phenylethyl)trimethoxysilane, CTMS, led to immobilization of the chloride group. Therefore, dried nanoparticles (300 mg) were dispersed in 18 mL of fresh anhydrous toluene in an argon environment in a two necked-round bottom flask. After 1 h sonication, excess amount of CTMS (6 mL) were added to the flask and the reaction was moved to an oil bath at 90 °C. The mixture was stirred at the same temperature for 48 h. Then the functionalized SNPs were collected by centrifugation. The synthesized nanoparticles were washed four times with anhydrous toluene to remove unreacted silane coupling agent. The complete purification was confirmed by UV-Vis spectroscopy. The prepared samples were dried under vacuum at room temperature for 48 h.

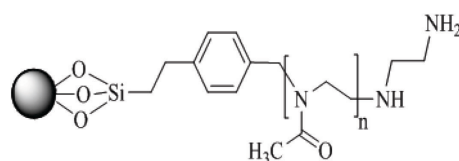
5.4.6 Preparation of PSNP-H via “grafting from” approach



PSNPs were prepared based on the cationic ring opening polymerization of 2-methyl-2-oxazoline using SNPs-CTMS as a nanoreactor to initiate the polymerization. Therefore, two series of hybrid nanoparticles, **PSNP-H**, were prepared to investigate the effect of reaction time and monomer/initiator ratio concentration on grafting density of the PMeOx-coated SNPs, respectively. It should be mentioned that all the polymerization were performed in a Schlenck-type flask under argon environment.

The first set of experiments (**PSNP-H**) were fabricated at various polymerization times while using constant ratio of initiator/monomer concentration. First, 50 mg of **SNP-CTMS** (containing 0.023 mmol of initiator) and 78 mg of KI (0.47 mmol) were dispersed in anhydrous acetonitrile (7.5 mL) by sonication for 1 h in order to bring about the exchange of the chloride anion with the iodide anion. Then, excess amount of 2-methyl-2-oxazoline (1 mL, 11.75 mmol) was added to the glass tube followed by stirring the reaction mixture in an oil bath at 120 °C at different polymerization times. Hence, three samples of **PSNP-H-1**, **PSNP-H-2**, and **PSNP-H-3** were prepared using three different reaction times of 1, 3, and 7 h, respectively. Then, the mixture was cooled down to reach the room temperature and 300 µl of piperidine (3.02 mmol) was added as a terminating agent and the reaction mixture was stirred overnight at room temperature. The solvent and the remaining excess of piperidine were removed at reduced pressure. The mixture was diluted with chloroform and precipitated in cold diethyl ether. Consequently, the product was collected by centrifugation and dried under vacuum for 24 h. The second set of experiments were also prepared like the first set while the concentration of MeOx/initiator was varied. Hence, another three samples were prepared using different amounts of MeOx, **PSNP-H-4** (10 µl, 5 eq.), **PSNP-H-5** (40 µl, 20 eq.), and **PSNP-H-6** (80 µl, 40 eq.). The polymerization of these samples were taken place at 120 °C for 24 h. The hybrid nanoparticles were collected like the former set. The prepared PMeOx-coated silica nanoparticles were dialyzed against water for 24 h.

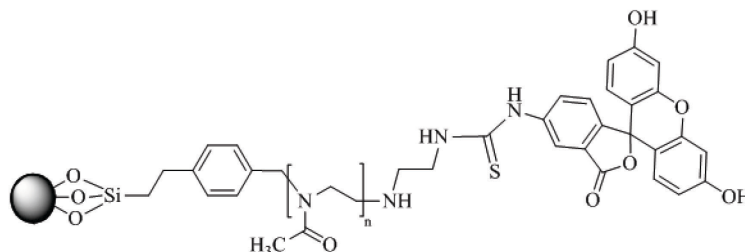
5.4.7 Synthesis of amine-functionalized hybrid nanoparticles (PSNP-I)



To terminate the polymerization reaction with amine group, first the cationic ring opening polymerization of 2-methyl-2-oxazoline by **SNP-CTMS** was taken place in the same reaction condition of **PSNP-H-2** (78 mg KI, 1 mL MeOx, 120 °C, 3 h). Then the reaction terminated by adding excess amount of ethylenediamine, EDA, (110 µl, 1.63 mmol) and the reaction mixture was moved to an oil bath at 50°C and stirred for 48 h. The solvent was removed at reduced pressure. The mixture was diluted with chloroform

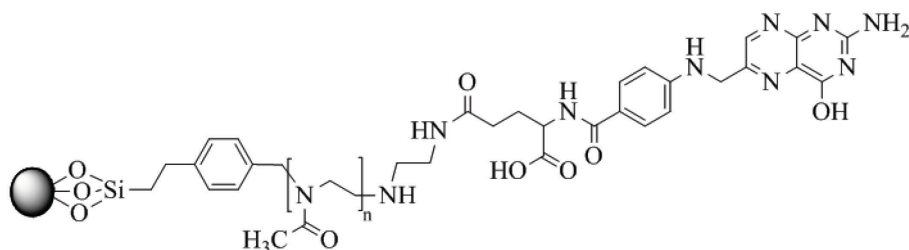
and precipitated in cold diethyl ether. Consequently, the product was collected by centrifugation and dried under vacuum for 24 h. The prepared amine-functionalized hybrid nanoparticles were dialyzed against deionized water for 48 h to remove the unreacted EDA. The prepared sample was dried by freeze-drying to obtain a white product. Finally, the presence of amine groups on the surface of hybrid nanoparticles were confirmed by ninhydrin test [221]. In ninhydrin test, 3 mg of **PSNP-I** were dispersed in 2 mL of absolute ethanol and centrifuged at 4500 rpm for 60 min. The obtained supernatant was mixed with 50 mg ninhydrin and stirred at 90°C for 25 min. More washing procedures will be required if the purple complex was observed; otherwise, the washed sample was dispersed in 16.4 mM ethanolic ninhydrine solution by 40 min sonication followed by stirring at 90°C for 25 min. The samples can be collected by centrifugation at 4500 rpm for 20 min. UV-Vis analysis was used to confirm the formation of complex and consequently verify the presence of amine group on the surface of hybrid nanoparticles.

5.4.8 Conjugation of FITC on PSNP-I (PSNP-I-FITC)



Fluorescein isothiocyanate (FITC) is an amine-reactive derivative fluorescein dye molecule, which was used to immobilize on the surface of **PSNP-I**. Hence, 10 mg of **PSNP-I** and excess amount of FITC (20 mg, 0.051 mmol) were added to the 3 mL of absolute ethanol. The mixture stirred at room temperature in the dark for 24 h. The particles were collected by centrifugation at 4500 rpm for 90 min and dried under vacuum. The prepared particles (**PSNP-I-FITC**) were dialyzed against water for 72 h to remove the unreacted FITC. The nanoparticles were then dried by freeze-drying to obtain a light yellow powder. The successful immobilization of FITC was confirmed by UV-Vis analysis and FT-IR.

5.4.9 Conjugation of folic acid on PSNP-I (PSNP-I-FA)



Folic acid as a cancer-targeting ligand was conjugated with **PSNP-I** according to the following procedure. Briefly, FA (30 mg, 0.068 mmol) was dissolved in dimethyl sulfoxide (DMSO, 16 mL) under sonication. Then, EDC.HCl (12.27 mg, 0.064 mmol) and NHS (7.37 mg, 0.064 mmol) were added as covalent coupling reagents and the solution was stirred in the dark for 6 h at room temperature. Next, **PSNP-I** (15 mg) was added into the activated FA solution, the mixture was continued to stir in the dark for 72 h. The FA-conjugated **PSNP-I** (**PSNP-I-FA**) were recovered by centrifugation at 4500 rpm for 90 min. The particles were dispersed in an appropriate amount of deionized-water, followed by dialysis against deionized water for 72 h to remove the unreacted FA [232]. The prepared nanoparticles were dried by freeze-drying to obtain a light yellow product. The successful conjugation of FA was confirmed by UV-Vis analysis and FT-IR.

5.4.10 Synthesis of Ru(bpy)-doped SNP coated with PMeOx (PSNP-J)

Ru(bpy)-doped silica nanoparticles (**SNP-Ru(bpy)**) were synthesized using W/O microemulsion method according to a previously reported in the literature [181,182,193]. The synthesis procedure is the same as preparation of SNPs. The only difference is the addition of 0.48 mL of Ru(bpy) dye solution (20 mM in deionized water) to the mixture rather than deionized water. The reaction was allowed to continue for 24 h at room temperature followed by the addition of 0.025 mL TEOS to get a simple polysiloxane coating. The obtained particles were required to be functionalized by CTM as it was reported followed by imitating the polymerization with KI. The prepared **PSNP-J** were characterized by FT-IR, TGA, and UV-Vis spectroscopy.

5.4.11 Etching silica nanoparticles

Sodium hydroxide (NaOH) solution can be used for etching silica nanoparticles. Hence, hybrid nanoparticles were first suspended in NaOH solution (4M) and stirred for 24 h at room temperature to etch the silica core completely. The suspension was diluted by adding more deionized-water followed by dialysis against deionized water for at least 72 h. Finally, the polymer chains were obtained by drying the suspension using freeze-drying. The complete removal of silica core was confirmed by FT-IR spectroscopy. The degrafted polymer chains were further analyzed with SEC.

Chapter 6. Synthesis of Polyoxazoline-Silica Hybrid Nanoparticles via *In situ* Immobilization and Polymerization of 2-Methyl-2-oxazoline

Introduction

In the past decade, silica nanoparticles have received great attention due to their wide variety of applications. However, the surface properties of SNPs usually require tailoring in order to fit the end applications [5]. Choosing an appropriate surface modification technique plays a significant role since it can directly affect the grafting density, molecular weight and polydispersity index of the polymer chains [233]. The surface modification via chemisorption, which leads to greater stability of the tethered polymer layer, mainly can be achieved via “grafting to”, “grafting from”, and “grafting through” approaches [234,235]. Recently, many research activities have been devoted to the design of a one-pot synthetic protocol due to advantages in time and cost efficiency [32,142]. The researchers mostly focus on a one-pot synthetic protocol based on the “grafting to” approach [146] (i.e., the functionalized polymer chains prepared separately followed by combining the functionalization of the core and the immobilization of polymer chain in one-pot system). For example, Tissandier et al. used a one-pot system to synthesize PEGylated SNPs containing FITC by combining click chemistry and reverse microemulsion. Therefore, alkyl functionalized SNPs containing FITC were prepared by reverse microemulsion followed by the addition of copper catalyst and azide-functionalized PEG chains [146]. The other protocol contains the formation of the polymer chains and immobilization in a reaction mixture. For instance, in 2007, Ranjan et al. reported the fabrication of PS-coated SNPs via tandem technique, in which RAFT polymerization and click chemistry takes place simultaneously [142]. To be more precise, the alkyne-functionalized RAFT agent participated in the RAFT polymerization as well as the copper-catalyzed azide–alkyne cycloaddition (CuAAC) reaction with azide-functionalized SNPs to form hybrid nanoparticles. In this method, polymerization occurred either from the surface of particles or in the solution. This approach resulted in higher grafting densities (of 0.51 chains/nm²) compared to those of the “grafting to” approach (0.29 chains/nm²), yet not as high as those of the “grafting from” approach (0.68

chains/nm²) [142]. This can be explained due to the steric hindrance from previously attached chains on the surface in the “grafting to” approach [16]. The versatility of this method, was investigated in 2010 by Huang et al. by synthesizing a series of well-defined homopolymers (di-, tri- and tetrablock copolymers) that could be efficiently grafted onto silica particles [32].

This chapter will explore the possibility of designing a one-step synthesis protocol for the fabrication of PMeOx-coated SNPs using a bifunctional initiator with one function for immobilizing on the surface of SNPs and another function for initiating the polymerization. The growth of polymer chains can therefore either be initiated in the solution or from the surface of the particles. There is still the possibility to immobilize the prepared polymer chains on the surface of the particles. This method is close to the “grafting through” approach; however, rather than using a macromonomer with a polymerizable unit, which requires an extra step, a bifunctional initiator was used. The chemical binding of the polymer chains through such a method involves the main aspects of both “grafting from” and “grafting to” approaches and is similar to the “grafting through” approach [165]. Figure 6.1 is a diagram showing the chemical grafting of polymer chains to the surface via a “grafting to” and “grafting from” approaches, as well as via this novel one-pot approach with the advantage of simplifying the surface modification of SNPs and potentially saving time and costs.

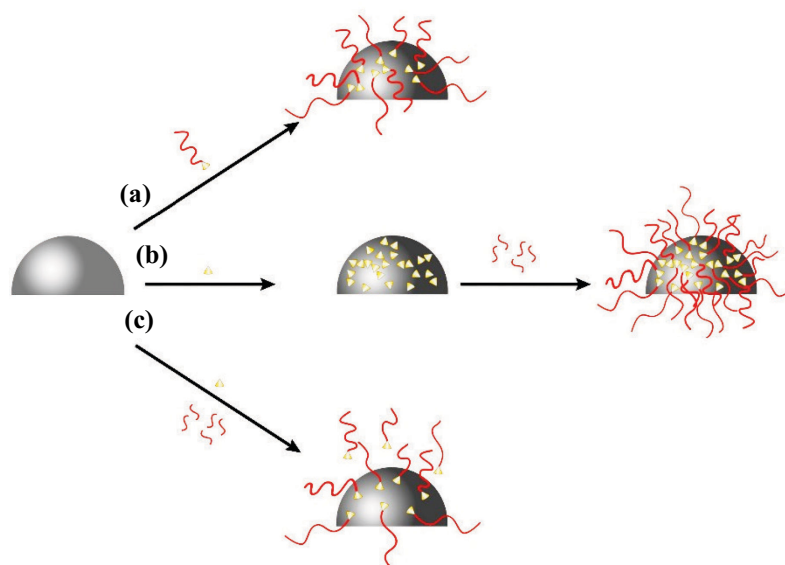


Figure 6.1 Schematic depiction of different approaches of chemical grafting of PMeOx chains to the silica surface: (a) “grafting to” (b) “grafting from”, and (c) in situ immobilization and polymerization.

Results and discussion

The “grafting to” approach is strongly self-limiting owing to the steric hindrance from previously attached chains on the surface [136], while the “grafting from” approach can overcome this drawback by first immobilizing initiators on the surface and then polymerizing a monomer directly from the surface [154,157–164,211–213]. The main purpose of this study is to design a synthetic protocol primarily based on the “grafting from” approach and with the advantage of greater time- and cost-efficiency through the reaction taking place in a one-pot system. For the preparation of the PMeOx-coated SNPs via *in situ* immobilization and polymerization of 2-methyl-2-oxazoline, (chloromethyl)phenylethyl)trimethoxysilane (CTMS) was therefore used as a bifunctional initiator, which can be immobilized on the surface of the SNP via silane coupling reaction and can at the same time initiate the polymerization of MeOx in the presence of a co-initiator (potassium iodide, KI) [106].

Figure 6.2 shows three different protocols designed to fabricate hybrid nanoparticles via a single-pot system. **PSNP-K** was prepared through such a process and is largely based on the “grafting to” approach. To be more precise, PMeOx chains were first synthesized in anhydrous acetonitrile at 120°C for 5 h, followed by the addition of SNPs to the reaction mixture. Polymer chains were therefore grafted on the surface of particles via a silane coupling reaction, between polymer chains containing a silane-coupling agent and hydroxyl groups on the surface of the silica particles. The main difference between the aforementioned method and the “grafting to” approach is a shortening of the reaction steps by using a single-pot system. In the second protocol (**PSNP-L**), the growth of polymer chains is initiated in the solution while SNPs are also present in the reaction mixture. In this protocol there is the possibility of a simultaneous silane coupling reaction between the hydroxyl groups on the surface of SNPs and both initiator and silane-functionalized polymer chains. In the synthetic protocol used for the fabrication of **PSNP-M**, a time interval was allowed for the immobilization of the initiators on the surface of the particles. The polymerization of the monomers was then initiated by adding the co-initiator and monomers to the reaction mixture. The idea was to decrease the steric repulsion by first immobilizing the initiators on the surface of the SNPs. Although the chain growth can proceed either from the surface or from the solution, the growth of polymer chains is expected to initiate more from the particle’s surface, which can lead to a greater grafting density.

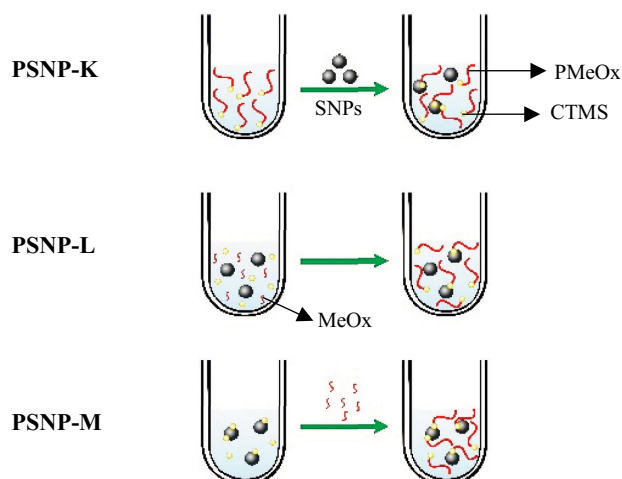


Figure 6.2 Schematic depiction for the synthesis of PMeOx-coated silica nanoparticles (**PSNP-K**, **PSNP-L**, and **PSNP-M**) via in situ immobilization and polymerization of 2-methyl-2-oxazoline.

The FT-IR spectra and TGA of these three hybrid nanoparticles are shown in Figure 6.3. In Figure 6.3-a, alongside the three main characteristic absorption bands of SNPs (symmetric vibration of Si–O (795 cm^{-1}), asymmetric vibration of Si–OH (935 cm^{-1}), and asymmetric vibration of Si–O (1100 cm^{-1}) [183]), the appearance of two extra absorption bands at 1622 cm^{-1} , corresponding to the carbonyl stretching mode of the amide backbone of the grafted PMeOx chain [186,187], and at 1430 cm^{-1} , assigning CH_x deformation mode of PMeOx [210], confirm the polymerization of MeOx and the successful grafting of PMeOx on the surface of the SNP. TGA results agree with FT-IR in that they indicate an additional mass loss of 5.16, 3.88, and 5.41% for **PSNP-K**, **PSNP-L**, and **PSNP-M**, respectively (Figure 6.3-b). The amount of the grafted polymer chains, Γ_{PMeOx} (mg m^{-2}), in these three samples was calculated based on their TGA results and summarized in Table 6.1. The lowest Γ_{PMeOx} value obtained when immobilization and polymerization of PMeOx chains takes place simultaneously in the reaction mixture (**PSNP-L**) and this is consistent with the theoretical expectations since it is a complex reaction and as Huang et al. also reported in a tandem reaction, that contains click chemistry and polymerization of the monomers, many parameters may affect the final results such as molecular weight of polymer chains, feed ratios, reaction time, and temperature [32]. The results show that using sequential reactions has a strong influence on the amount of grafted polymer chains and greater Γ_{PMeOx} values were obtained for

PSNP-K and **PSNP-M** compared to **PSNP-L** (Table 6.1). The amount of the grafted polymer chains in **PSNP-M** is only slightly greater than **PSNP-K**; however, a greater Γ_{PMeOx} value was expected for **PSNP-M**. Therefore, the effect of various parameters such as the time for immobilizing the initiator on the particle's surface (t_i), the reaction time (t_r , i.e. the time required for the immobilization of the polymer chains on the particle or/and polymerization of the MeOx), and the concentration of the initiator were investigated in relation to Γ_{PMeOx} values in order to optimize the reaction conditions. Table 6.1 summarizes the reaction conditions for all prepared trials.

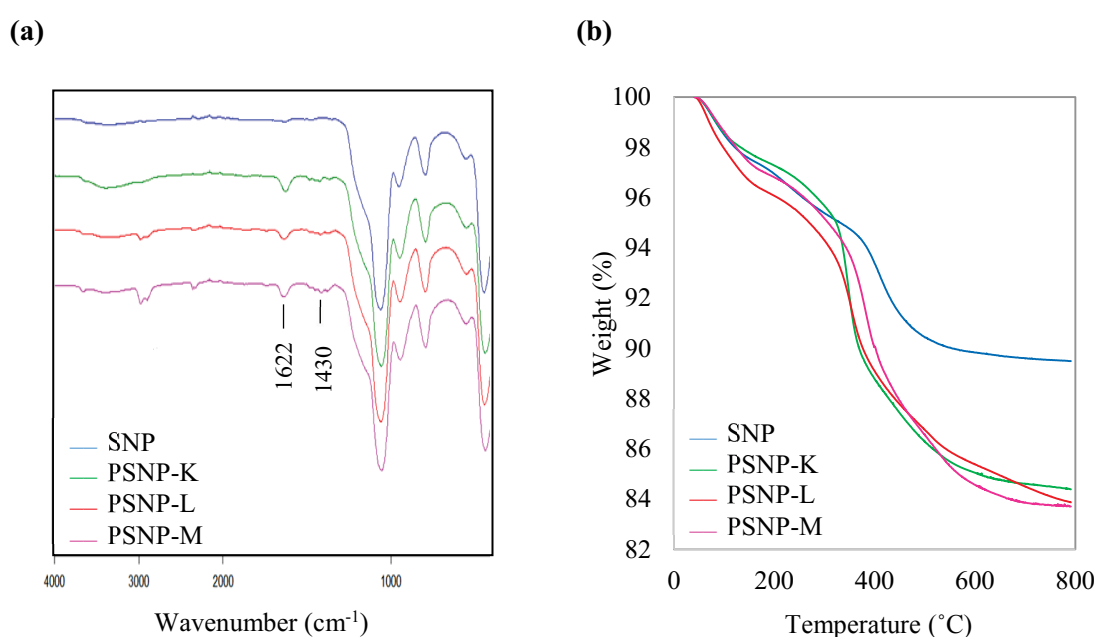


Figure 6.3 (a) FT-IR spectra of bare SNP, PSNP-K, PSNP-L, and PSNP-M **(b)** TGA of bare SNP, PSNP-K, PSNP-L, and PSNP-M.

In order to investigate the influence of the t_i on the amount of the grafted polymers, two reactions were performed under exactly the same **PSNP-M** conditions, with the t_i increased from 24 h to 48 h (**PSNP-M-1**) and 72 h (**PSNP-M-2**). The FT-IR spectra confirmed the formation of hybrid nanoparticles in both trials through the appearance of two characteristic PMeOx peaks at 1622 and 1430 cm⁻¹ (Figure 6.4-a). The Γ_{PMeOx} value showed a 30% increase from 1.06 to 1.38 mg m⁻² by increasing the t_i from 24 to 48 h. However, a further increase in t_i does not have a significant influence on the amount of the grafted polymer chains (**PSNP-M-2**), which can be explained by the low

concentration of the initiators in the reaction mixture. Therefore, 48 h would be a sufficient time for immobilizing the initiators on the particles' surface.

Table 6.1 Reaction condition and analytical data from the hybrid nanoparticles prepared via in situ immobilization and polymerization of MeOx.

Particle code	t_i ^a (h)	t_r ^b (h)	Feed ratio initiator/SNP	Mass loss ^c (%)	Γ_{PMeOx} ^d (mg m ⁻²)
PSNP-K	-	24	1	5.16	1.02
PSNP-L	-	24	1	3.88	0.78
PSNP-M	24	24	1	5.41	1.06
PSNP-M-1	48	24	1	7.03	1.38
PSNP-M-2	72	24	1	6.81	1.33
PSNP-M-3	48	48	1	7.03	1.38
PSNP-M-4	48	72	1	6.93	1.36
PSNP-M-5	48	24	2	7.01	1.37
PSNP-M-6	48	24	3	8.42	1.66

^a time required for immobilizing the initiator on the particle's surface; ^b reaction time; ^c mass loss data determined from the TGA from 150 to 650°C; ^d calculated from the mass loss data using eq. 7-1.

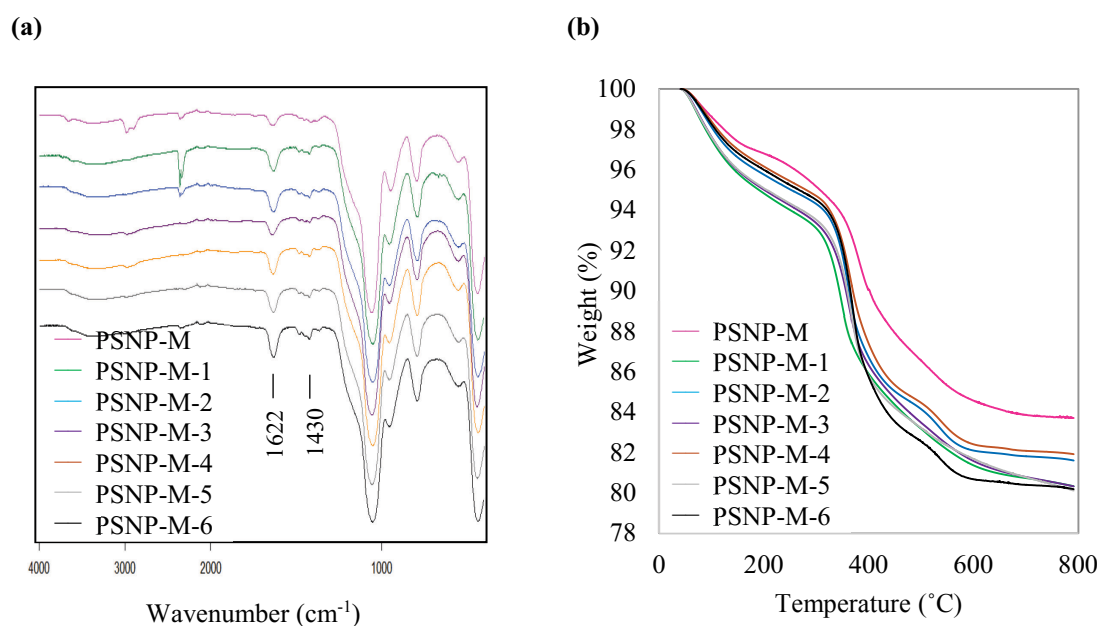


Figure 6.4 (a) FT-IR spectra of **PSNP-M**, **PSNP-M-1** to **PSNP-M-6** **(b)** TGA of **PSNP-M**, **PSNP-M-1** to **PSNP-M-6**.

As the t_r is an important parameter in all kinds of reactions, its effect was investigated in relation to the formation of hybrid nanoparticles. **PSNP-M-3** and **PSNP-**

M-4 were thus prepared by increasing the t_r from 24 h to 48 and 72 h, respectively. The values of Γ_{PMeOx} were calculated based on their TGA results (Figure 6.4-b) and showed that a longer reaction time cannot affect the amount of the grafted polymer chains. This could be explained by the fact that 5 h was known to be sufficient for a complete CROP of MeOx when CTMS is used as an initiator. Moreover, the Γ_{PMeOx} values showed that, once 24 h had passed, no further free polymer chains in the mixture could be grafted to the surface of the SNPs since the hydroxyl groups on the particle surface had been shielded by grafted PMeOx. Also, the steric repulsions had become more pronounced and prevented the silane end group of the PMeOx chains from approaching the hydroxyl groups on the surface of the SNPs [32,149]. The same behaviour was observed in the “grafting to” [165,236] and “grafting through” [165] approaches since these processes are strongly self-limiting. In addition, the incoming polymer chains require a transfer from a coiled conformation into a stretched (brush-like) conformation, which is unfavorable due to entropy loss [165,237].

Another parameter that can affect the grafting density of the polymer chains is the concentration of initiators immobilized on the surface of SNPs, which is directly affected by the t_i and the initiator concentration in the reaction mixture. The effect of the initiator concentration on the formation of hybrid nanoparticles was therefore investigated through synthesizing two more samples by increasing the initiator concentration by a factor of 2 and 3 in **PSNP-M-5** and **PSNP-M-6**, respectively. It should be noted that the monomer concentration was also increased proportional to the initiator, since otherwise shorter polymer chains would be formed. The greater amount of grafted polymer chains was achieved in **PSNP-M-6** (1.66 mg m^{-2}) as opposed to **PSNP-M-1** (1.38 mg m^{-2}). This was presumably because of the higher amount of initiators available on the particle’s surface which could initiate the CROP of MeOx. In general, the results obtained from the reaction optimization of the **PSNP-M** indicate that this synthetic protocol can overcome the limitations of **PSNP-K**, caused by the barrier formed by the surface-attached polymer chains against the penetration of further chains formed in the solution.

In order to obtain information regarding the molecular weight of the grafted PMeOx, the silica core was etched using sodium hydroxide solution and the polymer chains were collected for further analysis. In addition, free PMeOx chains that had formed in the solution could also be collected during the first washing cycle and were then treated with sodium hydroxide solution. The complete etching of the silica core was confirmed with FT-IR by the disappearance of the three characteristic peaks of silica particles at

1100, 935, and 795 cm^{-1} . The polymeric chains of the selected fabricated trials including **PSNP-M**, **PSNP-M-1**, **PSNP-M-4**, and **PSNP-M-6** were analyzed with size exclusion chromatography (SEC) and the results listed in Table 6.2. The results indicate that, regardless of the reaction conditions, the molecular weight of the free polymer chains are less than that of the grafted chains and their molecular weight distribution remains relatively low ($D < 1.24$) with monomodal distribution. However, the greater D with bimodal distribution was achieved for the grafted polymer chains, presumably because these can be obtained not only by growing from the particle surface but also via the silane coupling reaction between the free polymer chains and hydroxyl groups of the SNPs.

Table 6.2 Analytical data from the hybrid nanoparticles prepared via in situ immobilization and polymerization of MeOx.

Particle code	C ^a (%)	N ^a (%)	grafting density ^a (groups/nm ²)	Polymer layer thickness ^b (nm)	M _n ^c (g mol ⁻¹)	D ^c	M _n ^d (g mol ⁻¹)	D ^d
PSNP-M	7.01	0.78	0.19	-	6462	1.25	6310	1.2
PSNP-M-1	7.36	1.27	0.17	1.9 ± 2.33	7811	1.47	6449	1.15
PSNP-M-4	8.07	1.20	0.20	2.83 ± 0.75	7174	1.18	6853	1.13
PSNP-M-6	9.71	1.79	0.25	3.90 ± 0.34	7365	2.04	6308	1.09

^a determined from elemental analysis; ^b determined from the particle size before and after grafting using TEM and ImageJ software; ^c molecular weight and dispersity of the grafted polymer chains determined by size exclusion chromatography (SEC) in DMF with 5 g L⁻¹ LiBr at T=60°C; ^d molecular weight and dispersity of the free polymer chains prepared in the solution obtained via SEC.

These four samples were further characterized with elemental analysis (EA) and their results are listed in Table 6.2. The content of carbon and nitrogen increased by increasing the t_i (**PSNP-M-1**) and t_r (**PSNP-M-4**); however, there is not a significant difference in their grafting densities owing to the difference in the molecular weight of the grafted PMeOx chains. In other words, it is not easy to elucidate the extent to which these parameters can affect the grafting density since the molecular weight of polymer chains are not constant and longer polymer chains make immobilizing free polymer chains onto the surface of SNPs more difficult and decrease the grafting density as a result [165]. The EA results indicate that only increasing the concentration of the initiator in the reaction mixture (**PSNP-M-6**) leads to a greater grafting density (0.25 group of polymer chains/nm²), although longer polymer chains were also formed in this synthetic protocol.

This confirms the dominant effect of the “grafting from” approach compared to the “grafting to” approach in this method, in situ immobilization and polymerization of MeOx. Moreover, it should be noted that not all initiators can be immobilized on the surface of SNPs. Increasing the concentration of the initiator thus not only leads to an increase in the concentration of the initiators on the surface of particles but also to many of them being available in the solution. Hence, once the MeOx has been added to the reaction mixture, many short PMeOx chains will be formed with the possibility of easier penetration to reach the hydroxyl groups on the surface of SNPs and ultimately leading to a higher grafting density. The same behaviour was also reported for the surface modifications via the “grafting through” approach [165]. The fabricated hybrid nanoparticles of **PSNP-M-6** indicated intermediate grafting density between the “grafting to” approach using click chemistry (0.18 groups/nm²) and that prepared via a silane coupling reaction (0.30-0.46 groups/nm²). It should also be noted that the lower grafting density of **PSNP-M-6** compared to the “grafting to” approach can be explained by the longer polymer chains formed by this method.

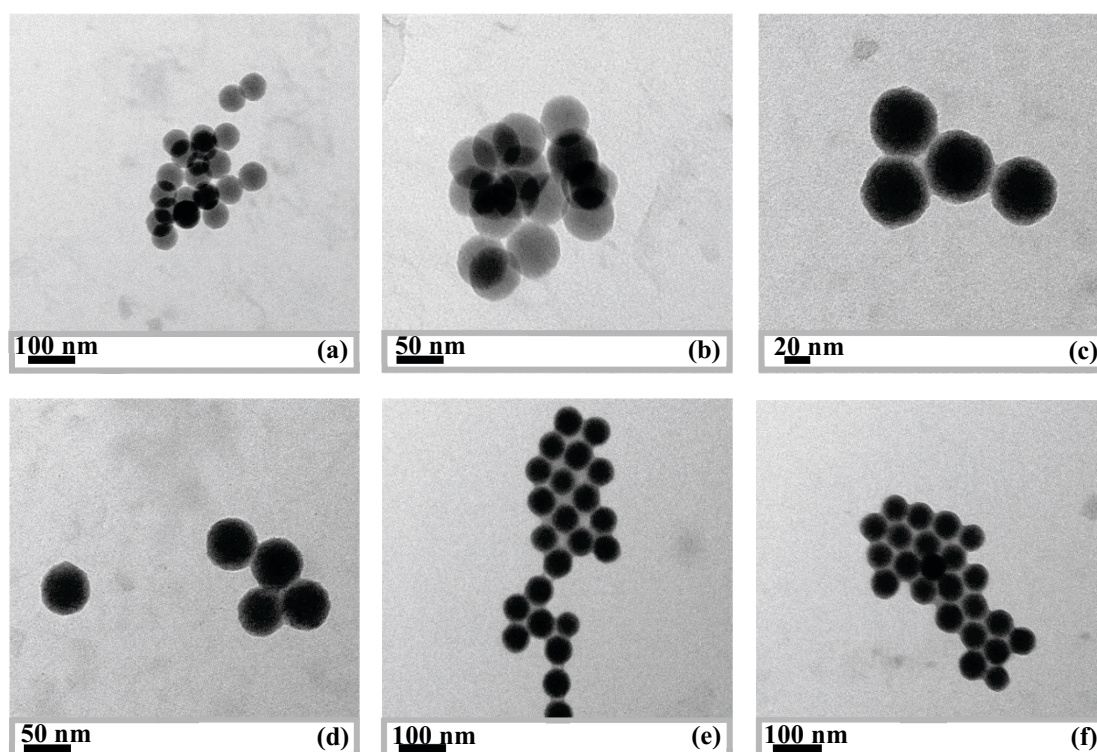


Figure 6.5 TEM images of (a,b) silica nanoparticles, (c,d) **PSNP-M-1** (e,f), and **PSNP-M-6** dispersed in isopropanol.

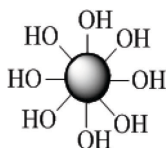
TEM images were used to investigate the morphology of the prepared nanoparticles and confirm the hypothesis of the formation of a homogeneous polymeric shell around the bare SNPs since in hybrid nanoparticles, the difference in density leads to the appearance of darker silica core compared to the polymeric shell. In Figure 6.5, the polymeric shell can be clearly identified for **PSNP-M-1** and **PSNP-M-6** and the thickness of the polymeric shell can be calculated by comparing the particle sizes of hybrid nanoparticles with bare SNPs. The thickness of the polymeric shell in hybrid nanoparticles was summarized in Table 6.2. The shell thickness of **PSNP-M-6** was measured around 3.90 nm, which is consistent with the results obtained in the “grafting to” and “grafting from” approaches.

Conclusion

PMeOx-coated silica nanoparticles were prepared via in situ immobilization and polymerization of MeOx in a one-pot system. CTMS was used as a bifunctional initiator, which can initiate the CROP of MeOx in the presence of a co-initiator and also immobilize on the surface of SNPs via silane coupling reaction. The results of the fabricated hybrid nanoparticles indicated that a greater amount of grafted polymer chains can be obtained by using sequential reactions (**PSNP-K** and **PSNP-M**) than using simultaneous reactions (**PSNP-L**). The synthetic protocol of the **PSNP-K** is largely dominated by the “grafting to” approach, a self-limiting process, while the method used for **PSNP-M** has the potential to overcome this limiting factor by allowing an appropriate time for the immobilization of the initiators on the surface of SNPs. Therefore, it leads to a more flexible process and enables control over the grafting density of the polymer chains through altering the immobilization time of initiators on the SNPs surface and the concentration of the initiator in the reaction mixture.

Experimental

6.4.1 Synthesis of silica nanoparticles (SNPs)



Monodisperse SNPs were prepared using the reverse microemulsion method according to the literature [181,230]. First, cyclohexane (7.5 mL), n -hexanol (1.8 mL), Triton X-100 (1.77 mL) were mixed followed by the addition of deionized water (0.5 mL), and TEOS (0.1 mL). After 15 min, 60 μ L of catalyst (NH_4OH) was added to initiate the polymerization of silica. The reaction was stirred for 24 h at room temperature. The isolation of the synthesized SNPs was taken place by the addition of the excess amount of acetone and consequently collected by centrifugation at 4500 rpm for 15 min. The synthesized samples were washed by at least three times with ethanol in order to remove the surfactant and other impurities and then were air dried and weighted for the yield (around 20 mg). The diameter of bare SNPs was calculated using TEM images and ImageJ software, which was around 56.9 ± 1.45 nm.

6.4.2 Synthesis of P MeO_x -coated SNPs

6.4.2.1 Synthesis of PSNP-K

Synthesized SNPs were dried in a vacuum oven at 70 $^\circ\text{C}$ for at least 48 h in order to reduce the aqueous contents on the surface of these particles. Dried SNPs were used for the synthesis of hybrid nanoparticles. All the hybrid nanoparticles were prepared in a Schlenk tube under an inert atmosphere (argon) using freshly distilled and dried solvent. A mixture of 57.7 μ L of ((chloromethyl)phenylethyl)trimethoxysilane (CTMS) (0.235 mmol, 1 eq.) and 78 mg of KI (0.47 mmol, 2 eq.) in acetonitrile (5 mL) was sonicated for 1 h in order to the exchange of the chloride anion with iodide anion. Then 1 mL of 2-methyl-2-oxazoline (11.75 mmol, 50 eq.) was added to the mixture and the glass tube was heated at the desired temperature (120 $^\circ\text{C}$). After 5 h, the mixture cooled down to reach the room temperature and 0.1 g of dried SNPs were added and the reaction mixture was heated to 100 $^\circ\text{C}$ and held for 24 h. In the next step, 70.6 μ L of piperidine (0.705 mmol, 3 eq.) was added and the reaction mixture was stirred overnight. The solvent and remaining

excess of piperidine were removed at reduced pressure. The mixture was diluted with chloroform and precipitated in cold diethyl ether. The product was recovered by centrifugation and dried in vacuum for 24 h. The product was washed three times with ethanol and methanol to remove either the free polymer chains or those physically adsorbed on the surface of particles. The prepared hybrid nanoparticles (**PSNP-K**) were dried at room temperature.

6.4.2.2 Synthesis of PSNP-L

PSNP-L prepared by dispersing SNPs (0.1 g) in 5 mL of acetonitrile. Followed by the addition of 57.7 μ l of CTMS (0.235 mmol, 1 eq.), 78 mg of KI (0.47 mmol, 2 eq.), and 1 mL of MeOx (11.75 mmol, 50 eq.). The mixture was sonicated for an hour and then heated at 120°C for 5 h under vigorous stirring and at 100°C for 24 h. In the next step, 70.6 μ l of piperidine (0.705 mmol, 3 eq.) was added to terminate the polymerization reaction and the reaction mixture was stirred overnight at room temperature. The hybrid nanoparticles recovered and washed similar to the aforementioned procedure named **PSNP-K**.

6.4.2.3 Synthesis of PSNP-M

PMeOx coating of SNPs in **PSNP-M** was performed by first dispersing SNPs (0.1 g) in 5 mL of acetonitrile and 57.7 μ l of CTMS (0.235 mmol, 1 eq.). The reaction mixture was stirred at 80°C for 24 h. Then 78 mg of KI (0.47 mmol, 2 eq.) was added and sonicated for 1 h, followed by the addition of 1 mL of MeOx (11.75 mmol, 50 eq.). The flask was moved to an oil bath at 120°C for 5 h and then decrease the temperature to 100°C for 24 h. In the last step, 70.6 μ l of piperidine (0.705 mmol, 3 eq.) was used as a terminating agent. The prepared hybrid nanoparticles of **PSNP-M** collected and washed for the characterization step.

6.4.3 Etching silica nanoparticles

Sodium hydroxide (NaOH) solution can be used for etching SNPs. Hence, hybrid nanoparticles and/or silane-functionalized polymer chains were first suspended in NaOH solution (4M) and stirred at room temperature for 24 h to etch the silica core. The suspension was diluted by adding more deionized-water followed by dialysis against deionized water for at least 72 h. Finally, the polymer chains were obtained by drying the suspension using freeze-drying. The complete removal of silica core was confirmed by FT-IR spectroscopy. The degrafted polymer chains were further analyzed with SEC.

Chapter 7. Characterization Techniques

7.1 Thermogravimetric analysis

Thermogravimetric analysis (TGAQ50 (TA instruments, Eschborn, Germany)) was used to verify the immobilized ligand, organic functional groups and/or polymer chains, on the surface of SNPs. The TG measurements were carried out under nitrogen environment at a scanning rate of 20°C/min from 40 to 800°C. The mass lost was measured as a function of the increasing temperature. Therefore, the amount of grafted polymer chains, Γ_{PMeOx} (mg m⁻²), were determined based on the data from TGA using eq. 7-1.[217]

$$\Gamma_{PMeOx} = \frac{\left(\frac{W_{PSNPs}}{100 - W_{PSNPs}} \right) \times 100 - W_{SNPs}}{S_{SPC} \times 100} \times 10^3 \quad (\text{eq. 7-1})$$

where W_{PSNPs} and W_{SNPs} are the weight loss percent between 150 and 650°C for the polymer-coated silica nanoparticles (PSNPs) and silica nanoparticles (SNPs), respectively. S_{SPC} is the specific surface area of silica nanoparticles (The value of S_{SPC} was calculated from the linear part of the BET plot and reached 69.7 m² g⁻¹).

7.2 Transmission electron microscopy

Transmission electron microscopy (TEM) images were performed using an energy filter transmission electron microscope (Philips CM200) to study the morphology of the synthesized particles. Samples were prepared by dispersing synthesized particles in an appropriate solvent (ethanol, methanol, isopropanol). Particle sizes were obtained by analyzing the TEM images using ImageJ software by taking into account more than 50 particles.

7.3 Fourier transform infrared spectroscopy

Fourier transform infrared (FT-IR) spectra were recorded with a Bruker Tensor 27 FT-IR spectrometer using a diffuse reflection apparatus (Cricket, Harrick Scientific).

Spectra were recorded over a range of 400-4000 cm^{-1} resolution and processed with the OPUS software in order to confirm the presence of the grafted ligand on the surface of silica nanoparticles.

7.4 Nuclear magnetic resonance spectroscopy

Nuclear magnetic resonance (NMR) spectroscopic studies were performed with DRX-500 (500 Hz) on FT-NMR instruments from Bruker at room temperature. The evaluation of the spectra was performed using the ACD Labs Program. The chemical shift (δ) reported in parts per million (ppm) and the coupling constants (J) in Hertz (Hz). Calibration was carried out on the residual protons of the deuterated solvent used, here deuterated chloroform (CDCl_3 : δ (1 H) = 7.24). Abbreviations for multiplicities and descriptors are: s = singlet, d = doublet, t = triplet, q = quartet, quint = quintet, m = multiplet, dd = doublet of doublets, dt = doublet of triplets, br= broad

7.5 Dynamic light scattering

The dynamic light scattering (DLS) experiments were performed using the Zetasizer Nano Instrument (Malvern). The instrument measures diffusion coefficient and by applying the Stokes Einstein equation, the hydrodynamic diameter of the particles will be calculated. A 4 mW He-Ne laser (633 nm wavelength) with a fixed detector angle of 173° was used for these measurements.

7.6 Nitrogen adsorption

Nitrogen adsorption measurement were performed by automatic adsorption instrument (Nova 4000e, Quantachrome Instruments, Boynton Beach, FL/USA). First, samples were placed in a glass cell and degassed under vacuum overnight at 50°C . The initial part of the obtained physisorption isotherm is attributed to monolayer-multilayer adsorption. Therefore, Brunauer-Emmett-Teller (BET) method was used to determine the specific surface area of silica nanoparticles.

7.7 Elemental analysis

Elemental analyses (EA) were performed at H. Kolbe Mikroanalytisches Laboratorium (Mulheim a. d. Ruhr, Germany) to measure the carbon, nitrogen, bromide, and chloride contents to quantify the ligand density on the surface of silica nanoparticles.

7.8 Size exclusion chromatography

Size exclusion chromatography (SEC) with PSS GRAM analytical 1000 Å and 30 Å columns equipped with a Knauer RI detector Smartline 2300 was used to measure the molecular weights of synthesized polymers. The molecular weights of samples were measured in DMF at 60°C, in which linear polystyrene was used as a standards for the POX.

7.9 Ultraviolet-visible spectroscopy

Ultraviolet-Visible (UV-Vis) Spectroscopy and Lambert-Beer law and were recorded on an Evolution 201 spectrophotometer (Thermo scientific). Therefore, a transparent solution of the modified NPs was prepared in an appropriate solvent and the extinction coefficient was measured at a suitable wavelength of maximum absorption (λ_{max}). The absorbance of a set of standard solutions of the reference substance at various concentrations were measured followed by plotting a calibration graph as the concentration corresponding to the absorbance of the solution. The concentration of the analyte in the sample solution is read from the plotted graph.

Chapter 8. Conclusions and Recommendations

Silica nanoparticle is one of the most well-known nanoparticles and has a wide variety of applications. In order to suppress the adsorption of proteins and improve their applications in biomedical fields as a result, surface modification of these particles with hydrophilic polymers is required [11,12]. Among the polymers that can be used as a shell for SNPs in biomedical applications, poly(2-oxazoline) (POx) and more specifically poly(2-methyl-2-oxazoline) and poly(2-ethyl-2-oxazoline) were proposed as promising alternatives for polyethylene glycol (PEG). PEG is the most interesting polymer in the biomedical field, but has some limitations owing to its possible interaction with the immune system and possible degradation under stress [21,23–25]. Hence, PMeOx was proposed since it is hydrophilic, biocompatible, has versatile end group chemistry [21], and high chemical stability [26]. In this thesis, PMeOx-coated SNPs were successfully prepared based on the chemical polymer attachment since they lead to an enhanced stability of the tethered polymer layer. Various design strategies were therefore employed including “grafting to”, “grafting from”, and “in situ immobilization and polymerization of MeOx” approaches, each with their own advantages and disadvantages. Moreover, the results indicate that the polymer grafting density of the synthesized hybrid nanoparticles largely depends on the methods used for the fabrication of these hybrid nanoparticles. This will be explained in more detail in this section.

First of all, the “grafting to” approach was used for the synthesis of PMeOx-coated SNPs based on two different methods: click chemistry and silane coupling reaction. In click chemistry, the alkyne-functionalized PMeOx (**P1**) was prepared and clicked to the azide-functionalized SNPs. In silane coupling reaction, trimethoxysilane-functionalized PMeOx (**P2**) was fabricated, which can be directly grafted on the surface of the silica nanoparticles. Since pre-fabricated polymer chains were used in this approach, characterizing the polymer chains was very straightforward. In the end, hybrid nanoparticles were successfully prepared by both click chemistry and silane coupling reaction. However, the silane coupling reaction indicated more promising results as it led to a higher grafting density (0.30-0.46 groups/nm²) compared to click chemistry (0.18 groups/nm²). Furthermore, the silane coupling reaction is able to shorten the reaction sequence and overcome the drawbacks of click chemistry such as the product's

dependency on the available functional group and the costly procedure of removing residual copper from the final product. The synthesis of PMeOx-coated silica nanoparticles via silane coupling reaction was further investigated under three different reaction conditions including: anhydrous acetonitrile at 120°C (**PSNP-B**), a mixture of ethanol and water at ambient condition (**PSNP-C**), and reverse microemulsion at ambient condition (**PSNP-D**). The highest grafting density of 0.45 chains/nm² was obtained for **PSNP-B** due to the greater mobility of the polymer chains in the solvent at high temperature. Therefore, the polymer chains can diffuse to the surface of the particle easier. The effect of three parameters i.e. temperature, reaction time, and polymer chains was investigated in relation to the grafting density of the final products. The synthesis of PMeOx-coated silica nanoparticles in reverse microemulsion medium was also investigated, where the synthesis of SNPs and the core-shell particle formation take place in a one-pot system. This synthetic protocol also led to a high grafting density (0.35 chains/nm²) with the advantage of being more time efficient. Moreover, this method is able to encapsulate imaging molecules such as Ru(bpy) in the silica matrix and consequently lead to the formation of fluorescent-dye hybrid nanoparticles.

Although PMeOx-coated SNPs were successfully prepared via the “grafting to” approach, the grafting densities are limited due to the steric hindrance originating from the polymeric chains already grafted. A further improvement in the grafting density of the hybrid nanoparticles was achieved with the “grafting from” approach. Therefore, ((chloromethyl)phenylethyl)trimethoxysilane (CTMS), which was already used for the synthesis of silane-functionalized PMeOx in the “grafting to” approach, was first immobilized on the surface of the SNPs. The polymerization of the MeOx was initiated from the surface using KI as a co-initiator. The average grafting density of ~1.45 chains/nm² was obtained for hybrid nanoparticles via this approach. The grafted PMeOx chains were characterized by treating hybrid nanoparticles with sodium hydroxide solution in order to etch the silica core. The hybrid particles prepared via this approach indicates that the molecular weight of the grafted PMeOx can be very well controlled by altering the polymerization time as well as the monomer/initiator ratio in the reaction. Moreover, these hybrid nanoparticles can be functionalized via the polymer chains and/or silica core. Hence, amine-functionalized PMeOx-coated SNPs were prepared by terminating the polymerization of MeOx with EDA, and then conjugated with biomolecules such as fluorescein (FITC) and folic acid (FA), acting as a fluorescein imaging molecule and cancer targeting ligand, respectively. Moreover, fluorescent-dye

hybrid nanoparticles were also prepared using Ru(bpy)-doped SNP with a greater polymer grafting density than that prepared via the “grafting to” approach.

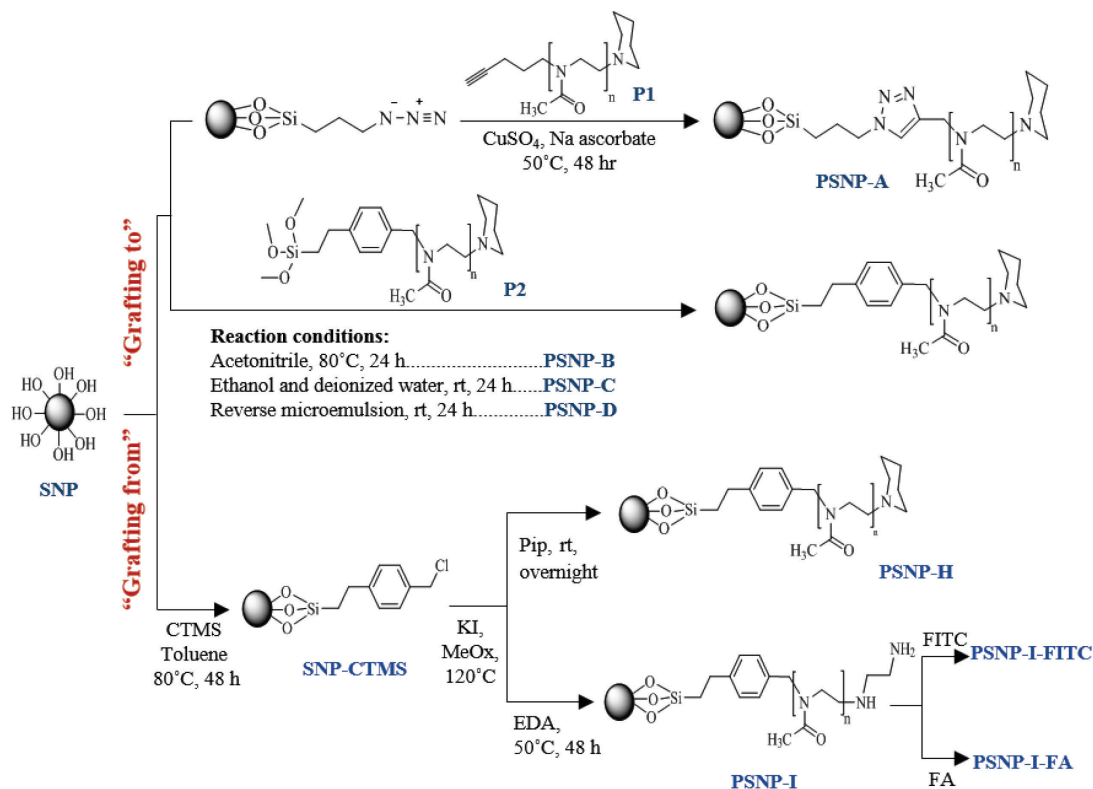


Figure 8.1 Schematic diagram of the formation process of PMeOx-coated SNPs via the “grafting to” approach using click chemistry (a) and silane coupling reaction (b) in different reaction conditions and also the “grafting from” approach using CTMS as an initiator and using different terminating agents for subsequent particle modification with (c) fluorescein (FITC) and (d) folic acid (FA).

Finally, a novel method was designed for the synthesis of PMeOx-coated SNPs entitled “in situ immobilization and polymerization of MeOx”. It is a simple and straightforward way to chemically attach PMeOx chains to the surface. In this one-pot system, CTMS was used as a bifunctional initiator, which can be immobilized on the surface of the SNPs and also initiate the CROP of MeOx. In other words, the PMeOx chain can continue to grow from the surface of the SNPs in a way similar to the “grafting from” approach or grow in the reaction mixture, with the potential to be grafted on the surface of the particles via a silane coupling reaction similar to the “grafting to” approach. Thus, this method consists of the main aspect of both the “grafting to” and “grafting from”

approache. The simultaneous immobilization and polymerization (**PSNP-L**) led to the formation of PMeOx-coated SNPs, although the amount of grafted polymer chains was very low. The protocol was further improved by the polymerization of MeOx followed by the addition of SNPs for the immobilization process (**PSNP-K**), which is largely limited by the “grafting to” step. Finally, in the last protocol (**PSNP-M**), a time interval for the immobilization of the initiators was considered in order to overcome the limiting factor (“grafting to” step). The aforementioned protocol was optimized by investigating the effect of the time interval for immobilization of the initiator, reaction time, and the initiator concentration. A grafting density of 0.25 chains/nm² was obtained for hybrid nanoparticles via this method. This method has the advantage of being time and cost-efficient.

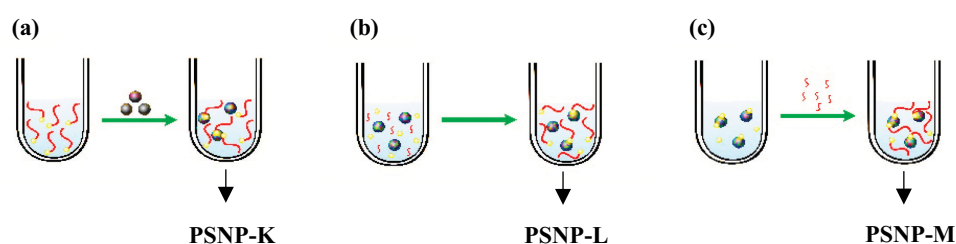


Figure 8.2 Schematic depiction of three synthetic protocol used for the synthesis of PMeOx-coated silica nanoparticles via in situ immobilization and polymerization of MeOx including **PSNP-K**, **PSNP-L**, and **PSNP-M**.

The results obtained in this research project indicate a successful synthesis and characterization of PMeOx-coated SNPs for biomedical applications using three different strategies. This study should naturally go beyond the current step and there are several points worthy of further investigation. Considering that these hybrid nanoparticles were prepared with the purpose of reducing protein adsorption in biological-related processes, nonspecific protein-binding tests [22] can be carried out to find out more about how these nanoparticles behave before and after surface modification. In addition, the cellular uptake of these hybrid nanoparticles and their *in vitro* cytotoxicity can be explored and compared with the bare SNP. With regard to the silica particle synthetic, mesoporous silica nanoparticles can replace the SNPs, as these have attracted considerable attention in drug delivery in particular due to their large surface area.

Chapter 9. References

- [1] K. Chatterjee, S. Sarkar, K. Jagajjanani Rao, S. Paria, Core/shell nanoparticles in biomedical applications, *Advances in Colloid and Interface Science* 209 (2014) 8–39.
- [2] N. Ahmed, H. Fessi, A. Elaissari, Theranostic applications of nanoparticles in cancer, *Drug Discovery Today* 17 (17-18) (2012) 928–934.
- [3] F. Peng, Z. Cao, X. Ji, B. Chu, Y. Su, Y. He, Silicon nanostructures for cancer diagnosis and therapy, *Nanomedicine* 10 (13) (2015) 2109–2123.
- [4] R. Ladj, A. Bitar, M.M. Eissa, H. Fessi, Y. Mugnier, R. Le Dantec, A. Elaissari, Polymer encapsulation of inorganic nanoparticles for biomedical applications, *International Journal of Pharmaceutics* 458 (1) (2013) 230–241.
- [5] M.C. Gomes, Â. Cunha, T. Trindade, J.P.C. Tomé, The role of surface functionalization of silica nanoparticles for bioimaging, *Journal of Innovative Optical Health Science* 9 (4) (2016) 1–16.
- [6] L. Tang, J. Cheng, Nonporous silica nanoparticles for nanomedicine application, *Nano Today* 8 (3) (2013) 290–312.
- [7] L. Wang, W. Zhao, W. Tan, Bioconjugated silica nanoparticles: development and applications, *Nano Research* 1 (2) (2008) 99–115.
- [8] S.S. Balamurugan, E. Soto-Cantu, R. Cueto, P.S. Russo, Preparation of organosoluble silica–polypeptide particles by “click” chemistry, *Macromolecules* 43 (1) (2010) 62–70.
- [9] A. Liberman, N. Mendez, W.C. Trogler, A.C. Kummel, Synthesis and surface functionalization of silica nanoparticles for nanomedicine, *Surface Science Reports* 69 (2-3) (2014) 132–158.
- [10] K. Wang, X. He, X. Yang, H. Shi, Functionalized silica nanoparticles: a platform for fluorescence imaging at the cell and small animal levels, *Accounts of Chemical Research* 46 (7) (2013) 1367–1376.
- [11] K. Natte, W. Österle, J.F. Friedrich, R. von Klitzing, G. Orts-Gil, Tuning interfacial properties and colloidal behavior of hybrid nanoparticles by controlling the polymer precursor, *Macromolecular Chemistry Physics* 213 (22) (2012) 2412–2419.
- [12] D. Drescher, G. Orts-Gil, G. Laube, K. Natte, R.W. Veh, W. Osterle, J. Kneipp, Toxicity of amorphous silica nanoparticles on eukaryotic cell model is determined by particle agglomeration and serum protein adsorption effects, *Analytical and Bioanalytical Chemistry* 400 (5) (2011) 1367–1373.
- [13] L. Tauhardt, K. Kempe, M. Gottschaldt, U.S. Schubert, Poly(2-oxazoline) functionalized surfaces: from modification to application, *Chemical Society Reviews* 42 (20) (2013) 7998–8011.

- [14] C. Barner-Kowollik, Handbook of RAFT polymerization, Wiley-VCH, Weinheim (2008).
- [15] P.S. Chinthamanipeta, S. Kobukata, H. Nakata, D.A. Shipp, Synthesis of poly(methyl methacrylate)–silica nanocomposites using methacrylate-functionalized silica nanoparticles and RAFT polymerization, *Polymer* 49 (26) (2008) 5636–5642.
- [16] J. Moraes, K. Ohno, T. Maschmeyer, S. Perrier, Synthesis of silica-polymer core-shell nanoparticles by reversible addition-fragmentation chain transfer polymerization, *Chemical Communications* 49 (80) (2013) 9077–9088.
- [17] M. Bialk, O. Prucker, J. Rühle, Grafting of polymers to solid surfaces by using immobilized methacrylates, *Colloids and Surfaces A: Physicochemical and Engineering Aspects* 198-200 (2002) 543–549.
- [18] N. Marshall, S.K. Sontag, J. Locklin, Surface-initiated polymerization of conjugated polymers, *Chemical Communications* 47 (20) (2011) 5681–5689.
- [19] S. Banerjee, T.K. Paira, T.K. Mandal, Surface confined atom transfer radical polymerization: Access to custom library of polymer-based hybrid materials for speciality applications, *Polymer Chemistry* 5 (14) (2014) 4153–4167.
- [20] A. Krieg, C. Weber, R. Hoogenboom, C.R. Becer, U.S. Schubert, Block copolymers of poly(2-oxazoline)s and poly(meth)acrylates: a crossover between cationic ring-opening polymerization (CROP) and reversible addition–fragmentation chain transfer (RAFT), *ACS Macro Letters* 1 (6) (2012) 776–779.
- [21] G. Volet, C. Amiel, Polyoxazoline adsorption on silica nanoparticles mediated by host-guest interactions, *Colloids and Surfaces B: Biointerfaces* 91 (2012) 269–273.
- [22] H. Xu, F. Yan, E.E. Monson, R. Kopelman, Room-temperature preparation and characterization of poly (ethylene glycol)-coated silica nanoparticles for biomedical applications, *Journal of Biomedical Materials Research. Part A* 66 (4) (2003) 870–879.
- [23] R. Luxenhofer, Y. Han, A. Schulz, J. Tong, Z. He, A.V. Kabanov, R. Jordan, Poly(2-oxazoline)s as polymer therapeutics, *Macromolecular Rapid Communications* 33 (19) (2012) 1613–1631.
- [24] B. Guillerm, S. Monge, V. Lapinte, J.-J. Robin, How to modulate the chemical structure of polyoxazolines by appropriate functionalization, *Macromolecular Rapid Communications* 33 (19) (2012) 1600–1612.
- [25] K. Knop, R. Hoogenboom, D. Fischer, U.S. Schubert, Poly(ethylene glycol) in drug delivery: pros and cons as well as potential alternatives, *Angewandte Chemie International Edition* 49 (36) (2010) 6288–6308.
- [26] F. Manzenrieder, R. Luxenhofer, M. Retzlaff, R. Jordan, M.G. Finn, Stabilization of virus-like particles with poly(2-oxazoline)s, *Angewandte Chemie International Edition* 50 (11) (2011) 2601–2605.
- [27] E.D.H. Mansfield, K. Sillence, P. Hole, A.C. Williams, V.V. Khutoryanskiy, POZylation: a new approach to enhance nanoparticle diffusion through mucosal barriers, *Nanoscale* 7 (32) (2015) 13671–13679.

- [28] H. Wang, L. Chen, Y. Feng, H. Chen, Exploiting core-shell synergy for nanosynthesis and mechanistic investigation, *Accounts of Chemical Research* 46 (7) (2013) 1636–1646.
- [29] R. Ghosh Chaudhuri, S. Paria, Core/shell nanoparticles: classes, properties, synthesis mechanisms, characterization, and applications, *Chemical Reviews* 112 (4) (2012) 2373–2433.
- [30] M.B. Gawande, A. Goswami, T. Asefa, H. Guo, A.V. Biradar, D.-L. Peng, R. Zboril, R.S. Varma, Core-shell nanoparticles: synthesis and applications in catalysis and electrocatalysis, *Chemical Society Reviews* 44 (21) (2015) 7540–7590.
- [31] M. Hood, M. Mari, R. Muñoz-Espí, Synthetic strategies in the preparation of polymer/inorganic hybrid nanoparticles, *Materials* 7 (5) (2014) 4057–4087.
- [32] Y. Huang, T. Hou, X. Cao, S. Perrier, Y. Zhao, Synthesis of silica-polymer hybrids by combination of RAFT polymerization and azide-alkyne cycloaddition ‘click’ reactions, *Polymer Chemistry* 1 (10) (2010) 1615–1623.
- [33] K.S. Kumar, V.B. Kumar, P. Paik, Recent advancement in functional core-shell nanoparticles of polymers: synthesis, physical properties, and applications in medical biotechnology, *Journal of Nanoparticles* 2013 (10) (2013) 1–24.
- [34] Zhao, S. Perrier, Synthesis of well-defined homopolymer and diblock copolymer grafted onto silica particles by z-Supported RAFT polymerization, *Macromolecules* 39 (25) (2006) 8603–8608.
- [35] O. Eckardt, C. Pietsch, O. Zumann, M. von der Lühe, D.S. Brauer, F.H. Schacher, Well-defined SiO₂@P(EtOx-stat -EI) core-shell hybrid nanoparticles via sol-gel processes, *Macromolecular Rapid Communications* 37 (4) (2016) 337–342.
- [36] N. Sounderya, Y. Zhang, Use of core/shell structured nanoparticles for biomedical applications, *Biomedical Engineering* 1 (1) (2008) 34–42.
- [37] Y. Zhao, B.G. Trewyn, I.I. Slowing, V.S.-Y. Lin, Mesoporous silica nanoparticle-based double drug delivery system for glucose-responsive controlled release of insulin and cyclic AMP, *Journal of the American Chemical Society* 131 (24) (2009) 8398–8400.
- [38] N.P. Sardesai, J.C. Barron, J.F. Rusling, Carbon nanotube microwell array for sensitive electrochemiluminescent detection of cancer biomarker proteins, *Analytical Chemistry* 83 (17) (2011) 6698–6703.
- [39] T. Chen, M.I. Shukoor, R. Wang, Z. Zhao, Q. Yuan, S. Bamrungsap, X. Xiong, W. Tan, Smart multifunctional nanostructure for targeted cancer chemotherapy and magnetic resonance imaging, *ACS Nano* 5 (10) (2011) 7866–7873.
- [40] X. Wu, M. Wu, J.X. Zhao, Recent development of silica nanoparticles as delivery vectors for cancer imaging and therapy, *Nanomedicine Nanotechnology, Biology, and Medicine* 10 (2) (2014) 297–312.
- [41] W.-H. Zhang, X.-X. Hu, X.-B. Zhang, Dye-doped fluorescent silica nanoparticles for live cell and in vivo bioimaging, *Nanomaterials* 6 (5) (2016) 81–98.
- [42] A.R. Kherlopian, T. Song, Q. Duan, M.A. Neimark, M.J. Po, J.K. Gohagan, A.F. Laine, A review of imaging techniques for systems biology, *BMC Systems Biology* 2 (74) (2008) 1–18.

- [43] T. Terai, T. Nagano, Fluorescent probes for bioimaging applications, *Current Opinion in Chemical Biology* 12 (5) (2008) 515–521.
- [44] T. Terai, T. Nagano, Small-molecule fluorophores and fluorescent probes for bioimaging, *European Journal of Physiology* 465 (3) (2013) 347–359.
- [45] O.S. Wolfbeis, An overview of nanoparticles commonly used in fluorescent bioimaging, *Chemical Society Reviews* 44 (14) (2015) 4743–4768.
- [46] D.O. Volkov, E.-B. Cho, I. Sokolov, Synthesis of ultrabright nanoporous fluorescent silica discoids using an inorganic silica precursor, *Nanoscale* 3 (5) (2011) 2036–2043.
- [47] S.J. Soenen, B.B. Manshian, T. Aubert, U. Himmelreich, J. Demeester, S.C. de Smedt, Z. Hens, K. Braeckmans, Cytotoxicity of cadmium-free quantum dots and their use in cell bioimaging, *Chemical Research in Toxicology* 27 (6) (2014) 1050–1059.
- [48] S.K. Nune, P. Gunda, P.K. Thallapally, Y.-Y. Lin, M.L. Forrest, C.J. Berkland, Nanoparticles for biomedical imaging, *Expert Opinion on Drug Delivery* 6 (11) (2009) 1175–1194.
- [49] D. Pantarotto, J.-P. Briand, M. Prato, A. Bianco, Translocation of bioactive peptides across cell membranes by carbon nanotubes, *Chemical Communications* (1) (2004) 16–17.
- [50] S.D. Topel, O. Topel, R.B. Bostancioglu, A.T. Koparal, Synthesis and characterization of Bodipy functionalized magnetic iron oxide nanoparticles for potential bioimaging applications, *Colloids and Surfaces B: Biointerfaces* 128 (2015) 245–253.
- [51] M.R. Hamblin, P. Avci, *Applications of nanoscience in photomedicine*, Woodhead Publishing, Cambridge (2015).
- [52] R.P. Bagwe, C. Yang, L.R. Hilliard, W. Tan, Optimization of dye-doped silica nanoparticles prepared using a reverse microemulsion method, *Langmuir* 20 (19) (2004) 8336–8342.
- [53] S.J. Soenen, B. Manshian, S.H. Doak, S.C. de Smedt, K. Braeckmans, Fluorescent non-porous silica nanoparticles for long-term cell monitoring: cytotoxicity and particle functionality, *Acta Biomaterialia* 9 (11) (2013) 9183–9193.
- [54] M. Benezra, O. Penate-Medina, P.B. Zanzonico, D. Schaer, H. Ow, A. Burns, E. DeStanchina, V. Longo, E. Herz, S. Iyer, J. Wolchok, S.M. Larson, U. Wiesner, M.S. Bradbury, Multimodal silica nanoparticles are effective cancer-targeted probes in a model of human melanoma, *The Journal of Clinical Investigation* 121 (7) (2011) 2768–2780.
- [55] J.-H. Park, L. Gu, G. von Maltzahn, E. Ruoslahti, S.N. Bhatia, M.J. Sailor, Biodegradable luminescent porous silicon nanoparticles for in vivo applications, *Nature Materials* 8 (4) (2009) 331–336.
- [56] M. Cho, W.-S. Cho, M. Choi, S.J. Kim, B.S. Han, S.H. Kim, H.O. Kim, Y.Y. Sheen, J. Jeong, The impact of size on tissue distribution and elimination by single intravenous injection of silica nanoparticles, *Toxicology Letters* 189 (3) (2009) 177–183.

- [57] Z. Xu, Y. Li, B. Zhang, T. Purkait, A. Alb, B.S. Mitchell, S.M. Grayson, M.J. Fink, Water-soluble PEGylated silicon nanoparticles and their assembly into swellable nanoparticle aggregates, *Journal of Nanoparticle Research* 17 (1) (2015) 1–16.
- [58] X. Huang, N. P, H. E, Characterization and comparison of mesoporous silica particles for optimized drug delivery, *Nanomaterials and Nanotechnology* 4 (2) (2014) 1–15.
- [59] J.L. Vivero-Escoto, R.C. Huxford-Phillips, W. Lin, Silica-based nanoprobe for biomedical imaging and theranostic applications, *Chemical Society Reviews* 41 (7) (2012) 2673–2685.
- [60] G. Bissadi, B. Kruczek, Thermal properties of silica/poly(2,6-dimethyl-1,4-phenylene oxide) films prepared by emulsion polymerization, *Journal of Thermal Analytical Calorimetry* 117 (1) (2014) 73–83.
- [61] K. Sinkó, Influence of chemical conditions on the nanoporous structure of silicate aerogels, *Materials* 3 (1) (2010) 704–740.
- [62] L.L. Hench, J.K. West, The sol-gel process, *Chemical Reviews* 90 (1) (1990) 33–72.
- [63] I.A. Rahman, V. Padavettan, Synthesis of silica nanoparticles by sol-gel: size-dependent properties, surface modification, and applications in silica-polymer nanocomposites - a review, *Journal of Nanomaterials* 2012 (30) (2012) 1–15.
- [64] Carcouet, Camille C M C, van de Put, Marcel W P, B. Mezari, Magusin, Pieter C M M, J. Laven, P.H.H. Bomans, H. Friedrich, A.C.C. Esteves, Sommerdijk, Nico A J M, van Benthem, Rolf A T M, G. de With, Nucleation and growth of monodisperse silica nanoparticles, *Nano Letters* 14 (3) (2014) 1433–1438.
- [65] B. Korzeniowska, R. Nooney, D. Wencel, C. McDonagh, Silica nanoparticles for cell imaging and intracellular sensing, *Nanotechnology* 24 (44) (2013) 442002 1–21.
- [66] W. Stöber, A. Fink, E. Bohn, Controlled growth of monodisperse silica spheres in the micron size range, *Journal of Colloid and Interface Science* 26 (1) (1968) 62–69.
- [67] F.J. Arriagada, K. Osseo-Asare, Phase and dispersion stability effects in the synthesis of silica nanoparticles in a non-ionic reverse microemulsion, *Colloids and Surfaces* 69 (2-3) (1992) 105–115.
- [68] A.P. Demchenko, P.R. Callis, G. Bergamini, A.M. Brouwer, *Advanced fluorescence reporters in chemistry and biology*, Springer, Heidelberg, (2010).
- [69] C.-L. Chang, H.S. Fogler, Kinetics of silica particle formation in nonionic W/O microemulsions from TEOS, *AIChE Journal* 42 (11) (1996) 3153–3163.
- [70] V.P. Chauhan, Z. Popovic, O. Chen, J. Cui, D. Fukumura, M.G. Bawendi, R.K. Jain, Fluorescent nanorods and nanospheres for real-time in vivo probing of nanoparticle shape-dependent tumor penetration, *Angewandte Chemie International Edition* 50 (48) (2011) 11417–11420.
- [71] Y. Yang, C. Yu, Advances in silica based nanoparticles for targeted cancer therapy, *Nanomedicine: Nanotechnology, Biology and Medicine* 12 (2) (2016) 317–332.
- [72] F. Alexis, E. Pridgen, L.K. Molnar, O.C. Farokhzad, Factors affecting the clearance and biodistribution of polymeric nanoparticles, *Molecular Pharmaceutics* 5 (4) (2008) 505–515.

- [73] G.H. Bogush, M.A. Tracy, C.F. Zukoski, Preparation of monodisperse silica particles: control of size and mass fraction, *Journal of Non-Crystalline Solids* 104 (1) (1988) 95–106.
- [74] J.W. Kim, L.U. Kim, C.K. Kim, Size control of silica nanoparticles and their surface treatment for fabrication of dental nanocomposites, *Biomacromolecules* 8 (1) (2007) 215–222.
- [75] S. Liang, C.L. John, S. Xu, J. Chen, Y. Jin, Q. Yuan, W. Tan, J.X. Zhao, Silica-based nanoparticles: design and properties, in: A.P. Demchenko (Ed.), *Advanced fluorescence reporters in chemistry and biology II*, Springer Berlin Heidelberg, Berlin, Heidelberg, (2010) 229–251.
- [76] N. Jaramillo, C. Paucar, C. García, Influence of the reaction time and the triton x-100/cyclohexane/methanol/H₂O ratio on the morphology and size of silica nanoparticles synthesized via sol–gel assisted by reverse micelle microemulsion, *Journal of Materials Science* 49 (9) (2014) 3400–3406.
- [77] H. Yoo, J. Pak, Synthesis of highly fluorescent silica nanoparticles in a reverse microemulsion through double-layered doping of organic fluorophores, *Journal of Nanoparticle Research* 15 (5) (2013) 1–10.
- [78] N.P. Truong, M.R. Whittaker, C.W. Mak, T.P. Davis, The importance of nanoparticle shape in cancer drug delivery, *Expert Opinion on Drug Delivery* 12 (1) (2015) 129–142.
- [79] S. Barua, S. Mitragotri, Challenges associated with penetration of nanoparticles across cell and tissue barriers: a review of current status and future prospects, *Nano Today* 9 (2) (2014) 223–243.
- [80] Y. Geng, P. Dalhaimer, S. Cai, R. Tsai, M. Tewari, T. Minko, D.E. Discher, Shape effects of filaments versus spherical particles in flow and drug delivery, *Nature Nanotechnology* 2 (4) (2007) 249–255.
- [81] H. Nakamura, Y. Matsui, Silica gel nanotubes obtained by the sol-gel method, *Journal of American Chemical Society* 117 (9) (1995) 2651–2652.
- [82] X. Yang, H. Tang, K. Cao, H. Song, W. Sheng, Q. Wu, Templated-assisted one-dimensional silica nanotubes: synthesis and applications, *Journal of Materials Chemistry* 21 (17) (2011) 6122–6135.
- [83] J. Yu, X. Bai, J. Suh, S.B. Lee, S.J. Son, Mechanical capping of silica nanotubes for encapsulation of molecules, *Journal of the American Chemical Society* 131 (43) (2009) 15574–15575.
- [84] M. Kim, J. Hong, J. Lee, C.K. Hong, S.E. Shim, Fabrication of silica nanotubes using silica coated multi-walled carbon nanotubes as the template, *Journal of Colloid and Interface Science* 322 (1) (2008) 321–326.
- [85] M. Yamanaka, Y. Miyake, S. Akita, K. Nakano, Sol–gel transcription of semi-fluorinated organogel fiber into fluorocarbon-functionalized silica nanotubes, *Chemistry of Materials* 20 (6) (2008) 2072–2074.
- [86] R.P. Bagwe, L.R. Hilliard, W. Tan, Surface modification of silica nanoparticles to reduce aggregation and nonspecific binding, *Langmuir* 22 (9) (2006) 4357–4362.

- [87] K.-M. Kim, H.M. Kim, W.-J. Lee, C.-W. Lee, T.-i. Kim, J.-K. Lee, J. Jeong, S.-M. Paek, J.-M. Oh, Surface treatment of silica nanoparticles for stable and charge-controlled colloidal silica, *International Journal of Nanomedicine* 9 (2) (2014) 29–40.
- [88] J.R. Lakowicz, C.D. Geddes, *Topics in fluorescence spectroscopy*, Plenum Press, New York (1991).
- [89] A. van Blaaderen, A. Vrij, Synthesis and characterization of colloidal dispersions of fluorescent, monodisperse silica spheres, *Langmuir* 8 (12) (1992) 2921–2931.
- [90] G.T. Hermanson, *Bioconjugate techniques*, Elsevier/Academic Press, Amsterdam (2013).
- [91] A. Auger, J. Samuel, O. Poncelet, O. Raccurt, A comparative study of non-covalent encapsulation methods for organic dyes into silica nanoparticles, *Nanoscale Research Letters* 6 (1) (2011) 328–340.
- [92] L. Wang, K. Wang, S. Santra, X. Zhao, L.R. Hilliard, J.E. Smith, Y. Wu, W. Tan, Watching silica nanoparticles glow in the biological world, *Analytical Chemistry* 78 (3) (2006) 646–654.
- [93] N. Thepwiwatjit, A. Thattiyaphong, P. Limsuwan, K. Tuitemwong, P. Tuitemwong, Antibody-conjugated Rubpy dye-doped silica nanoparticles as signal amplification for microscopic detection of vibrio cholerae O1, *Journal of Nanomaterials* 2013 (3) (2013) 1–7.
- [94] X. Mu, C. Wu, J. Lai, J. Chen, J. Zheng, C. Li, Y. Zhao, A facile and general approach for the synthesis of fluorescent silica nanoparticles doped with inert dyes, *Chinese Science Bulletin* 56 (31) (2011) 3242–3246.
- [95] Y. Matsumura, H. Maeda, A new concept for macromolecular therapeutics in cancer chemotherapy: mechanism of tumorotropic accumulation of proteins and the antitumor agent smancs, *Cancer Research* 46 (12 Pt 1) (1986) 6387–6392.
- [96] S. Salmaso, P. Caliceti, Stealth properties to improve therapeutic efficacy of drug nanocarriers, *Journal of Drug Delivery* 2013 (2013) 1–19.
- [97] T.X. Viegas, M.D. Bentley, J.M. Harris, Z. Fang, K. Yoon, B. Dizman, R. Weimer, A. Mero, G. Pasut, F.M. Veronese, Polyoxazoline: chemistry, properties, and applications in drug delivery, *Bioconjugate Chemistry* 22 (5) (2011) 976–986.
- [98] N.T. Thanh, L.A. Green, Functionalisation of nanoparticles for biomedical applications, *Nano Today* 5 (3) (2010) 213–230.
- [99] F.C. Gaertner, R. Luxenhofer, B. Blechert, R. Jordan, M. Essler, Synthesis, biodistribution and excretion of radiolabeled poly(2-alkyl-2-oxazolines), *Journal of Controlled Release Society* 119 (3) (2007) 291–300.
- [100] A. Makino, S. Kobayashi, Chemistry of 2-oxazolines: A crossing of cationic ring-opening polymerization and enzymatic ring-opening polyaddition, *Journal of Polymer Science Part A: Polymer Chemistry* 48 (6) (2010) 1251–1270.
- [101] T. Kagiya, S. Narisawa, T. Maeda, K. Fukui, Ring-opening polymerization of 2-substituted 2-oxazolines, *Journal of Polymer Science Part B: Polymer Letters* 4 (7) (1966) 441–445.

- [102] K. AOI, Polymerization of oxazolines, *Progress in Polymer Science* 21 (1) (1996) 151–208.
- [103] J.S. Hrkach, K. Matyjaszewski, Reaction of 2-methyl-2-oxazoline with trimethylsilyl initiators: an unusual mode of ring opening, *Macromolecules* 25 (8) (1992) 2070–2075.
- [104] P. Dubois, O. Coulembier, J.M. Raquez, *Handbook of ring-opening polymerization*, Wiley-VCH, Weinheim (2009) 141–164.
- [105] T. Saegusa, H. Ikeda, H. Fujii, Isomerization polymerization of 2-oxazoline. II. propagating species and mechanism of unsubstituted 2-oxazoline polymerization, *Polymer Journal* 3 (2) (1972) 176–180.
- [106] R. Weberskirch, R. Hettich, O. Nuyken, D. Schmaljohann, B. Voit, Synthesis of new amphiphilic star polymers derived from a hyperbranched macroinitiator by the cationic ‘grafting from’ method, *Macromolecular Chemistry Physics* 200 (4) (1999) 863–873.
- [107] N. Adams, U.S. Schubert, Poly(2-oxazolines) in biological and biomedical application contexts, *Advanced Drug Delivery Reviews* 59 (15) (2007) 1504–1520.
- [108] M. Litt, A. Levy, J. Herz, Polymerization of Cyclic Imino Ethers. X. Kinetics, chain transfer, and repolymerization, *Journal of Macromolecular Science: Part A: Chemistry* 9 (5) (1975) 703–727.
- [109] J.M. Warakowski, B.P. Thill, Evidence for long chain branching in polyethyloxazoline, *Journal of Polymer Science Part A: Polymer Chemistry* 28 (13) (1990) 3551–3563.
- [110] F. Hu, S. Xie, L. Jiang, Z. Shen, Living cationic ring-opening polymerization of 2-oxazolines initiated by rare-earth metal triflates, *RSC Advances* 4 (104) (2014) 59917–59926.
- [111] C. Legros, *Engineering of poly(2-oxazoline)s for potential use in biomedical applications*, University of Waterloo (2015).
- [112] K. Kempe, S. Onbulak, U.S. Schubert, A. Sanyal, R. Hoogenboom, pH degradable dendron-functionalized poly(2-ethyl-2-oxazoline) prepared by a cascade “double-click” reaction, *Polymer Chemistry* 4 (11) (2013) 3236.
- [113] M.W.M. Fijten, C. Haensch, B.M. van Lankvelt, R. Hoogenboom, U.S. Schubert, Clickable poly(2-oxazoline)s as versatile building blocks, *Macromolecular Chemistry Physics* 209 (18) (2008) 1887–1895.
- [114] K. Kempe, R. Hoogenboom, M. Jaeger, U.S. Schubert, Three-fold metal-free efficient (“click”) reactions onto a multifunctional poly(2-oxazoline) designer scaffold, *Macromolecules* 44 (16) (2011) 6424–6432.
- [115] J.C. Rueda, H. Komber, J.C. Cedrón, B. Voit, G. Shevtsova, Synthesis of new hydrogels by copolymerization of poly(2-methyl-2-oxazoline) bis(macromonomers) and N-vinylpyrrolidone, *Macromolecular Chemistry Physics* 204 (7) (2003) 947–953.
- [116] M. Einzmann, W.H. Binder, Novel functional initiators for oxazoline polymerization, *Journal of Polymer Science Part A: Polymer Chemistry* 39 (16) (2001) 2821–2831.

- [117] Y. Yang, K. Kataoka, F.M. Winnik, Synthesis of diblock copolymers consisting of hyaluronan and poly(2-ethyl-2-oxazoline), *Macromolecules* 38 (6) (2005) 2043–2046.
- [118] T.-X. Lav, P. Lemechko, E. Renard, C. Amiel, V. Langlois, G. Volet, Development of a new azido-oxazoline monomer for the preparation of amphiphilic graft copolymers by combination of cationic ring-opening polymerization and click chemistry, *Reactive and Functional Polymers* 73 (8) (2013) 1001–1008.
- [119] R. Luxenhofer, R. Jordan, Click chemistry with poly(2-oxazoline)s, *Macromolecules* 39 (10) (2006) 3509–3516.
- [120] A. Gress, A. Völkel, H. Schlaad, Thio-click modification of poly[2-(3-butenyl)-2-oxazoline], *Macromolecules* 40 (22) (2007) 7928–7933.
- [121] C. Taubmann, R. Luxenhofer, S. Cesana, R. Jordan, First aldehyde-functionalized poly(2-oxazoline)s for chemoselective ligation, *Macromolecular bioscience* 5 (7) (2005) 603–612.
- [122] S. Cesana, J. Auernheimer, R. Jordan, H. Kessler, O. Nuyken, First poly(2-oxazoline)s with pendant amino groups, *Macromolecular Chemistry and Physics* 207 (2) (2006) 183–192.
- [123] S. Cesana, A. Kurek, M.A. Baur, J. Auernheimer, O. Nuyken, Polymer-bound thiol groups on poly(2-oxazoline)s, *Macromolecular Rapid Communications* 28 (5) (2007) 608–615.
- [124] M.T. Zarka, O. Nuyken, R. Weberskirch, Amphiphilic polymer supports for the asymmetric hydrogenation of amino acid precursors in water, *Chemistry* 9 (14) (2003) 3228–3234.
- [125] A. Levy, M. Litt, Polymerization of cyclic iminoethers. V. 1,3-oxazolines with hydroxy-, acetoxy-, and carboxymethyl-alkyl groups in the 2 position and their polymers, *Journal of Polymer Science Part A: Polymer Chemistry* 6 (7) (1968) 1883–1894.
- [126] S. Konieczny, C.P. Fik, N.J.H. Aversch, J.C. Tiller, Organosoluble enzyme conjugates with poly(2-oxazoline)s via pyromellitic acid dianhydride, *Journal of Biotechnology* 159 (3) (2012) 195–203.
- [127] C. Krumm, S. Konieczny, G.J. Dropalla, M. Milbradt, J.C. Tiller, Amphiphilic polymer conetworks based on end group cross-linked poly(2-oxazoline) homo- and triblock copolymers, *Macromolecules* 46 (9) (2013) 3234–3245.
- [128] M. Glassner, K. Kempe, U.S. Schubert, R. Hoogenboom, C. Barner-Kowollik, One-pot synthesis of cyclopentadienyl endcapped poly(2-ethyl-2-oxazoline) and subsequent ambient temperature diels-alder conjugations, *Chemical Communications* 47 (38) (2011) 10620–10622.
- [129] K. Kempe, K.L. Killops, J.E. Poelma, H. Jung, J. Bang, R. Hoogenboom, H. Tran, C.J. Hawker, U.S. Schubert, L.M. Campos, Strongly phase-segregating block copolymers with sub-20 nm features, *CS Macro Letters* 2 (8) (2013) 677–682.
- [130] G. David, V. Alupei, B.C. Simionescu, End-capping of living poly(2-methyl-2-oxazoline) with maleic acid, *European Polymer Journal* 37 (7) (2001) 1353–1358.

- [131] M. Miyamoto, K. Naka, M. Tokumizu, T. Saegusa, End capping of growing species of poly(2-oxazoline) with carboxylic acid: a novel and convenient route to prepare vinyl- and carboxy-terminated macromonomers, *Macromolecules* 22 (4) (1989) 1604–1607.
- [132] R.R. Bhat, M.R. Tomlinson, T. Wu, J. Genzer, Surface-grafted polymer gradients: formation, characterization, and applications, in: R. Jordan, *Surface-initiated polymerization II*, Springer-Verlag, Berlin/Heidelberg (2006) 51–124.
- [133] D. Li, Q. Zheng, Y. Wang, H. Chen, Combining surface topography with polymer chemistry: exploring new interfacial biological phenomena, *Polymer Chemistry* 5 (1) (2014) 14–24.
- [134] D.S. Achilleos, M. Vamvakaki, End-grafted polymer chains onto inorganic nano-objects, *Materials* 3 (3) (2010) 1981–2026.
- [135] B. Radhakrishnan, R. Ranjan, W.J. Brittain, Surface initiated polymerizations from silica nanoparticles, *Soft Matter* 2 (5) (2006) 386–396.
- [136] B. Zdyrko, I. Luzinov, Polymer brushes by the "grafting to" method, *Macromolecular Rapid Communications* 32 (12) (2011) 859–869.
- [137] W. Taylor, R.A.L. Jones, Producing high-density high-molecular-weight polymer brushes by a "grafting to" method from a concentrated homopolymer solution, *Langmuir the ACS Journal of Surfaces and Colloids* 26 (17) (2010) 13954–13958.
- [138] G. Liu, H. Cheng, L. Yan, G. Zhang, Study of the kinetics of the pancake-to-brush transition of poly(N-isopropylacrylamide) chains, *The Journal of Physical Chemistry B* 109 (47) (2005) 22603–22607.
- [139] H.-S. Lee, L.S. Penn, In situ study of polymer brushes as selective barriers to diffusion, *Macromolecules* 41 (21) (2008) 8124–8129.
- [140] F. Hoffmann, T. Wolff, S. Minko, M. Stamm, Photochemical structuring and fixing of structures in binary polymer brush layers via 2pi+2pi photodimerization, *Journal of Colloid and Interface Science* 282 (2) (2005) 349–358.
- [141] M. Motornov, R. Sheparovych, I. Tokarev, Y. Roiter, S. Minko, Nonwetable thin films from hybrid polymer brushes can be hydrophilic, *Langmuir the ACS Journal of Surfaces and Colloids* 23 (1) (2007) 13–19.
- [142] R. Ranjan, W.J. Brittain, Tandem RAFT polymerization and click chemistry: an efficient approach to surface modification, *Macromolecular Rapid Communications* 28 (21) (2007) 2084–2089.
- [143] V. Maurice, C. Slostowski, N. Herlin-Boime, G. Carrot, Polymer-grafted silicon nanoparticles obtained either via peptide bonding or click chemistry, *Macromolecular Chemistry and Physics* 213 (23) (2012) 2498–2503.
- [144] R. Ranjan, W.J. Brittain, Combination of living radical polymerization and click chemistry for surface modification, *Macromolecules* 40 (17) (2007) 6217–6223.
- [145] N. Li, W.H. Binder, Click-chemistry for nanoparticle-modification, *Journal of Materials Chemistry* 21 (42) (2011) 16717.
- [146] C. Tissandier, N. Diop, M. Martini, S. Roux, O. Tillement, T. Hamaide, One-pot synthesis of hybrid multifunctional silica nanoparticles with tunable coating by click

- chemistry in reverse w/o microemulsion, *Langmuir the ACS Journal of Surfaces and Colloids* 28 (1) (2012) 209–218.
- [147] P. Paoprasert, J.W. Spalanka, D.L. Peterson, R.E. Ruther, R.J. Hamers, P.G. Evans, P. Gopalan, Grafting of poly(3-hexylthiophene) brushes on oxides using click chemistry, *Journal of Materials Chemistry* 20 (13) (2010) 2651–2658.
- [148] M. Kar, P.S. Vijayakumar, B.L.V. Prasad, S. Sen Gupta, Synthesis and characterization of poly-L-lysine-grafted silica nanoparticles synthesized via NCA polymerization and click chemistry, *Langmuir the ACS Journal of Surfaces and Colloids* 26 (8) (2010) 5772–5781.
- [149] Y. Huang, Q. Liu, X. Zhou, S. Perrier, Y. Zhao, Synthesis of silica particles grafted with well-defined living polymeric chains by combination of RAFT polymerization and coupling reaction, *Macromolecules* 42 (15) (2009) 5509–5517.
- [150] M.M. Rahman, M. Takafuji, Hirotaka, Noncrystalline L-phenylalanine-silica hybrid composite materials for high selective reversed phase liquid chromatography, in: J. Cuppoletti, Metal, ceramic and polymeric composites for various uses, InTech, Rijeka (2011).
- [151] W.J. Brittain, S. Minko, A structural definition of polymer brushes, *Polymer Science Part: A Polymer Chemistry* 45 (16) (2007) 3505–3512.
- [152] Z. Zhang, M.-L. Chen, X.-D. Cheng, Z.-G. Shi, B.-F. Yuan, Y.-Q. Feng, A facile approach for the polymer grafting of silica based on tandem reversible addition fragmentation chain transfer/click chemistry and its application in high performance liquid chromatography, *Journal of Chromatography A* 1351 (2014) 96–102.
- [153] R. Inoubli, S. Dagr  ou, A. Khoukh, F. Roby, J. Peyrelasse, L. Billon, ‘Graft from’ polymerization on colloidal silica particles: elaboration of alkoxyamine grafted surface by in situ trapping of carbon radicals, *Polymer* 46 (8) (2005) 2486–2496.
- [154] L. Wu, U. Glebe, A. B  ker, Surface-initiated controlled radical polymerizations from silica nanoparticles, gold nanocrystals, and bionanoparticles, *Polymer Chemistry* 6 (29) (2015) 5143–5184.
- [155] R. Jordan, K. Martin, H.J. R  der, K.K. Unger, Lipopolymers for surface functionalizations. 1. synthesis and characterization of terminal functionalized poly(N-propionylethylenimine)s, *Macromolecules* 34 (26) (2001) 8858–8865.
- [156] T.K. Mandal, M.S. Fleming, D.R. Walt, Production of hollow polymeric microspheres by surface-confined living radical polymerization on silica templates, *Chemistry of Materials* 12 (11) (2000) 3481–3487.
- [157] R. Jordan, A. Ulman, J.F. Kang, M.H. Rafailovich, J. Sokolov, Surface-initiated anionic polymerization of styrene by means of self-assembled monolayers, *Journal of American Chemical Society* 121 (5) (1999) 1016–1022.
- [158] B. Zhao, W.J. Brittain, W. Zhou, S.Z.D. Cheng, Nanopattern formation from tethered PS- b -PMMA brushes upon treatment with selective solvents, *Journal of American Chemical Society* 122 (10) (2000) 2407–2408.
- [159] A. Juang, O.A. Scherman, R.H. Grubbs, N.S. Lewis, Formation of covalently attached polymer overlayers on Si(111) surfaces using ring-opening metathesis polymerization methods, *Langmuir* 17 (5) (2001) 1321–1323.

- [160] T. von Werne, T.E. Patten, Preparation of structurally well-defined polymer–nanoparticle hybrids with controlled/living radical polymerizations, *Journal of American Chemical Society* 121 (32) (1999) 7409–7410.
- [161] T. von Werne, T.E. Patten, Atom transfer radical polymerization from nanoparticles: a tool for the preparation of well-defined hybrid nanostructures and for understanding the chemistry of controlled/“living” radical polymerizations from surfaces, *Journal of American Chemical Society* 123 (31) (2001) 7497–7505.
- [162] C. Bartholome, E. Beyou, E. Bourgeat-Lami, P. Chaumont, N. Zydowicz, Nitroxide-mediated polymerizations from silica nanoparticle surfaces: “graft from” polymerization of styrene using a triethoxysilyl-terminated alkoxyamine initiator, *Macromolecules* 36 (21) (2003) 7946–7952.
- [163] Y. Tsujii, M. Ejaz, K. Sato, A. Goto, T. Fukuda, Mechanism and kinetics of RAFT-mediated graft polymerization of styrene on a solid surface. 1. experimental evidence of surface radical migration, *Macromolecules* 34 (26) (2001) 8872–8878.
- [164] N. Zammarelli, M. Luksin, H. Raschke, R. Hergenröder, R. Weberskirch, "Grafting-from" polymerization of PMMA from stainless steel surfaces by a RAFT-mediated polymerization process, *Langmuir the ACS Journal of Surfaces and Colloids* 29 (41) (2013) 12834–12843.
- [165] M. Henze, D. Mädge, O. Prucker, J. Rühle, “Grafting through”: mechanistic aspects of radical polymerization reactions with surface-attached monomers, *Macromolecules* 47 (9) (2014) 2929–2937.
- [166] P. Datta, J. Genzer, “Grafting through” polymerization involving surface-bound monomers, *Journal of Polymer Science Part A: Polymer Chemistry* 54 (2) (2016) 263–274.
- [167] D. Roy, M. Semsarilar, J.T. Guthrie, S. Perrier, Cellulose modification by polymer grafting: a review, *Chemical Society Reviews* 38 (7) (2009) 2046–2064.
- [168] B.-J. Chang, O. Prucker, E. Groh, A. Wallrath, M. Dahm, J. Rühle, Surface-attached polymer monolayers for the control of endothelial cell adhesion, *Colloids and Surfaces A: Physicochemical and Engineering Aspects* 198-200 (2002) 519–526.
- [169] H. Murata, B.-J. Chang, O. Prucker, M. Dahm, J. Rühle, Polymeric coatings for biomedical devices, *Surface Science* 570 (1-2) (2004) 111–118.
- [170] T. Ogoshi, Y. Chujo, Synthesis of colloidal polyoxazoline/silica hybrids prepared in an aqueous solution, *Polymer* 47 (11) (2006) 4036–4041.
- [171] H. Li, B. Meng, S.-H. Chai, H. Liu, S. Dai, Hyper-crosslinked β -cyclodextrin porous polymer: an adsorption-facilitated molecular catalyst support for transformation of water-soluble aromatic molecules, *Chemical Science* 7 (2) (2016) 905–909.
- [172] N. Tsubokawa, S. Yoshikawa, Grafting of polymers with controlled molecular weight onto ultrafine silica surface, *Journal of Polymer Science Part A: Polymer Chemistry* 33 (3) (1995) 581–586.
- [173] F. Rehfeldt, M. Tanaka, L. Pagnoni, R. Jordan, Static and dynamic swelling of grafted poly(2-alkyl-2-oxazoline)s, *Langmuir* 18 (12) (2002) 4908–4914.

- [174] Y. Chujo, E. Ihara, K. Suzuki, T. Saegusa, Synthesis of amphiphilic silane coupling agents based on poly(2-ethyl-2-oxazoline) and their reactions with tetraethoxysilane, *Polymer Bulletin* 31 (3) (1993) 317–322.
- [175] T. Loontjens, L. Rique-Lurbet, Synthesis of α -alkyl ω -trimethoxysilane polyoxazolines and their application as coatings on glass fibres, *Designed Monomers and Polymers* 2 (3) (1999) 217–229.
- [176] Y. Chujo, E. Ihara, H. Ihara, T. Saegusa, A novel silane coupling agent. 1. synthesis of trimethoxysilyl-terminated poly(N-acetyleneimine), *Macromolecules* 22 (5) (1989) 2040–2043.
- [177] J.E. Hein, V.V. Fokin, Copper-catalyzed azide-alkyne cycloaddition (CuAAC) and beyond: new reactivity of copper(I) acetylides, *Chemical Society Reviews* 39 (4) (2010) 1302–1315.
- [178] K.A. Smith, D.L. Pickel, K. Yager, K. Kisslinger, R. Verduzco, Conjugated block copolymers via functionalized initiators and click chemistry, *Journal of Polymer Science Part A: Polymer Chemistry* 52 (2) (2014) 154–163.
- [179] H.C. Kolb, M.G. Finn, K.B. Sharpless, Click chemistry: diverse chemical function from a few good reactions, *Angewandte Chemie International Edition* 40 (11) (2001) 2004–2021.
- [180] C. Rosu, S. Selcuk, E. Soto-Cantu, P.S. Russo, Progress in silica polypeptide composite colloidal hybrids: from silica cores to fuzzy shells, *Colloid and Polymer Science* 292 (5) (2014) 1009–1040.
- [181] W. Lian, S.A. Litherland, H. Badrane, W. Tan, D. Wu, H.V. Baker, P.A. Gulig, D.V. Lim, S. Jin, Ultrasensitive detection of biomolecules with fluorescent dye-doped nanoparticles, *Analytical Biochemistry* 334 (1) (2004) 135–144.
- [182] Y. Sun, X. Wang, J. Wu, Y. Fu, J. Zhang, H. Li, W. Li, Effects of surfactant/water ratio and dye amount on the fluorescent silica nanoparticles, *Colloid Journal* 72 (5) (2010) 723–729.
- [183] X. Mei, D. Chen, N. Li, Q. Xu, J. Ge, H. Li, B. Yang, Y. Xu, J. Lu, Facile preparation of coating fluorescent hollow mesoporous silica nanoparticles with pH-sensitive amphiphilic diblock copolymer for controlled drug release and cell imaging, *Soft Matter* 8 (19) (2012) 5309–5316.
- [184] W. Li, Y. Xu, Y. Zhou, W. Ma, S. Wang, Y. Dai, Silica nanoparticles functionalized via click chemistry and ATRP for enrichment of Pb(II) ion, *Nanoscale Research Letters* 7 (1) (2012) 485–492.
- [185] J. Lin, H. Chen, Y. Yuan, Y. Ji, Mechanochemically conjugated PMHS/nano-SiO₂ hybrid and subsequent optimum grafting density study, *Applied Surface Science* 257 (21) (2011) 9024–9032.
- [186] T. Ogoshi, K.-M. Kim, Y. Chujo, Synthesis and characterization of transparent poly(2-methyl-2-oxazoline) (POZO) – vanadium oxide (V₂O₅) hybrids with reversible formation, *Journal of Materials Chemistry* 13 (9) (2003) 2202–2207.
- [187] C.V. de Macedo, M.S. da Silva, T. Casimiro, E.J. Cabrita, A. Aguiar-Ricardo, Boron trifluoride catalyzed polymerisation of 2-substituted-2-oxazolines in supercritical carbon dioxide, *Green Chemistry* 9 (9) (2007) 948–953.

- [188] R. Jordan, N. West, A. Ulman, Y.-M. Chou, O. Nuyken, Nanocomposites by surface-initiated living cationic polymerization of 2-oxazolines on functionalized gold nanoparticles, *Macromolecules* 34 (6) (2001) 1606–1611.
- [189] I. Cianga, V.M. Mercore, M. Grigoras, Y. Yagci, Poly(thienyl-phenylene)s with macromolecular side chains by oxidative polymerization of well-defined macromonomers, *Journal of Polymer Science Part A: Polymer Chemistry* 45 (5) (2007) 848–865.
- [190] S. Xu, S. Hartvickson, J.X. Zhao, Increasing surface area of silica nanoparticles with a rough surface, *ACS Applied Materials & Interfaces* 3 (6) (2011) 1865–1872.
- [191] X. Hun, Z. Zhang, A novel sensitive staphylococcal enterotoxin C1 fluoroimmunoassay based on functionalized fluorescent core-shell nanoparticle labels, *Food Chemistry* 105 (4) (2007) 1623–1629.
- [192] A. Guerrero-Martínez, J. Pérez-Juste, L.M. Liz-Marzán, Recent progress on silica coating of nanoparticles and related nanomaterials, *Advanced Materials* 22 (11) (2010) 1182–1195.
- [193] M. Qhobosheane, S. Santra, P. Zhang, W. Tan, Biochemically functionalized silica nanoparticles, *Analyst* 126 (8) (2001) 1274–1278.
- [194] N. Iwakuma, P. Sharma, M.J. Delano, L.L. Moldawer, B.M. Moudgil, R. Grobmyer, Differential uptake of PEG-silica-FITC nanoparticles by human breast cancer cells, *NSTI Nanotechnology Conference and Trade Show, Santa Clara* (2007).
- [195] D. Ma, A.J. Kell, S. Tan, Z.J. Jakubek, B. Simard, Photophysical properties of dye-doped silica nanoparticles bearing different types of dye–silica interactions, *Journal of Physical Chemistry C* 113 (36) (2009) 15974–15981.
- [196] F. Olivero, F. Renò, F. Carniato, M. Rizzi, M. Cannas, L. Marchese, A novel luminescent bifunctional POSS as a molecular platform for biomedical applications, *Dalton Transactions* 41 (25) (2012) 7467–7473.
- [197] A. Pinna, L. Malfatti, G. Galleri, R. Manetti, S. Cossu, G. Rocchitta, R. Migheli, P.A. Serra, P. Innocenzi, Ceria nanoparticles for the treatment of Parkinson-like diseases induced by chronic manganese intoxication, *RSC Advances* 5 (26) (2015) 20432–20439.
- [198] A. Soleimani Dorcheh, M.H. Abbasi, Silica aerogel; synthesis, properties and characterization, *Journal of Materials Processing Technology* 199 (1-3) (2008) 10–26.
- [199] D. Li, Q. He, J. Li, Smart core/shell nanocomposites: intelligent polymers modified gold nanoparticles, *Advances in Colloid and Interface Science* 149 (1-2) (2009) 28–38.
- [200] S. Kobayashi, H. Uyama, Polymerization of cyclic imino ethers: From its discovery to the present state of the art, *Journal of Polymer Science Part A: Polymer Chemistry* 40 (2) (2002) 192–209.
- [201] H. Schlaad, C. Diehl, A. Gress, M. Meyer, A.L. Demirel, Y. Nur, A. Bertin, Poly(2-oxazoline)s as smart bioinspired polymers, *Macromolecular Rapid Communications* 31 (6) (2010) 511–525.

- [202] K. Yoshinaga, Y. Hidaka, Cationic graft-polymerization of 2-methyl-2-oxazoline on monodispersed polymer-coated ultrafine silica particles, *Polymer Journal* 26 (9) (1994) 1070–1079.
- [203] J. Ueda, W. Gang, K. Shirai, T. Yamauchi, N. Tsubokawa, Cationic graft polymerization onto silica nanoparticle surface in a solvent-free dry-system, *Polymer Bulletin* 60 (5) (2008) 617–624.
- [204] T. Lehmann, J. Rhe, Polyethyloxazoline monolayers for polymer supported biomembrane models, *Macromolecular Symposia* 142 (1) (1999) 1–12.
- [205] J.-H. Lee, Y.-C. An, D.-S. Choi, M.-J. Lee, K.-M. Kim, J.-H. Lim, Fabrication of a nano-porous polyoxazoline-coated tip for scanning probe nanolithography, *Macromolecular Symposia* 249-250 (1) (2007) 307–311.
- [206] G. Qi, L. Fu, E.P. Giannelis, Sponges with covalently tethered amines for high-efficiency carbon capture, *Nature Communications* 5 (2014) 5796–5803.
- [207] R. Jordan, A. Ulman, Surface initiated living cationic polymerization of 2-oxazolines, *Journal of American Chemical Society* 120 (2) (1998) 243–247.
- [208] G. Bayramoglu, B. Karagoz, N. Bicak, M.Y. Arica, Surface-initiated ring-opening polymerization of poly(2-methyl-2-oxazoline) from Poly(bromoethyl methacrylate/methyl methacrylate) microspheres and modification into PEI: immobilization of α -amylase by adsorption and cross-linking, *Industrial and Engineering Chemistry Research* 53 (37) (2014) 14263–14271.
- [209] N. Zhang, M. Steenackers, R. Luxenhofer, R. Jordan, Bottle-brush brushes: cylindrical molecular brushes of poly(2-oxazoline) on glassy carbon, *Macromolecules* 42 (14) (2009) 5345–5351.
- [210] N. Zhang, T. Pompe, I. Amin, R. Luxenhofer, C. Werner, R. Jordan, Tailored poly(2-oxazoline) polymer brushes to control protein adsorption and cell adhesion, *Macromolecular Bioscience* 12 (7) (2012) 926–936.
- [211] K. Matyjaszewski, N.V. Tsarevsky, Nanostructured functional materials prepared by atom transfer radical polymerization, *Nature Chemistry* 1 (4) (2009) 276–288.
- [212] Y. Li, B.C. Benicewicz, Functionalization of silica nanoparticles via the combination of surface-initiated RAFT polymerization and click reactions, *Macromolecules* 41 (21) (2008) 7986–7992.
- [213] H. Sabouri, K. Ohno, S. Perrier, Well-defined colloidal crystal films from the 2D self-assembly of core-shell semi-soft nanoparticles, *Polymer Chemistry* 6 (41) (2015) 7297–7307.
- [214] R. Mohammadi, Molecularly imprinted core shell nanoparticles by surface initiated RAFT polymerization, *Technische Universitt Dortmund* (2014).
- [215] M. Kowczyk-Sadowy, R. Świsłocka, H. Lewandowska, J. Piekut, W. Lewandowski, Spectroscopic (FT-IR, FT-Raman, ^1H - and ^{13}C -NMR), theoretical and microbiological study of trans o-coumaric acid and alkali metal o-coumarates, *Molecules* 20 (2) (2015) 3146–3169.
- [216] S.S. Deshmukh, V.I. Kovalchuk, V.Y. Borovkov, J.L. d'Itri, FTIR spectroscopic and reaction kinetics study of the interaction of CF_3CFCl_2 with $\gamma\text{-Al}_2\text{O}_3$, *Journal of Physical Chemistry B* 104 (6) (2000) 1277–1284.

- [217] M. Joubert, C. Delaite, E. Bourgeat Lami, P. Dumas, Synthesis of poly(ϵ -caprolactone)–silica nanocomposites: from hairy colloids to core–shell nanoparticles, *New Journal of Chemistry* 29 (12) (2005) 1601–1609.
- [218] K. Nagase, J. Kobayashi, A. Kikuchi, Y. Akiyama, H. Kanazawa, T. Okano, Effects of graft densities and chain lengths on separation of bioactive compounds by nanolayered thermoresponsive polymer brush surfaces, *Langmuir the ACS Journal of Surfaces and Colloids* 24 (2) (2008) 511–517.
- [219] R. Luxenhofer, Y. Han, A. Schulz, J. Tong, Z. He, A.V. Kabanov, R. Jordan, Poly(2-oxazoline)s as polymer therapeutics, *Macromolecular Rapid Communications* 33 (19) (2012) 1613–1631.
- [220] M. Nickels, J. Xie, J. Cobb, J.C. Gore, W. Pham, Functionalization of iron oxide nanoparticles with a versatile epoxy amine linker, *Journal of Materials Chemistry* 20 (23) (2010) 4776–4780.
- [221] S. Hozhabr Araghi, M.H. Entezari, Amino-functionalized silica magnetite nanoparticles for the simultaneous removal of pollutants from aqueous solution, *Applied Surface Science* 333 (2015) 68–77.
- [222] E. Soto-Cantu, R. Cueto, J. Koch, P.S. Russo, Synthesis and rapid characterization of amine-functionalized silica, *Langmuir* 28 (13) (2012) 5562–5569.
- [223] A. Pourjavadi, Z.M. Tehrani, A.A. Moghanaki, Folate-conjugated pH-responsive nanocarrier designed for active tumor targeting and controlled release of gemcitabine, *Pharmaceutical Research* 33 (2) (2016) 417–432.
- [224] J.A. Reddy, C. Abburi, H. Hofland, S.J. Howard, I. Vlahov, P. Wils, C.P. Leamon, Folate-targeted, cationic liposome-mediated gene transfer into disseminated peritoneal tumors, *Gene therapy* 9 (22) (2002) 1542–1550.
- [225] G. Destito, R. Yeh, C.S. Rae, M.G. Finn, M. Manchester, Folic acid-mediated targeting of cowpea mosaic virus particles to tumor cells, *Chemistry & Biology* 14 (10) (2007) 1152–1162.
- [226] Y. Liu, Yang, Lou, Xu, Wu, Investigation of folate-conjugated fluorescent silica nanoparticles for targeting delivery to folate receptor-positive tumors and their internalization mechanism, *International Journal of Nanomedicine* (2011) 2023–2032.
- [227] M. Sheikh Mohamed, A.C. Poulouse, S. Veerananarayanan, R. Romero Aburto, T. Mitcham, Y. Suzuki, Y. Sakamoto, P.M. Ajayan, R.R. Bouchard, Y. Yoshida, T. Maekawa, D. Sakthi Kumar, Plasmonic fluorescent CdSe/Cu₂S hybrid nanocrystals for multichannel imaging and cancer directed photo-thermal therapy, *Nanoscale* 8 (15) (2016) 7876–7888.
- [228] J. Bin, Y. Xiao, Z.T. Lin, Y.L. Deng, Y. Chen, D.E. Le, J. Bin, M. Li, Y. Liao, Y. Liu, G.B. Jiang, H. Wang, High molecular weight chitosan derivative polymeric micelles encapsulating superparamagnetic iron oxide for tumor-targeted magnetic resonance imaging, *International Journal of Nanomedicine* 5 (10) (2015) 1155–1172.
- [229] J.K. Herr, J.E. Smith, C.D. Medley, D. Shangguan, W. Tan, Aptamer-conjugated nanoparticles for selective collection and detection of cancer cells, *Analytical Chemistry* 78 (9) (2006) 2918–2924.

- [230] S. Santra, K. Wang, R. Tapeç, W. Tan, Development of novel dye-doped silica nanoparticles for biomarker application, *Journal of Biomedical Optics* 6 (2) (2001) 160–166.
- [231] D. Gao, Z. Zhang, M. Wu, C. Xie, G. Guan, D. Wang, A surface functional monomer-directing strategy for highly dense imprinting of TNT at surface of silica nanoparticles, *Journal of the American Chemical Society* 129 (25) (2007) 7859–7866.
- [232] X. Wang, S. Yao, H.Y. Ahn, Y. Zhang, M.V. Bondar, J.A. Torres, K.D. Belfield, Folate receptor targeting silica nanoparticle probe for two-photon fluorescence bioimaging, *Biomedical Optics Express* 1 (2) (2010) 453–462.
- [233] Y. Jiao, P. Akcora, Accelerated brush growth on nanoparticle surfaces by reversible addition-fragmentation chain transfer polymerization, *Journal of Polymer Science Part A: Polymer Chemistry* 52 (12) (2014) 1700–1705.
- [234] M. Sobani, V. Haddadi-Asl, M. Salami-Kalajahi, H. Roghani-Mamaqani, S.-A. Mirshafiei-Langari, K. Khezri, “Grafting through” approach for synthesis of polystyrene/silica aerogel nanocomposites by in situ reversible addition-fragmentation chain transfer polymerization, *Journal of Sol-Gel Science and Technology* 66 (2) (2013) 337–344.
- [235] S.C. Radzinski, J.C. Foster, J.B. Matson, Preparation of bottlebrush polymers via a one-pot ring-opening polymerization (ROP) and ring-opening metathesis polymerization (ROMP) grafting-through strategy, *Macromolecular Rapid Communications* 37 (7) (2016) 616–621.
- [236] A. Kopf, J. Baschnagel, J. Wittmer, K. Binder, On the adsorption process in polymer brushes: a monte carlo study, *Macromolecules* 29 (5) (1996) 1433–1441.
- [237] R.C. Advincula, *Polymer brushes: synthesis, characterization, applications*, Wiley-VCH, Weinheim (2004).
- [238] L. Severaa, L. Adriaenssens, J. Vávraa, D. Šamana, I. Čisarováb, P. Fiedlera, F. Teplýa, Highly modular assembly of cationic helical scaffolds: rapid synthesis of diverse helquats via differential quaternization, *Tetrahedron* 66 (19) (2010) 3537–3552.

Chapter 10. Appendix

10.1 Nomenclature

10.1.1 Abbreviations

ABDMMS	(4-Aminobutyl)dimethylethoxysilane
APTES	3-Aminopropyltriethoxysilane
APTMS	3-Aminopropyl trimethoxysilane
ATRP	Atom transfer radical polymerization
BET	Brunauer-Emmett-Teller
BMBA	4-(Bromomethyl)benzoic acid
CROP	Cationic ring opening polymerization
CSNPs	Core-shell nanoparticles
CT	Computed tomography
CTMS	((Chloromethyl)phenylethyl)trimethoxysilane
CuAAC	Copper-catalysed azide-alkyne cycloaddition
DCM	Dichloromethane
DLS	Dynamic light scattering
DFM	Dimethylformamide
EA	Elemental analysis
EDA	Ethylene diamine
EPR	Enhancing the permeability and retention effect
EtOx	2-Ethyl-2-oxazoline
FA	Folic acid
FITC	Fluorescein isothiocyanate
FT-IR	Fourier transform infrared
GPS	3-Glycidoxypropyl trimethoxysilane
IPOX	2-Isopropenyl-2-oxazoline
IPTES	(3-Isocyanatopropyl) triethoxysilane
MeOTf	Methyl trifluoromethane sulfonate

MeOx	2-Methyl-2-oxazoline
MPTMS	(3-Mercaptopropyl)trimethoxysilane
MRI	Magnetic resonance imaging
NMP	Nitroxide-mediated polymerization
NMR	Nuclear magnetic resonance
NPs	Nanoparticles
PDI	Polydispersity index
PEG	Polyethylene glycol
PET	Positron emission tomography
PEtOx	Poly(2-ethyl-2-oxazoline)
PGA	Polyglutamic acid
PLGA	Poly(lactic and polyglutamic acid)
PMeOx	Poly(2-methyl-2-oxazoline)
POx	Poly(2-oxazoline)
PSA	Polysialic acid
PSNP	Poly(2-methyl-2-oxazoline)-silica nanoparticles
PVP	Polyvinylpyrrolidone
PynOx	2-(Pent-4-ynyl)-2-oxazoline
P β CD	β -Cyclodextrin polymer
RAFT	Reversible addition–fragmentation chain-transfer
Ru(bpy)	Tris(bipyridine)ruthenium(II) chloride
SEC	Size-exclusion chromatography
SEM	Scanning electron microscope
SNPs	Silica nanoparticles
TEM	Transmission electron microscopy
TEOS	Tetraethoxysilane
TGA	Thermal gravimetric analysis
TMOS	Tetramethoxysilane
UV-Vis	Ultraviolet-Visible Spectroscopy
W/O	Water in oil

10.1.2 Symbols

c_{dye}	Concentration of the dye dispersed in a solvent	$\mu\text{mol mL}^{-1}$
\mathcal{D}	Dispersity	-
M_n	Number-average molecular weight	g mol^{-1}
M_w	Weight-average molecular weight	g mol^{-1}
n	Degree of polymerization	-
S_{SPC}	Specific surface area of silica nanoparticles	$\text{m}^2 \text{g}^{-1}$
t_i	Initiator immobilization's time	h
t_r	Reaction time	h
W_{PSNP}	Weight loss percent of polymer-coated silica nanoparticles between 150 and 650°C	-
W_{SNP}	Weight loss percent of silica nanoparticles between 150 and 650°C	-
Γ_{PMeOx}	Amount of the grafted poly(2-methyl-2-oxazoline)	mg m^{-2}

10.2 List of Figures

Figure 1.1	Schematic illustration of cancer diagnosis and therapy with nanoparticles ...	2
Figure 2.1	General classification of core-shell nanoparticles based on the properties of their shells and material-types	3
Figure 2.2	Scheme of a multifunctional core-shell nanoparticle for biomedical applications.....	4
Figure 2.3	Schematic diagram of the (a) mesoporous silica nanoparticles and (b) nonporous silica nanoparticles loaded with cargos.	7
Figure 2.4	Hydrolysis and condensation reactions of the silica precursor	8
Figure 2.5	Schematic diagram of Stöber method and reverse microemulsion to synthesize silica nanoparticles	9
Figure 2.6	Schematic representation of the controlled physicochemical properties of SNPs.....	10
Figure 2.7	Schematic representation of two synthetic approaches to fabricate dye-doped silica nanoparticles: (a) Stöber method and (b) reverse microemulsion method	14
Figure 2.8	General polymerization mechanism of cationic-ring opening polymerization of 2-oxazolines	17
Figure 2.9	Polymerization mechanism of 2-oxazoline containing a covalent propagation species	18
Figure 2.10	Mechanism of chain transfer and chain coupling	19
Figure 2.11	Possible ways to synthesize functionalized poly(2-oxazoline)s	20
Figure 2.12	Functionalized POx using functionalized initiator (I), monomer (R), or terminating agent (T).....	21
Figure 2.13	Different strategies for the surface modification with a polymer	23
Figure 2.14	Schematic representation of (a) copper(I)-catalyzed azide/alkyne-cycloaddition for NP-surface modification via the click chemistry (b) the silane coupling reaction between hydroxyl groups on the surface of SNPs and silane-functionalized polymer chain.....	25
Figure 2.15	Schematic description of (a) SNP coated with β -cyclodextrin polymer (P β CD) as a host layer and alkyl-functionalized PMeOx as a guest layer, (b) photochemical attachment of POx chains to silica surfaces by illumination of polymer-covered monolayers of a benzophenone derivative	30
Figure 4.1	Various coupling agents that can be used for the direct termination of the living oxazolinium species and consequently binding them to silica surface (FP.1-6), preparation of POx with three silane-functionalized groups (FP.7).....	34
Figure 4.2	Synthesis of (a) alkyne-/azide-functionalized SNPs by grafting or co-condensation approaches (b) various clickable POx.....	35

Figure 4.3 Schematic diagram of the formation process of poly(2-methyl-2-oxazoline)-silica nanoparticles (PSNP) by using click chemistry (approach 1) and silane coupling reaction (approach 2) in different reaction conditions.....	36
Figure 4.4 Schematic diagram of the formation process of poly(2-methyl-2-oxazoline)-silica nanoparticles using click chemistry	38
Figure 4.5 TEM images of silica nanoparticles prepared by reverse microemulsion....	39
Figure 4.6 (a) FT-IR spectra of SNP, SNP-Br, SNP-N ₃ , PSNP-A. (b) Thermogravimetric analysis of SNP, SNP-Br, SNP-N ₃ , PSNP-A.	39
Figure 4.7 TEM image of (a,b) silica-azide nanoparticles, poly(2-methyl-2-oxazoline)-silica nanoparticles (PSNP-A) dispersed in (c,d) methanol and (e,f) isopropanol	42
Figure 4.8 Schematic diagram of the formation process of poly(2-methyl-2-oxazoline) silica nanoparticles using silane coupling reaction in various reaction conditions.	43
Figure 4.9 (a) FT-IR spectra of SNP, PSNP-B, PSNP-C, and PSNP-D (b) Thermogravimetric analysis of SNP, PSNP-B, PSNP-C, and PSNP-D	44
Figure 4.10 Schematic strategy for the synthesis of PMeOx-silica hybrid nanoparticles using water in oil micro emulsion (PSNP-D)	46
Figure 4.11 TEM images of (a,b) silica nanoparticles, poly(2-methyl-2-oxazoline)-silica nanoparticles (PSNP-B) dispersed in (c,d) methanol and (e,f) isopropanol	47
Figure 4.12 Schematic diagram for the formation process of poly(2-methyl-2-oxazoline) dye-doped silica nanoparticles in one-pot system by using reverse microemulsion method	48
Figure 4.13 (a) FT-IR spectra of SNP, SNP-Ru(bpy), PSNP-E, SNP-FITC, and PSNP-F (b) TGA of SNP, SNP-Ru(bpy), PSNP-E, SNP-FITC, and PSNP-F.	49
Figure 4.14 TEM images of SNP-Ru(bpy) (a), PSNP-E dispersed in methanol (b) and isopropanol (c) SNP-FITC (d), PSNP-F dispersed in methanol (e) and isopropanol (f)..	50
Figure 4.15 (a) FT-IR spectra of bare SNP, PSNP-B-1, PSNP-B-2, PSNP-B-3, and PSNP-B-4 (b) TGA of bare SNP, PSNP-B-1, PSNP-B-2, PSNP-B-3, and PSNP-B-4	53
Figure 4.16 (a) FT-IR spectra of bare SNP, PSNP-B-5, PSNP-B-6, PSNP-B-7, and PSNP-B-8 (b) TGA of bare SNP, PSNP-B-5, PSNP-B-6, PSNP-B-7, and PSNP-B-8...	54
Figure 4.17 (a) FT-IR spectra of bare SNP, PSNP-B-9, PSNP-B-10, PSNP-B-11, and PSNP-B-12 (b) TGA of bare SNP, PSNP-B-9, PSNP-B-10, PSNP-B-11, and PSNP-B-12	55
Figure 4.18 (a) FT-IR spectra of bare SNP, PSNP-D-1, PSNP-D-2, PSNP-D-3, and PSNP-D-4 (b) TGA of bare SNP, PSNP-D-1, PSNP-D-2, PSNP-D-3, and PSNP-D-4..	56
Figure 4.19 (a) FT-IR spectra of bare SNP, PSNP-D-5, PSNP-D-6, PSNP-D-7, and PSNP-D-8 (b) TGA of bare SNP, PSNP-D-5, PSNP-D-6, PSNP-D-7, and PSNP-D-8...	57

Figure 5.1 Schematic strategy for the synthesis of PMeOx-coated SNPs using “grafting-from” approach followed by further functionalization of the hybrid nanoparticle via (a) the functionalization of the polymer chains or (b) doping fluorescent dye molecules in the core of the hybrid nanoparticle.....	67
Figure 5.2 Reaction scheme for the synthesis of poly(2-methyl-2-oxazoline)-silica hybrid nanoparticles by means of surface-initiated cationic ring opening polymerization using 4-(bromomethyl)benzoic acid (BMBA) as an initiator	69
Figure 5.3 (a) FT-IR spectra of SNP, SNP-NH ₂ , SNP-BMBA, and PSNP-G (b) TGA of SNP, SNP-NH ₂ , SNP-BMBA, and PSNP-G	69
Figure 5.4 Synthesis of poly(2-methyl-2-oxazoline)-silica hybrid nanoparticles, (a) by means of surface-initiated cationic ring-opening polymerization using((chloromethyl)phenylethyl)trimethoxysilane (CTMS) as an initiator, (b) using different terminating agents for subsequent particle modification with (c) fluorescein (FITC) and (d) folic acid (FA).	71
Figure 5.5 (a) FT-IR spectra of the SNP and SNP-CTMS (b) TGA of SNP and SNP-CTMS	72
Figure 5.6 TEM images of (a,b) SNP-CTMS	73
Figure 5.7 (a) FT-IR spectra of SNP, PSNP-H-1, PSNP-H-2, and PSNP-H-3 (b) TGA of SNP, PSNP-H-1, PSNP-H-2, and PSNP-H-3	74
Figure 5.8 TEM images of (a) PSNP-H-1, (b) PSNP-H-2, and (c) PSNP-H-3.....	75
Figure 5.9 (a) FT-IR spectra of SNP, PSNP-H-4, PSNP-H-5, and PSNP-H-6 (b) TGA of SNP, PSNP-H-4, PSNP-H-5, and PSNP-H-6	78
Figure 5.10 TEM images of (a) PSNP-H-4, (b) PSNP-H-5, and (c) PSNP-H-6.....	78
Figure 5.11 Schematic representation of the modification sequence of PMeOx-silica hybrid nanoparticles functionalized with amine groups (PSNP-I) conjugated with: (a) folic acid, PSNP-I-FA, and (b) fluorescein isothiocyanate, PSNP-I-FITC.....	80
Figure 5.12 UV-Vis absorption spectra of ninhydrin and PSNP-I.....	80
Figure 5.13 UV-Vis absorption spectra of (a) PSNP-I, PSNP-I-FITC, and bare FITC (b) PSNP-I, PSNP-I-FA, and pure FA.	81
Figure 5.14 FT-IR spectra of PSNP-I, PSNP-I-FITC, and PSNP-I-FA	82
Figure 5.15 Schematic strategy for the synthesis of Ru(bpy)-doped SNPs coated with PMeOx using the “grafting-from” approach.....	83
Figure 5.16 (a) FT-IR spectra of SNP, SNP-Ru(bpy), and PSNP-J (b) TGA of SNP-Ru(bpy), and PSNP-J	84
Figure 6.1 Schematic depiction of different approaches of chemical grafting of PMeOx chains to the silica surface: (a) “grafting to” (b) “grafting from”, and (c) in situ immobilization and polymerization.	94
Figure 6.2 Schematic depiction for the synthesis of PMeOx-coated silica nanoparticles (PSNP-K, PSNP-L, and PSNP-M) via in situ immobilization and polymerization of 2-methyl-2-oxazoline.....	96

Figure 6.3 (a) FT-IR spectra of bare SNP, PSNP-K, PSNP-L, and PSNP-M (b) TGA of bare SNP, PSNP-K, PSNP-L, and PSNP-M.....	97
Figure 6.4 (a) FT-IR spectra of PSNP-M, PSNP-M-1 to PSNP-M-6 (b) TGA of PSNP-M, PSNP-M-1 to PSNP-M-6.	98
Figure 6.5 TEM images of (a,b) silica nanoparticles, (c,d) PSNP-M-1 (e,f), and PSNP-M-6 dispersed in isopropanol	101
Figure 8.1 Schematic diagram of the formation process of PMeOx-coated SNPs via the “grafting to” approach using click chemistry (a) and silane coupling reaction (b) in different reaction conditions and also the “grafting from” approach using CTMS as an initiator and using different terminating agents for subsequent particle modification with (c) fluorescein (FITC) and (d) folic acid (FA).....	113
Figure 8.2 Schematic depiction of three synthetic protocol used for the synthesis of PMeOx-coated silica nanoparticles via in situ immobilization and polymerization of MeOx including PSNP-K, PSNP-L, and PSNP-M.....	114
Figure 10.1 ¹ H NMR spectrum of alkyne-functionalized PMeOx (P1).....	141
Figure 10.2 ¹ H NMR spectrum of trimethoxysilane-functionalized PMeOx (P2)	141
Figure 10.3 (a) UV-Vis absorption spectra of Ru(bpy) in PBS buffer at different concentrations (b) the relation between absorbance and Ru(bpy) concentration.	142
Figure 10.4 (a) UV-Vis absorption spectra of FITC in PBS buffer at different concentrations (b) the relation between absorbance and FITC concentration.....	143
Figure 10.5 (a) UV-Vis absorption spectra of FA in DMSO at different concentrations (b) the relation between absorbance and FA concentration.....	143

10.3 List of Tables

Table 4.1 Elemental analysis of modified SNPs using click chemistry and shell thickness in the synthesized hybrid particle.....	40
Table 4.2 Analytical data for the polymers P1 and P2.	41
Table 4.3 Elemental analysis of modified SNPs using silane coupling reaction and shell thickness in the synthesized hybrid particle.	44
Table 4.4 Particle size and concentration of dyes inside silica matrix before and after the formation of the polymeric shell	51
Table 4.5 Analytical data from the PSNP-B by varying the reaction temperature, time, and feed ratio	53
Table 4.6 Analytical data from the PSNP-D by varying reaction time and feed ratio ...	56
Table 5.1 Shell thickness of the PMeOx-coated SNPs by varying time reaction and monomer/initiator ratio concentration.....	76
Table 5.2 Analytical data from PMeOx grafted from the silica nanoparticles surface. .	76
Table 6.1 Reaction condition and analytical data from the hybrid nanoparticles prepared via in situ immobilization and polymerization of MeOx	98
Table 6.2 Analytical data from the hybrid nanoparticles prepared via in situ immobilization and polymerization of MeOx.....	100

10.4 ^1H NMR spectra of P1 and P2

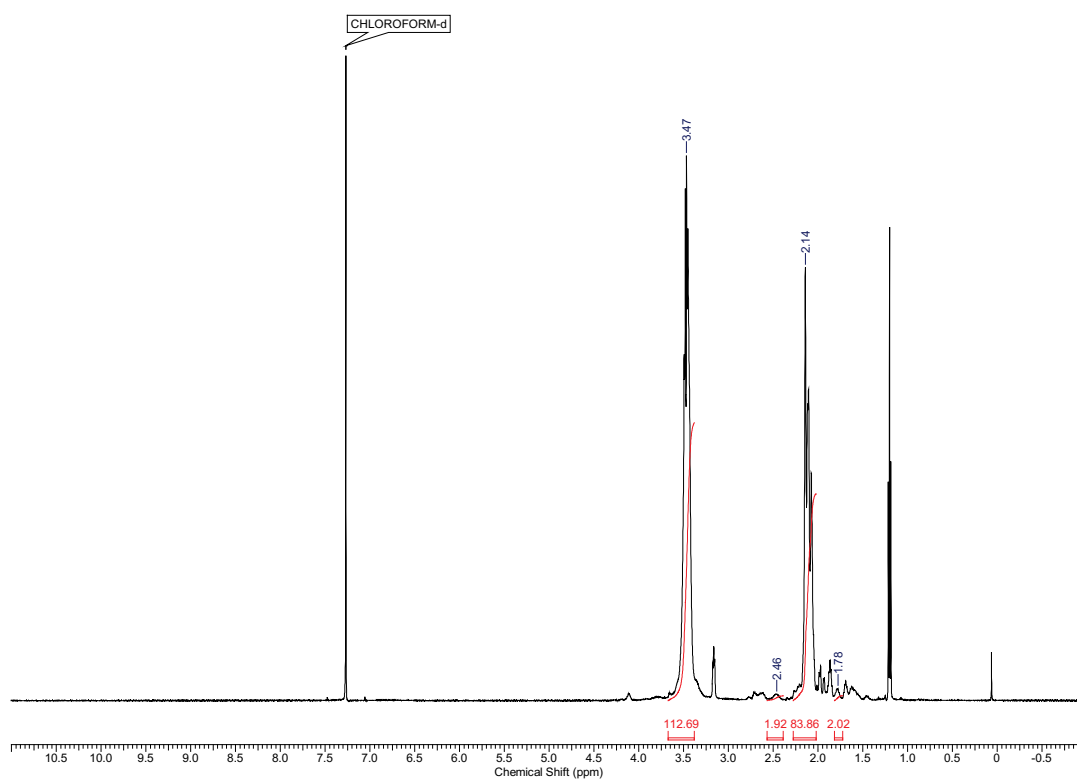


Figure 10.1 ^1H NMR spectrum of alkyne-functionalized PMeOx (P1).

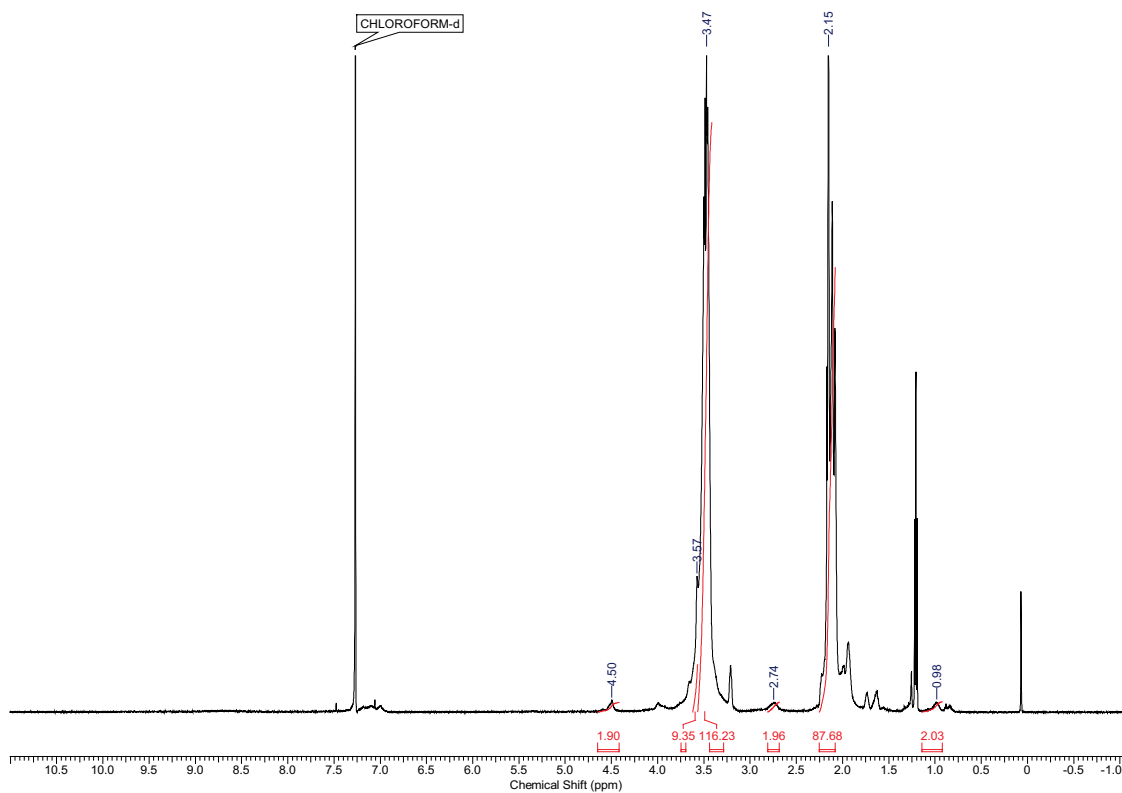


Figure 10.2 ^1H NMR spectrum of trimethoxysilane-functionalized PMeOx (P2).

10.5 UV-Vis Calibration

The concentration of the dye molecules, such as Ru(bpy) and FITC which were encapsulated either inside the silica core or immobilized on the surface of hybrid nanoparticles, and also a cancer-targeting ligand, such as folic acid (FA), as a cancer-targeting ligand which were conjugated to the surface of particles, can be calculated by using UV-Vis spectroscopy. Therefore, the calibration curves of these molecules are required to be plotted. Figure 10.3 indicates the absorption spectra of a series of standard solutions containing Ru(bpy) dye molecules at different concentration in PBS buffer. It is obvious that the absorbance at 452 nm for Ru(bpy) increased correspondingly by increasing the dye concentration. For Ru(bpy) dye molecules, the absorbance increased linearly with the dye concentration in the range of 0.25 to 1.75 (10^{-8} mol/mL) ($\Delta\text{Abs.} = 0.1092 \times c_{\text{Ru(bpy)}} + 0.0693$) with a correlation coefficient of 0.991.

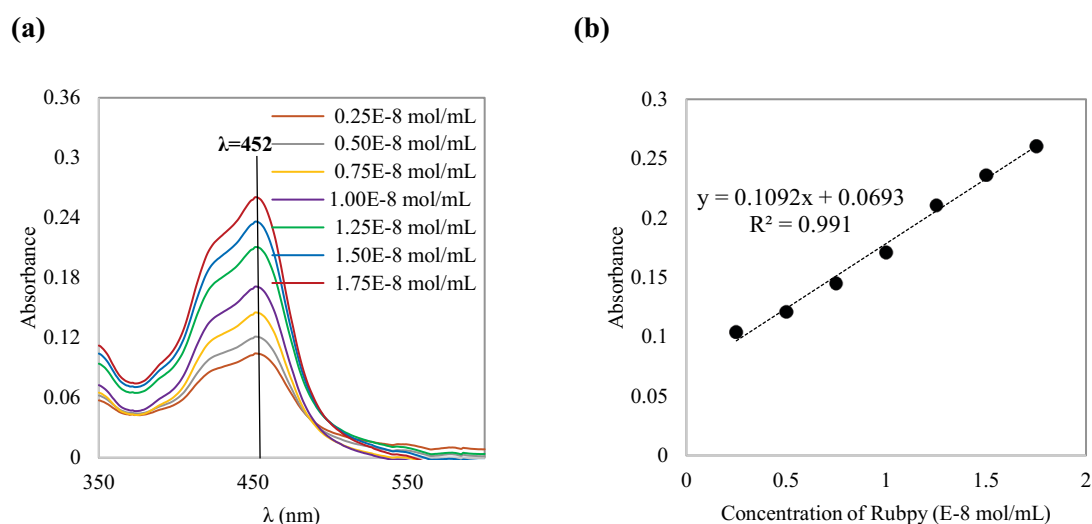


Figure 10.3 (a) UV-Vis absorption spectra of Ru(bpy) in PBS buffer at different concentrations **(b)** the relation between absorbance and Ru(bpy) concentration.

Figure 10.4 indicates the absorption spectra of a series of standard solutions containing FITC dye molecules at different concentration in PBS buffer. For FITC dye molecules, the absorbance at 482 nm was increased linearly with the dye concentration in the range of 0.25 to 2 (10^{-8} mol/mL) ($\Delta\text{Abs.} = 0.0384 \times c_{\text{FITC}} + 0.0008$) with a correlation coefficient of 0.9937. Finally, the absorption spectra of a series of standard solutions containing FA molecules with different concentrations in DMSO was shown in

Figure 10.5. It is obvious that the absorbance at 360 nm for FA increased correspondingly by increasing the concentrations of these molecules.

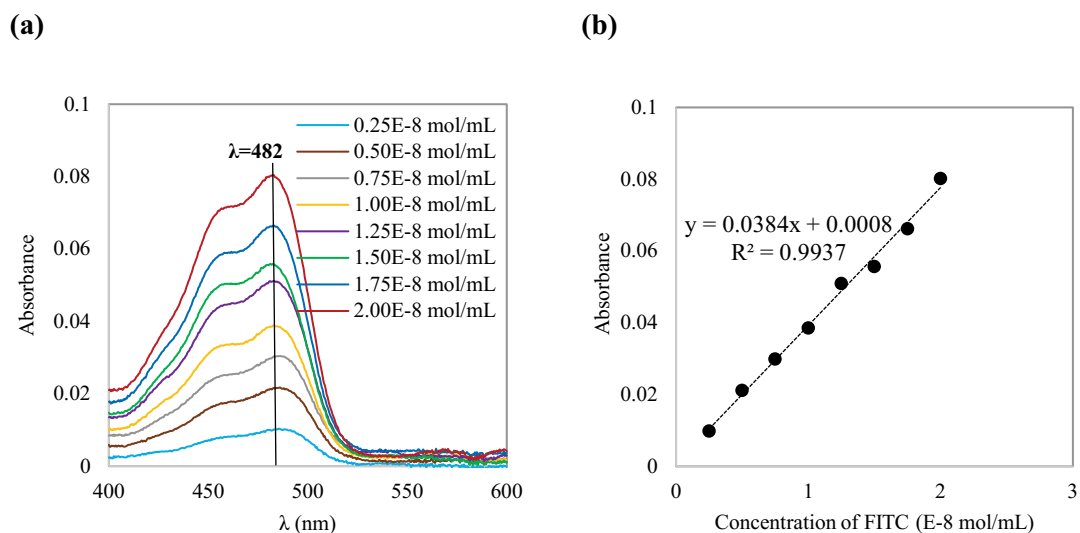


Figure 10.4 (a) UV-Vis absorption spectra of FITC in PBS buffer at different concentrations (b) the relation between absorbance and FITC concentration.

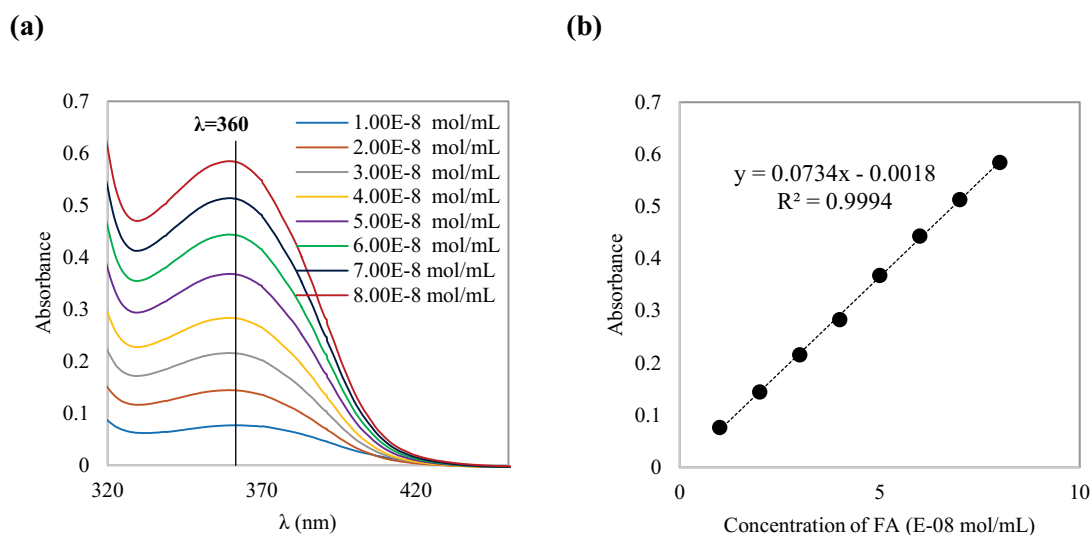


Figure 10.5 (a) UV-Vis absorption spectra of FA in DMSO at different concentrations (b) the relation between absorbance and FA concentration.

Eidesstattliche Versicherung (Affidavit)

Name, Vorname
(Surname, first name)

Matrikel-Nr.
(Enrolment number)

Belehrung:

Wer vorsätzlich gegen eine die Täuschung über Prüfungsleistungen betreffende Regelung einer Hochschulprüfungsordnung verstößt, handelt ordnungswidrig. Die Ordnungswidrigkeit kann mit einer Geldbuße von bis zu 50.000,00 € geahndet werden. Zuständige Verwaltungsbehörde für die Verfolgung und Ahndung von Ordnungswidrigkeiten ist der Kanzler/die Kanzlerin der Technischen Universität Dortmund. Im Falle eines mehrfachen oder sonstigen schwerwiegenden Täuschungsversuches kann der Prüfling zudem exmatrikuliert werden, § 63 Abs. 5 Hochschulgesetz NRW.

Die Abgabe einer falschen Versicherung an Eides statt ist strafbar.

Wer vorsätzlich eine falsche Versicherung an Eides statt abgibt, kann mit einer Freiheitsstrafe bis zu drei Jahren oder mit Geldstrafe bestraft werden, § 156 StGB. Die fahrlässige Abgabe einer falschen Versicherung an Eides statt kann mit einer Freiheitsstrafe bis zu einem Jahr oder Geldstrafe bestraft werden, § 161 StGB.

Die oben stehende Belehrung habe ich zur Kenntnis genommen:

Official notification:

Any person who intentionally breaches any regulation of university examination regulations relating to deception in examination performance is acting improperly. This offence can be punished with a fine of up to EUR 50,000.00. The competent administrative authority for the pursuit and prosecution of offences of this type is the chancellor of the TU Dortmund University. In the case of multiple or other serious attempts at deception, the candidate can also be unenrolled, Section 63, paragraph 5 of the Universities Act of North Rhine-Westphalia.

The submission of a false affidavit is punishable.

Any person who intentionally submits a false affidavit can be punished with a prison sentence of up to three years or a fine, Section 156 of the Criminal Code. The negligent submission of a false affidavit can be punished with a prison sentence of up to one year or a fine, Section 161 of the Criminal Code.

I have taken note of the above official notification.

Ort, Datum
(Place, date)

Unterschrift
(Signature)

Titel der Dissertation:
(Title of the thesis):

Ich versichere hiermit an Eides statt, dass ich die vorliegende Dissertation mit dem Titel selbstständig und ohne unzulässige fremde Hilfe angefertigt habe. Ich habe keine anderen als die angegebenen Quellen und Hilfsmittel benutzt sowie wörtliche und sinngemäße Zitate kenntlich gemacht.

Die Arbeit hat in gegenwärtiger oder in einer anderen Fassung weder der TU Dortmund noch einer anderen Hochschule im Zusammenhang mit einer staatlichen oder akademischen Prüfung vorgelegen.

I hereby swear that I have completed the present dissertation independently and without inadmissible external support. I have not used any sources or tools other than those indicated and have identified literal and analogous quotations.

The thesis in its current version or another version has not been presented to the TU Dortmund University or another university in connection with a state or academic examination.*

***Please be aware that solely the German version of the affidavit ("Eidesstattliche Versicherung") for the PhD thesis is the official and legally binding version.**

Ort, Datum
(Place, date)

Unterschrift
(Signature)